Observational Consequences of Unstable Stellar Interiors

Cover illustration:
The massive binary star Eta Carinae and evolutionary tracks of a fast rotating and a slowly rotating massive star. Credit: NASA, Hubble Space Telescope

ISBN/EAN 9789490122744

Observational consequences of unstable stellar interiors

Waarneembare gevolgen van instabiliteiten
in het binnenste van sterren
(met een samenvatting in het Nederlands)

Proefschrift

ter verkrijging van de graad van doctor aan de Universiteit Utrecht op gezag van de rector magnificus, prof. dr. J.C. Stoof, ingevolge het besluit van het college voor promoties in het openbaar te verdedigen op vrijdag 6 november 2009 des middags te 2.30 uur

door

Matteo Cantiello

geboren op 28 oktober 1979 te Cecina, Italië

Promotor: Prof. dr. N. Langer

This research has been supported in part by the Netherlands Research School for Astronomy (NOVA).

“You must have chaos within you to give birth to a dancing star”
F. Nietzsche - Thus Spoke Zarathustra

Contents

CHAPTER 1

Introduction

It is hard to escape a deep sense of awe during a starry night, even more if one realizes that we are looking at a tiny fraction of the stars populating our galaxy, the Milky-Way. The importance of stars partly comes from their sheer number. It has been determined that there are 10^{11}-10^{12} stars in our Galaxy, and there are perhaps 10^{11}-10^{12} galaxies in our universe. Therefore a simple estimate leads to the mind-blowing number of 10^{22}-10^{24} stars.

The night sky looks still and peaceful, but stars are not eternal. They are born, live and die. This is a tale with gravity as protagonist. The same force that is responsible for the initial cloud of gas to form the protostar, has to be counteracted by the gradient of the internal pressure. Only in this way a star can be in hydrostatic equilibrium. The required energy is mostly provided by nuclear reactions in the stellar interiors, which turn a small fraction of the rest mass into energy. Thermonuclear reactions in the stellar interior release energy and at the same time synthesize, starting from hydrogen, heavier elements. This process is called stellar nucleosynthesis. Studying stars humans discovered that, aside from hydrogen, all of the elements we are made of have been synthesized inside stars. A star is a self-regulating system, because the amount of energy released by nuclear burning is exactly the amount needed to counteract the gravitational force. If the equilibrium is perturbed, the star readjust its structure, such that the nuclear reactions provide again the right amount of energy.

In this way stars can be stable for long timescales during hydrogen burning (the so-called main sequence). This phase cannot last forever, since the amount of fuel inside of stars is finite, and energy is released only from the fusion of isotopes lighter than iron. When a sufficient amount of energy can no longer be extracted from the rest mass of the star, the battle against gravity is lost. Then the final fate of the star depends on the mass of the object: low mass stars end their lives as white dwarfs, while massive stars (more massive than about 8 solar masses) die in spectacular explosions (see Fig. 1.1).

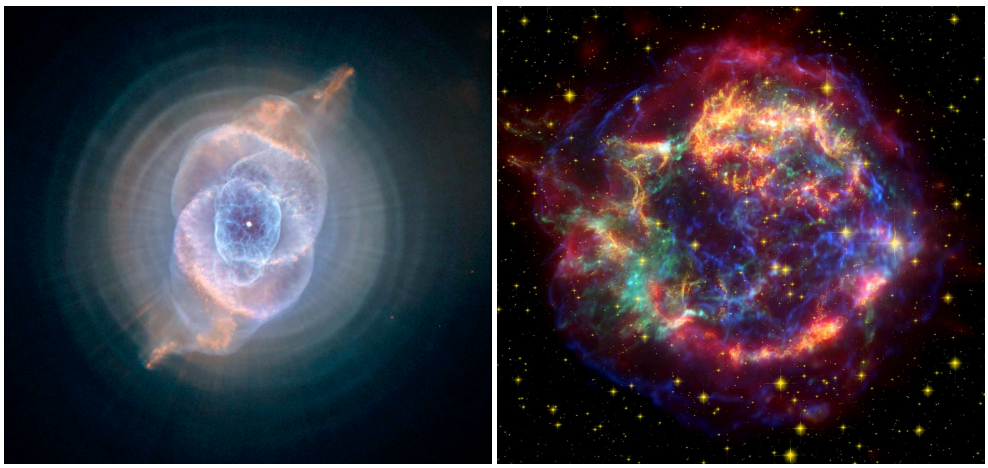

Figure 1.1: Left: A classic planetary nebula, the Cat's Eye (NGC 6543), is 3000 light years away from the Earth and represents a final phase in the life of a sun-like star. The nebula's dying central star is loosing material, which forms the beautiful and intricate structures visible in the picture. These layers are rich in material processed in the stellar interiors, which in this way is ejected in the interstellar medium and will take part to the formation of new stars and planets. Credit: NASA, ESA, HEIC, and The Hubble Heritage Team. Right: While low-mass stars die quietly, slowly releasing material in the interstellar medium, massive stars pass with a blast. The supernova which is produced during the collapse of stars more massive than about $8\,M_{\odot}$, is a powerful explosion that ejects material at very high speed. As fireworks leave beautiful lights and colors in the sky, supernovae also leave their colorful signature: supernova remnants. The picture shows Cassiopeia A, one of the best-studied supernova remnants. Observations of this remnant at different wavelength permit to identify heavy elements in the debris left by the stellar explosion. This material, as in the case of the planetary nebula, will be recycled and will form new stars and planets. Credit: NASA/JPL-Caltech/STScI/CXC/SAO.

Most of the work presented in this thesis focuses on state-of-the-art evolutionary calculations of massive single and binary stars, including some of the complex hydrodynamical phenomena that affect their interiors. Massive stars represent a small fraction of the total number of stars, but their importance for astrophysics is enormous. Massive stars play a key-role in the evolution of galaxies from the era of re-ionization until today. They are the prime contributors to the energy and momentum input into the interstellar medium through both stellar winds and supernovae (SNe); they are responsible for the bulk of ionizing radiation, and they are the principal sources of enrichment of the Universe with heavy elements via winds and SNe. The death of massive stars is one of the most interesting and spectacular phenomena in astrophysics. Not only does it result in the most energetic explosions in the Universe (SNe, long gamma-ray bursts (GRBs) and pair creation supernovae), but it leaves exotic remnants such as pulsars, magnetars and black holes.

1.1 The unstable stellar interiors

In order to predict stellar nucleosynthesis, the stellar interior has to be modeled.

The interior of stars is not quiet. The main reason is that huge amounts of energy are produced in the inner parts of a star, creating strong temperature gradients. This energy eventually escapes from the inside of the star through its surface, transported from below through radiative transfer or convection. Convection, in particular, results in turbulent motions of the stellar plasma; a clear example of this process is visible at the surface of the Sun (see Fig. 1.2). In general such motions are able to transport chemical species and angular momentum. In the case of convection the turbulent motions are also able to excite waves, which can propagate and transport energy through the star. In the presence of rotation, further instabilities of the stellar plasma can develop. Rotation also contributes to the generation of magnetic fields, which provide further instabilities and mixing processes. Thermohaline mixing is driven by another instability that may occur in the stellar interior in regions where an inversion in the mean molecular weight is created. Finally, in the case of extremely high temperatures, the production of electron-positron pairs from photons can destabilize the stellar core and induce collapse. This results in the so-called pair creation supernovae (PCSN).

Before discussing the instabilities which have been studied in this thesis, it is important to emphasize that modern stellar evolution calculations do not solve the full 3D hydrodynamic equations in the stellar interior. The reason is that this is computationally impossible. The timescale of the evolution of a star (nuclear timescale) is much longer than the timescale of the hydrodynamical processes occurring in its interior (dynamical or thermal timescale). As a consequence a numerical time-step resolving convection or any other hydrodynamical process for the entire stellar evolution would results in almost endless calculations. At least with the actual computational facilities. The trick is to restrict the simulations to 1D, and implement complex hydrodynamical phenomena as diffusion processes. The code is still solving the 1D hydrodynamic equations, but the transport of chemical species and angular momentum resulting from complex instabilities, is implemented through a diffusion scheme. An analytical approach is used to estimate the speed of mixing and angular momentum transport as function of physics parameters. This permits the calculation of a diffusion coefficient for each physical process considered; these coefficients are added together and enter the diffusion equation. Therefore the single processes can be modeled, but it is clear that this approach will neglect possible interactions between different instabilities.

1.1.1 Convection

Convection is a circulational mass and heat transfer in a fluid, driven by buoyancy generated by a strong temperature gradient. Strong convection results in turbulent motions which can efficiently mix the fluid. In stellar calculations convection is implemented through the so-called Mixing Length Theory, in which buoyant fluid elements (blobs) are assumed to travel some distance before dissolving and releasing their excess heat. The turbulent cascade is not considered in this implementation, while a local mean flow velocity is calculated.

In a radiative layer of a star there are three ways to turn on convection: either the luminosity increases, the adiabatic gradient decreases (for example in the case of partial ionization)

Figure 1.2: Photosphere of the Sun. The small scale pattern is called granulation, and is caused by the surface emergence of convective elements. The interaction of convection and rotation results in the generation of magnetic fields, which can rise due to buoyancy and reach the surface of the Sun. A group of sun-spots is clearly visible at the picture's center. These appear dark due to magnetic fields up to a few kG which inhibit convection, resulting in a less efficient flux transport. Credit: Dutch Open Telescope.

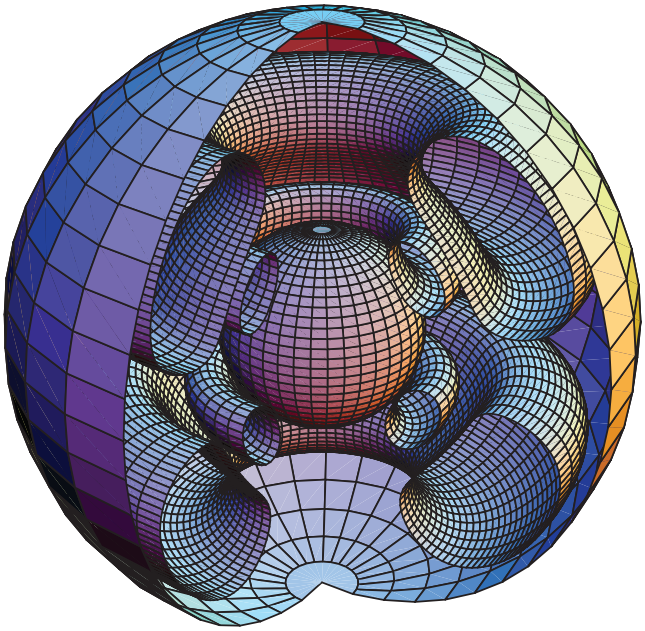

Figure 1.3: Eddington-Sweet circulation in a rotating 20 $M_\odot$ model with $v_{\rm ini} = 300\,{\rm km\,s^{-1}}$ at the beginning of the H-burning phase. The streamlines are in the meridian plane. In the upper hemisphere on the right section, matter is turning counterclockwise along the outer stream line and clockwise along the inner one. The outer sphere is the star surface and has a radius equal to 5.2 $R_\odot$. The inner sphere is the outer boundary of the convective core. It has a radius of 1.7 $R_\odot$. Credit: G. Meynet & A. Maeder

or the opacity gets larger. In 1992 at the Los Alamos Laboratories, Rogers & Iglesias included the spin-orbit coupling in their atomic physics calculations. A huge amount of new transitions, especially for iron, came from the line splitting due to the presence of the Russel-Saunders coupling in the hamiltonian of the atom. This created a new peak in the opacity tables which are used for stellar evolution calculations. In hot massive stars this peak can trigger convection below the surface. The study of these sub-surface convective regions and of their possible observational consequences in massive stars is the topic of Chapter 2.

1.1.2 Rotational instabilities

In the presence of rotation the stellar structure is modified by the centrifugal acceleration. Since the radiative energy flux depends on the effective gravity, the luminosity and temperature of the star become a function of the latitude (von Zeipel 1924). An imbalance in temperature between the pole and the equator is created, which in turn drives a meridional circulation in the stellar interiors (Fig. 1.3). This flow is called "Eddington-Sweet" circulation, and in massive spinning stars it is believed to be the most important rotational mixing

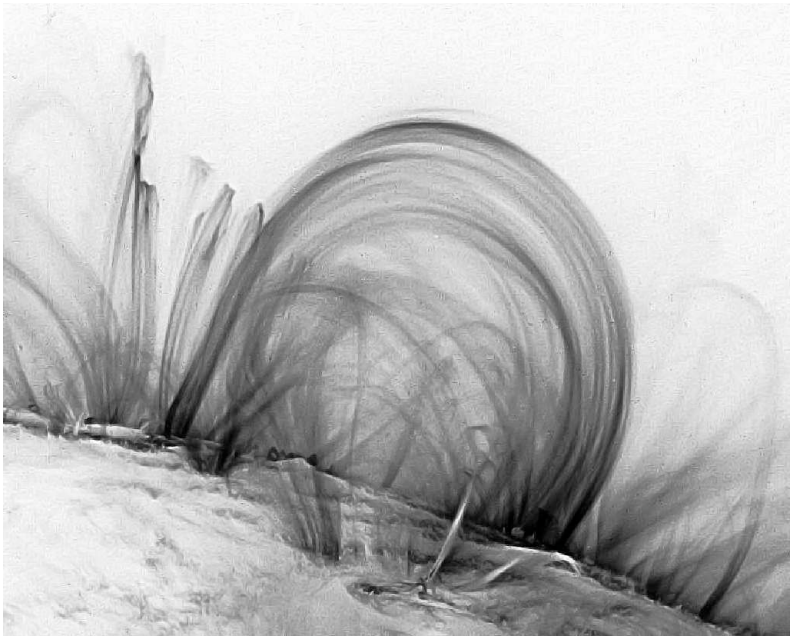

Figure 1.4: The magnetic field in the solar atmosphere shapes the structures that we see, as the emitting gas can generally only move along the field. This creates the thin loops arching above the solar limb in the picture. These active regions produce flares, which could have a role in affecting the Earth's climate. For comparison the Earth would fit about ten times inside the big loop. Credit: TRACE (NASA).

process. Shear mixing is also very significant in the case of strong differential rotation, even if the presence of magnetic fields tend to keep a star close to rigid rotation, reducing the influence of shear. In the case of a very fast rotator, rotational mixing can be so efficient that in the interior a compositional gradient can not be created, and the star evolves "quasi-chemically homogenous". In this thesis different situations in which rotational mixing plays an important role on stellar evolution have been investigated. In Chapter 3 a study of rotating, close massive binaries is presented. These stars are rapidly rotating because their surface velocity is synchronized with the orbital velocity through the action of tides. Offering the possibility to obtain the stellar parameters with high accuracy, these stars can be used as a test case for the study of rotational mixing. A new evolutionary scenario for the production of the observed massive black hole binaries is also proposed. Another way to spin up a star is by mass accretion. This is studied in Chapter 4, where the accretion process in a massive binary system is discussed. An intriguing result is that such a system could be the progenitor of a long gamma-ray burst. In Chapter 5 we show that rotational mixing allows very massive stars to explode as pair creation supernovae.

1.1.3 Magnetic fields

In a star, as in many other astrophysical environments, part of the kinetic and thermal energy of the plasma can be converted into magnetic energy. This is called a "dynamo process", and requires special configurations of the fluid motions. Once a magnetic field is produced inside a star, it plays an important role for the transport of angular momentum and chemical species. In the stellar evolution code used for the studies in this thesis, the so-called "Spruit-Tayler" dynamo is included. This dynamo process accounts for the generation of a magnetic field in radiative layers of a star which experience differential rotation.
Magnetic fields can also be generated at the boundaries of convective regions. Such dynamo process is believed to give rise to the solar cycle and produce the magnetic fields of sun-spots (see Fig. 1.2 and 1.4). In Chapter 2 we propose that also in the envelope of massive stars a similar dynamo process can occur. Sub-surface convective regions in rotating massive stars could play a role in generating magnetic fields. Emerging at the surface, such magnetic fields could have important observational consequences, which are discussed in details in Section 2.4.4.

1.1.4 Thermohaline mixing

Thermohaline mixing is a hydrodynamic instability that arises when an unstable gradient in composition is stabilized by a gradient in temperature. Because it involves the diffusion of two different components (particles and heat) it belongs to the more general class of double-diffusive instabilities. In the oceans this instability can occur, for example, in regions where the evaporation leaves a warm layer of saltier water on top of less salty, cooler water. In this situation the saltier water can sink only after exchanging its heat excess. The optimal configuration for an efficient heat exchange requires a large contact surface; long fingers satisfy this requirement (see Fig. 1.5).
A similar process occurs in stars in case of inverse mean molecular weight gradients in a thermally stabilized medium. This can take place during the accretion of material in a binary system or in the case of off-center burning. In Chapter 6 the role of thermohaline mixing in red giants is discussed. This mixing process can help explain the intriguing surface abundances observed in these stars. In particular it could be responsible for the destruction of ^{3}He in low mass stars. Such stars are net producers of ^{3}He in standard stellar evolution calculations, but the amount of ^{3}He observed in the interstellar medium matches the predictions of Big-Bang nulceosynthesis. Therefore thermohaline mixing could help to reconcile predictions of stellar evolution calculations with the observations and Big-Bang nulceosynthesis.

1.1.5 Pair production

A star in hydrostatic equilibrium is dynamically stable only if the adiabatic index $\gamma_{\rm ad}$ is greater than $4/3$ (e.g. Kippenhahn & Weigert 1990). In the core of very massive stars, temperatures in excess of $\sim 10^9$ K results in photons having an energy exceeding the rest mass of two electrons. Therefore photons in the fields of nuclei can form electro-positron pairs. As such

Figure 1.5: Thermohaline mixing in a glass of water. A layer of warm, salty water colored with a dye, is standing on top of a layer of fresh, cold water. While losing their heat content, finger-like structures slowly make their way to the bottom of the glass. Also shear develops at the finger's top, resulting in Kelvin-Helmoltz instability.

massive stars are radiation pressure dominated, removing photons means removing the main source of pressure, resulting in a decrease of the adiabatic index below $4/3$. If $\gamma_{\rm ad} < 4/3$ in an appreciably large region, the core is destabilized and collapses. As the temperature rapidly increases, oxygen is ignited explosively, which may lead to the disruption of the star in a pair creation supernova. For a PCSN to occur, stars not only need to be born massive, but they have to avoid loosing too much of their mass. Since massive star winds are metallicity dependent, a threshold in metallicity for the occurrence of PCSN is expected. This threshold has been studied in Chapter 5, leading to an estimate of the PCSN rate as function of redshift.

1.2 Binary stars

Most stars are binaries. This statement still comes as a surprise to some astronomers, but the role of binaries in astrophysics is of primary importance. From the point of view of stellar evolution, modeling binaries poses an additional challenge, since mass transfer, angular momentum transfer and tides need to be included during the calculation. The binary stellar evolution code used in this thesis has this capability, and at the same time includes the same physics as implemented in the most advanced codes for single stars. In this sense the binary stellar evolution code is unique, and allowed to explore novel evolutionary scenarios.

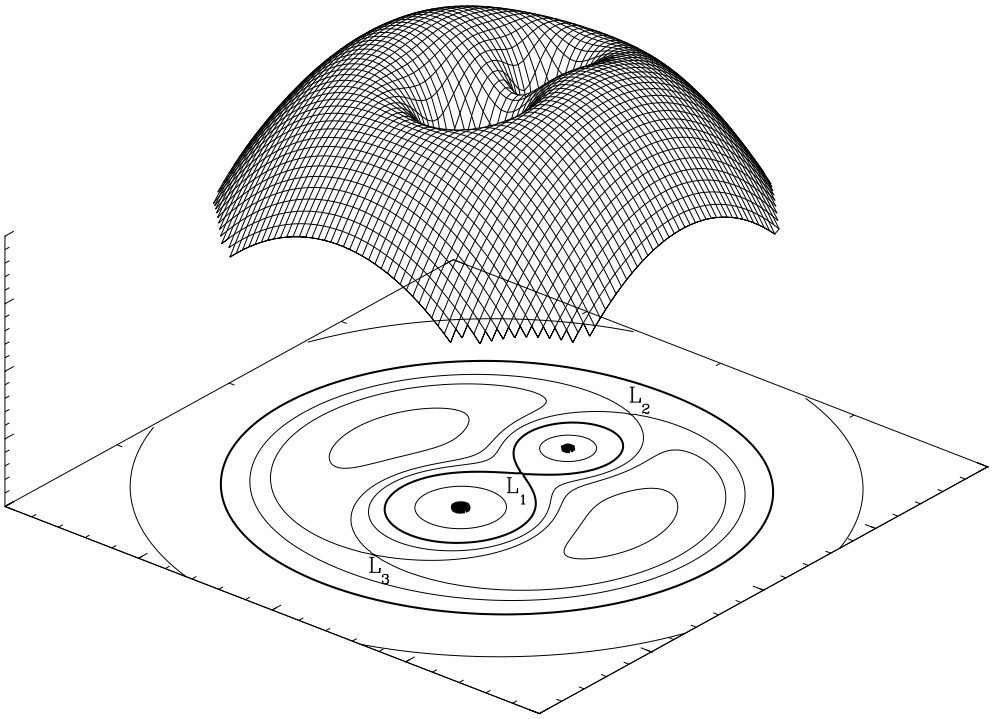

Figure 1.6: A three-dimensional representation of the Roche potential in a binary star with a mass ratio of 2, in the co-rotating frame. The droplet-shaped figures in the equipotential plot at the bottom of the figure are called the Roche lobes of each star. L1, L2 and L3 are the points of Lagrange where forces cancel out. Mass can flow through the saddle point L1 from one star to its companion, if the star fills its Roche lobe. Credit: Marc van der Sluys.

1.2.1 The influence of tides

In a close binary, angular momentum and kinetic energy can be exchanged between the two stars and their orbit through tidal torques and dynamical deformation. The system tends to evolve towards a state of minimum mechanical energy due to dissipative processes. This is an equilibrium state, where the orbit is circular, the spins of the stars are aligned and perpendicular to the orbital plane and the stars are in synchronous rotation with the orbital motion, such that $P_{\rm spin} = P_{\rm orbit}$. Therefore in very close systems tides can spin up the stars to rapid rotation, synchronous with their orbital revolution. As a consequence rotational instabilities are expected to rapidly mix processed material from the core to the stellar surface. Since these short-period binaries often show eclipses, their parameters can be determined with high accuracy. If their surface abundances can be measured, such systems can be extremely useful as test-cases for the concept of rotational mixing, as discussed in Chapter 3.

1.2.2 Mass accretion and spin-up

In the case of a star in a binary system, one can define a region of space within which orbiting material is gravitationally bound to the star. Such a region is called the Roche lobe (see Fig. 1.6). During the evolution of the star, its radius can expand past its Roche lobe, resulting in material falling toward the companion star. Part of the material is accreted from the star, resulting in mass and angular momentum transfer. The specific angular momentum transferred in such a process depends on the binary parameters (mass of the two components and orbital separation). However, the total mass and angular momentum accreted depend on how the star reacts to the in-falling material.
The amount of specific angular momentum in the in-falling material is, in general, huge, and the outer layers of the accreting star are easily spun up to critical rotation, i.e. the rotational velocity for which the centrifugal acceleration equalizes the gravity. When this occurs, no more material can be added to the stellar surface until angular momentum is transferred to deeper layers of the star, for example by magnetic fields or rotational instabilities. Since these processes are included in the code used in this thesis, it is possible to assess the final budget of accreted mass and angular momentum in the case of a mass transfer event. This capability has been exploited in Chapter 4, where it is shown that in a close, massive binary system, it is possible to spin-up one component to critical rotation. The amount of angular momentum transferred is enough for rotational instabilities to mix the star and induce quasi-chemically homogeneous evolution. The accretor becomes a fast rotating Wolf-Rayet star and at the end of its life can form a long GRB.

1.3 This thesis

In Chapter 2 we present the first extensive study of convection in the outer envelope of hot massive stars. The investigation regards sub-surface convection zones which are caused by opacity peaks associated with iron ionization. We determine the occurrence and properties of these convection zones as function of the stellar parameters. We then confront our results with observations of OB stars. This work strongly suggests the

existence of a physical connection between sub-photospheric convective motions and small scale stochastic velocities in the photosphere of O- and B-type stars. Moreover clumping in the inner parts of the winds of OB stars could be caused by the same mechanism, and magnetic fields produced in the sub-surface convective regions could appear at the surface of OB stars as diagnosed by discrete absorption components in ultraviolet absorption lines.

In Chapter 3 the consequences of rotational mixing for massive main sequence stars in short-period binaries is investigated. In these systems the tides are thought to spin up the stars to rapid rotation, synchronous with their orbital revolution. Such systems can be used to test the concept of rotational mixing. As these short-period binaries often show eclipses, their parameters can be determined with high accuracy. These close binary stars can also provide an alternative channel for the formation of tight Wolf-Rayet binaries with a main sequence companion and might explain massive black hole binaries such as the intriguing system M33 X-7.

Chapter 4 reports the study of a new binary channel for the production of rapidly rotating Wolf-Rayet stars. In massive close binaries this is achieved through mass accretion and consecutive quasi-chemically homogeneous evolution. At low enough metallicity this provides a viable channel for the production of long gamma-ray bursts. This scenario suggests that a possibly large fraction of long GRBs occurs in runaway stars. More generally, this provides a means for massive stars to obtain high rotation rates, which could naturally explain the existence of fast rotators.

Chapter 5 Pair creation supernovae (PCSN) are thought to be produced from very massive low metallicity stars. The spectacularly bright SN 2006gy does show several signatures expected from PCSN. In this chapter we investigate the metallicity threshold below which PCSN can form and estimate their occurrence rate. We find that hydrogen-rich PCSN could occur at metallicities as high as $Z_{\odot}/3$, which — assuming standard IMFs (Initial Mass Function) are still valid to estimate their birth rates — results in a rate of about one PCSN per 1000 supernovae in the local universe, and one PCSN per 100 supernovae at a redshift of $z = 5$.

In Chapter 6 we investigate the role of thermohaline mixing during the evolution of low-mass stars. We compare thermohaline mixing with other mixing processes acting in these stars, and discuss its possible role in changing surface abundances. We show for the first time that thermohaline mixing can be present also during core helium burning and beyond, and has the potential to change the surface abundances also during the AGB phase.

1.4 Outlook

Stars are the physicist's playground. There are few objects in nature for which an understanding requires such a variety of physical theories involved than stars. Classical mechanics, ther-

modynamics, electrodynamics, nuclear physics, quantum mechanics and general relativity are the necessary ingredients to investigate their birth, life and death.

We are living in a very exciting time for stellar astrophysics. Thanks to the amazing progresses in the observations, it is possible to measure with unprecedented precision the properties of stars, even for objects very far away. An example are the measurements of rotational velocities and surface abundances obtained by the VLT-FLAMES survey of massive stars, allowing to study, for the first time, a significant sample of fast rotators in the magellanic clouds. Magnetic fields in massive stars have been detected only recently (e.g., Henrichs et al. 2000; Hubrig et al. 2008), and some observations suggest that surface abundance anomalies in massive stars could be related to the presence of magnetic fields (Morel et al. 2006, 2008; Hunter et al. 2008a). Statistical studies show that a large fraction of stars is in binary systems (e.g., Sana et al. 2008), stressing the central role of binarity in stellar physics.

From the theoretical point of view, all these new, exciting observations represent a stimulating challenge. Many physical processes once considered "of secondary importance", now turned out to be vital. This is underlined by the fact that the last ten years have seen a steep increase of papers devoted to study the role of rotation, magnetic fields and binarity. This thesis shows how the detailed inclusion of processes like sub-surface convection, rotation, magnetic fields, binarity and thermohaline mixing in stellar evolution calculations has profound consequences for stellar evolution and nucleosynthesis.

However, a lot of work still need to be done. The devil is in the details, and it appears more and more likely that these details are of primary importance to understand extraordinary phenomena like SNe and GRBs.

CHAPTER 2

Sub-surface convection zones in hot massive stars and their observable consequences

M. Cantiello, N. Langer, I. Brott, A. de Koter, S. N. Shore, J. S. Vink,
A. Voegler, D. J. Lennon and S.-C. Yoon

Astronomy & Astrophysics, 2009, **499**, 279-290

Abstract We study the convection zones in the outer envelope of hot massive stars which are caused by opacity peaks associated with iron and helium ionization. We determine the occurrence and properties of these convection zones as function of the stellar parameters. We then confront our results with observations of OB stars. A stellar evolution code is used to compute a grid of massive star models at different metallicities. In these models, the mixing length theory is used to characterize the envelope convection zones. We find the iron convection zone (FeCZ) to be more prominent for lower surface gravity, higher luminosity and higher initial metallicity. It is absent for luminosities below about $10^{3.2}\,L_\odot$, $10^{3.9}\,L_\odot$, and $10^{4.2}\,L_\odot$ for the Galaxy, LMC and SMC, respectively. We map the strength of the FeCZ on the Hertzsprung-Russell diagram for three metallicities, and compare this with the occurrence of observational phenomena in O stars: microturbulence, non-radial pulsations, wind clumping, and line profile variability. The confirmation of all three trends for the FeCZ as function of stellar parameters by empirical microturbulent velocities argues for a physical connection between sub-photospheric convective motions and small scale stochastic velocities in the photosphere of O- and B-type stars. We further suggest that clumping in the inner parts of the winds of OB stars could be caused by the same mechanism, and that magnetic fields produced in the FeCZ could appear at the surface of OB stars as diagnosed by discrete absorption components in ultraviolet absorption lines.

2.1 Introduction

Massive stars, in a general sense, have convective cores and radiative envelopes (Kippenhahn & Weigert 1990). The introduction of the so called “iron peak" in stellar opacities (Iglesias et al. 1992) led, however, to the prediction of a small convection zone in the envelope of sufficiently luminous massive main sequence models (Stothers & Chin 1993). It is often accompanied by an even smaller convection zone which originates from an opacity peak associated with partial helium ionization. These two convection zones comprise almost negligible amount of mass. The reality of the iron opacity bump, as predicted by various groups (e.g., Iglesias et al. 1992; Badnell et al. 2005), is unambiguous. It is most obvious in the field of stellar pulsations. Only the inclusion of this feature allows an agreement of observed and predicted instability regimes in the HR diagram, from the white dwarf regime (e.g. Saio 1993; Charpinet et al. 1997), for main sequence stars (e.g., β Cephei stars; see Deng & Xiong 2001, and references therein), and up to hot supergiants (Saio et al. 2006).

While the envelope convection zones may, at first glance, be negligible for the internal evolution of hot massive stars, they may cause observable phenomena at the stellar surface. The reason is that the zones are located very close to the photosphere for some mass interval (see below). Here, we will discuss which observed features in hot stars might be produced by these near surface convection zones. In particular, we examine whether a link exists between these convective regions and observable small scale velocity fields at the stellar surface and in the stellar wind, “microturbulence". A similar idea has been used to explain microturbulence in low mass stars (Edmunds 1978), in which deeper envelope convection zones reach the photosphere. While Edmunds (1978) concludes that the same mechanism *cannot* explain microturbulent velocities in O and B stars, the iron-peak induced sub-photospheric convection zones in these stars had not yet been discovered. We demonstrate in this paper that these convection zones may not only cause motions which are observable, but possibly even directly affect the evolution: First, we discuss how photospheric velocity fields may affect the structure of massive star winds by inducing clumping at the base of the wind and thereby affecting the stellar mass-loss. And second, we argue that the near surface convection zones may generate magnetic fields which – if they migrate to the surface – further affect the stellar wind mass-loss and, more significantly, the associated stellar angular momentum loss.

We construct grids of massive main sequence star models, for various metallicities, that allow us to predict the occurrence and properties of sub-surface convection zones as function of the stellar parameters (Sect. 2.3). We then compare the model predictions with observed stellar properties, e.g., empirically derived microturbulent velocities and observations of wind clumping in hot massive stars (Sect. 2.4).

2.2 Method

Our stellar models are calculated with a hydrodynamic stellar evolution code. This code can calculate the effect of rotation on the stellar structure, rotationally induced chemical mixing, and the transport of angular momentum by magnetic torques (see Petrovic et al. 2005b; Yoon et al. 2006, and references therein). Compositional mixing is treated as a diffusive process.

The rate of change of a nuclear species of mass fraction X_i is calculated as

$$\left(\frac{\partial X_i}{\partial t}\right) = \left(\frac{\partial}{\partial m}\right)\left[(4\pi r^2\rho)^2\, D\left(\frac{\partial X_i}{\partial m}\right)\right] + \left(\frac{\mathrm{d}X_i}{\mathrm{d}t}\right)_{\mathrm{nuc}}, \tag{2.1}$$

where D is the diffusion coefficient constructed from the sum of individual diffusion coefficients for the range of mixing processes (see Heger et al. 2000, and references therein). The second term on the right hand side is the schematic symbol to stand for all nuclear reactions. The contributions to the diffusion coefficient are convection, semiconvection and thermohaline mixing. For rotating models also the contributions from rotationally induced mixing and magnetic diffusion are computed. The transport of angular momentum is also treated as a diffusive process (Endal & Sofia 1978; Pinsonneault et al. 1989; Heger et al. 2000).

The Ledoux criterion is used to determine which regions of the star are unstable to convection:

$$\nabla_{\mathrm{ad}} - \nabla + \frac{\varphi}{\delta}\,\nabla_\mu \leq 0 \tag{2.2}$$

(e.g., Kippenhahn & Weigert 1990) where ∇_{ad} is the adiabatic temperature gradient and ∇_μ is the gradient in the mean molecular weight. The diffusion coefficient, D, in convective regions is approximated with

$$D = \frac{1}{3}\alpha H_P v_c \tag{2.3}$$

where H_P is the pressure scale height, v_c is the convective velocity, and α the mixing length parameter. We fix $\alpha = 1.5$, which results from evolutionary tracks of the Sun (e.g. Abbett et al. 1997; Ludwig et al. 1999); a sensitivity study of the α dependence of our scenario will be presented in future work. The convective velocity, v_c, is calculated using the mixing length theory (Böhm-Vitense 1958) (MLT hereafter) and the convective contribution to the diffusion coefficient becomes:

$$D = \frac{1}{3}\,\alpha^{2/3} H_P \left[\frac{c}{\varkappa\rho}\, g\beta\,(1-\beta)\nabla_{\mathrm{ad}}(\nabla_{\mathrm{rad}} - \nabla_{\mathrm{ad}})\right]^{1/3}, \tag{2.4}$$

where $\varkappa$ is the opacity, ρ is the density, β is the ratio of gas pressure to total pressure, g is the local gravitational acceleration, and c is the speed of light. Here, ∇_{rad} and ∇_{ad} are the radiative and adiabatic gradients, respectively.

We use the solar composition proposed by Asplund et al. (2005). The opacities in our code are extracted from the OPAL tables (Iglesias & Rogers 1996). Fig. 2.1 shows the opacity coefficient as function of temperature in our 60 $\mathrm{M}_\odot$ models for various metallicities. The peaks at $\log T \simeq 4.7$ and $\log T \simeq 5.3$ are caused by helium and iron, respectively. The peak at $\log T \simeq 6.2 - 6.3$ is caused by carbon, oxygen and iron.

We use the metallicity dependent mass-loss predictions of Vink et al. (2001).

2.2.1 The helium convection zone

In the very weak helium convection zone, radiative diffusion is the dominant energy transport mechanism, which may have consequences for the development of convection. In fact, in viscous fluids the Ledoux-criterion is not strictly correct, since it ignores any dissipative

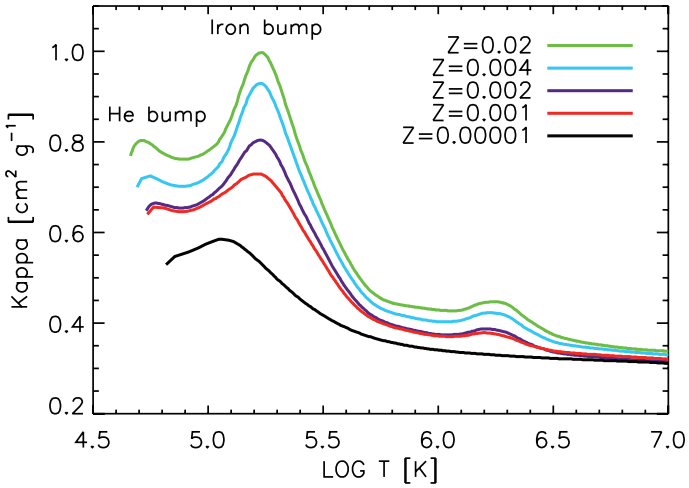

Figure 2.1: Opacity in the interior of 60 $M_\odot$ zero age main sequence stars of various metallicities (see legend) as a function of temperature, from the surface up to a temperature of 10^7 K. The different colors refer to different metallicities, as shown in the legend.

effect on the evolution of a perturbation. A more accurate criterion can be expressed in terms of the non-dimensional Rayleigh number, Ra which for compressible, stratified convection, is

$$\mathrm{Ra} \simeq \frac{(\nabla - \nabla_{\mathrm{ad}})L^3 g}{\kappa\nu}. \tag{2.5}$$

Here L is the thickness of the convective layer, and κ and ν are, respectively, the thermal diffusivity and the kinematic (molecular) viscosity (e.g, Shore 1992, p. 328).

For convection to develop, Ra must exceed some critical value, Ra_c. The estimate of Ra in the helium convective region depends on the choice of the viscosity coefficient. For the Spitzer formula (Spitzer 1962),$\mathrm{Ra} > \mathrm{Ra}_c$, and the region can be considered convective. In contrast, for the radiative viscosity (e.g, Kippenhahn & Weigert 1990, p. 445), $\mathrm{Ra} < \mathrm{Ra}_c$. There is an additional uncertainty in these estimates since the expressions for the radiative transport coefficients in our models are strictly correct only in the diffusion limit. Likewise, the value of the heat capacity c_P can vary by an order of magnitude depending on whether the radiative energy reservoir aT^4 is coupled to the internal energy of the gas or not. Since the helium convection zone occurs very close to the surface in our models, these additional uncertainties could be relevant.

Ideally, the properties of the helium convection zone could be studied through multi-dimensional hydrodynamic calculations. However, the large thermal diffusivity poses a onerous computational challenge since it makes the problem numerically stiff: the diffusive timescale is much shorter than the dynamical one, which leads to very short time steps if an explicit solver is used (unfortunately, most codes used for compressible convection are explicit). Any simulation would have only limited value unless it includes a sufficiently realistic

treatment of the coupling between plasma and radiation.

In the presence of strong wind mass-loss, another consideration related to the He convective zone becomes important, due to the fact that it comprises only a tiny amount of mass. Convection can set in only if the turnover time $\tau_{\rm turn} \simeq H_P/v_c$ is shorter than the time scale for which convection is predicted to prevail at a fixed Lagrangian mass shell inside the convection zone, $\tau_{\rm conv}$, which is $\tau_{\rm conv} \simeq \Delta M_{\rm conv}/\dot{M}$. We find a critical mass-loss rate $\dot{M} \sim 10^{-6}\,{\rm M}_\odot{\rm yr}^{-1}$, above which convection has no time to develop in the helium region, since the wind is removing an amount of mass equivalent to the mass of the convection zone before a convective eddy can turn over (see Tab. 2.1). For a metallicity Z=0.02, stars above 40 $\rm M_\odot$ cannot develop the He convection zone, and in a 20 $\rm M_\odot$ such a layer is convective only for 10 - 100 turnovers before convection moves to a lower mass coordinate. None of these concerns is significant for the iron convection zone (FeCZ hereafter), where convection is always fully developed. Moreover the convective velocities for the FeCZ are always found to be much higher than those in the helium convection zones. We disregard the occurrence of the helium convection zones unless it is explicitly mentioned.

2.3 Results

We calculated a grid of non-rotating stellar evolution sequences for initial masses between $5\,{\rm M}_\odot$ and $100\,{\rm M}_\odot$, at metallicities of Z=0.02, Z=0.008 and Z=0.004, roughly corresponding to the Galaxy, the LMC and the SMC, respectively. Additionally, we computed several models at lower metallicity. Since rapid rotation can change the properties of sub-surface convection (Maeder et al. 2008), we calculated a few rotating models to evaluate the effects of rotation on our results. These effects are discussed in Section 2.3.1.

Figures 2.2 and 2.3 show the evolution of the radial extent and location of the sub-surface convection zones in $20\,{\rm M}_\odot$ and $60\,{\rm M}_\odot$ models during the main sequence phase.

As outlined above, the He opacity bump at around $\log T \simeq 4.7$ is responsible for a convective zone which occurs close to the stellar surface and is very inefficient: only a very small fraction of the heat flux is transported by bulk motions in this region. The upper boundary is typically found at an optical depth in the range $2 \leq \tau \leq 10$, where τ is the Rosseland mean optical depth. Below this convective zone, the Fe opacity bump at around $\log T \simeq 5.3$ is associated with a more efficient and extended convective region.

The radial extent of the FeCZ is quite substantial, i.e. a significant fraction of one solar radius, which corresponds typically to 2 - 10 pressure scale heights, comprising a mass on the order of $10^{-6}\,{\rm M}_\odot$ to $10^{-5}\,{\rm M}_\odot$, while the amount of mass between the top of the FeCZ and the stellar surface is around several times $10^{-7}\,{\rm M}_\odot$ (cf. Table 1). In the $20\,{\rm M}_\odot$ model the upper border of the FeCZ is located at $\tau \approx 140$ on the ZAMS, and at $\tau \approx 370$ on the cool side of the main sequence band. In the $60\,{\rm M}_\odot$ model the upper border at ZAMS is located at $\tau \approx 15$, reaching $\tau \approx 260$ during the late main sequence evolution. Convective velocities predicted by the MLT are on the order of 10s of $\rm km\,s^{-1}$, where more extended zones achieve higher velocities. For a quantitative analysis, we define an average convective velocity

$$\langle v_c \rangle := \frac{1}{\alpha H_P} \int_{{\rm R_c}-\alpha H_P}^{\rm R_c} v_c(r)\, dr \qquad (2.6)$$

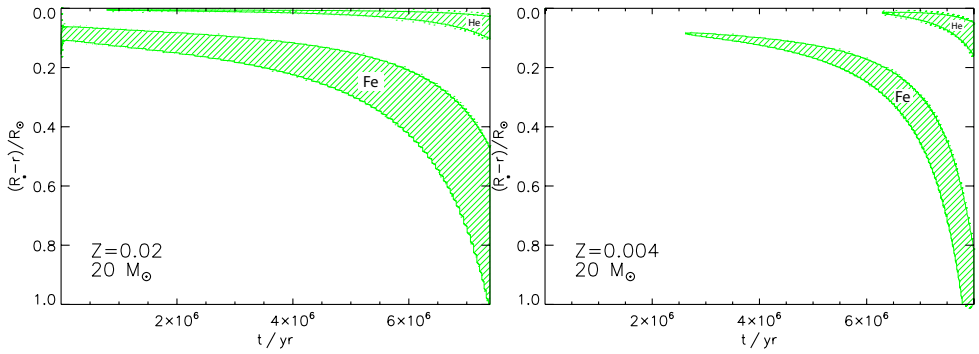

Figure 2.2: Evolution of the radial extent of the helium and iron convective regions (hatched) as function of time, from the zero age main sequence to roughly the end of core hydrogen burning, for a 20 $M_\odot$ star. The top of the plot represents the stellar surface. Only the upper 1 $R_\odot$ of the star is shown in the plot, while the stellar radius itself increases during the evolution. Left panel: The star has a metallicity of Z=0.02, and its effective temperature decreases from 35 000 K to 25 000 K during the main sequence phase. Right panel: The star has a metallicity of Z=0.004, and its effective temperature decreases from 37 000 K to 27 000 K during the main sequence phase. The extent of the convection zones is smaller than in the case shown above, and the iron zone is absent for the first 2.5 million years.

Table 2.1: Properties of the envelope convection zones in our 20 and 60 $M_\odot$ models of solar metallicity. These are the same models shown in the top panel of Fig. 2.2 and in Fig. 2.3. The values in the table refer to t=6.41×10^6 for the 20 $M_\odot$ model and t=2.37×10^6 for the 60 $M_\odot$ model.

M	Zone	H_P	$\langle v_c \rangle$	$\Delta M_{\rm conv}$ [a]	$\Delta M_{\rm top}$ [b]	$N_{\rm cells}$ [c]	$\tau_{\rm turn}$ [d]	$\tau_{\rm conv}$ [e]	$\dot{M}$
$M_\odot$		$R_\odot$	km s^{-1}	$M_\odot$	$M_\odot$		days	days	$M_\odot$yr^{-1}
20	He	0.025	0.08	7.6×10^{-9}	1.9×10^{-9}	1.8×10^{5}	2.5	38	7.3×10^{-8}
20	Fe	0.08	2.40	3.6×10^{-6}	5.8×10^{-7}	1.8×10^{4}	0.25	18250	7.3×10^{-8}
60	Fe	0.24	2.25	1.6×10^{-5}	9.8×10^{-7}	8.5×10^{3}	0.83	1570	3.7×10^{-6}

[a] Mass contained in the convective region.
[b] Mass in the radiative layer between the stellar surface and the upper boundary of the convective zone.
[c] Expected number of convective cells, $N_{\rm cells} := (R_\star/H_{\rm P})^2$.
[d] Convective turnover time, $\tau_{\rm turn} := H_{\rm P}/\langle v_c \rangle$.
[e] Time that a piece of stellar material spends inside a convective region, $\tau_{\rm conv} := \Delta M_{\rm conv}/\dot{M}$.

where R_c is the upper boundary of the convective zone, and where we set $\alpha = 1.5$.

From Figures 2.2 and 2.3, three trends for the extent of the sub-surface convection zones are noticeable. First, with increasing time during the main sequence evolution, these zones become more extended, and are located deeper inside the stellar envelope. This is because the stellar envelope expands, and becomes cooler, while the temperature of the opacity peak remains nearly constant. In our 20 $M_\odot$ model at Z=0.02, the mass of the He convective zone increases from about 10^{-9} $M_\odot$ to 2×10^{-7} $M_\odot$, and that of the FeCZ is growing from 2×10^{-6} $M_\odot$ to 10^{-4} $M_\odot$. For sufficiently hot models, the helium convection zones can even vanish (Fig. 2.2, lower panel). Second, comparing the 20 $M_\odot$ and the 60 $M_\odot$ model at Z=0.02

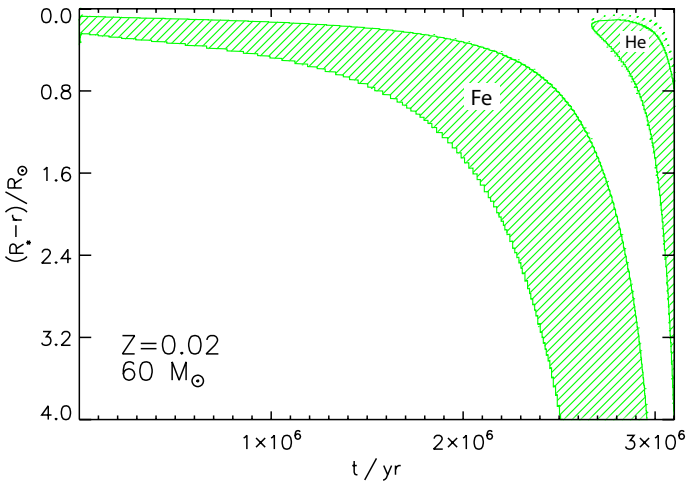

Figure 2.3: Same as Fig. 2.2, but for a 60 $M_\odot$ star at Z=0.02. Note the different vertical scale, spanning the upper 4 $R_\odot$ of the star. The effective temperature decreases from 48 000 K to 18 000 K during the main sequence phase.

demonstrates that the FeCZ becomes more prominent for higher luminosity. This is because the opacity is not substantially changing among main sequence models at the same metallicity, such that a higher luminosity renders a larger portion of the envelope convectively unstable (both in radius and mass fraction). Our models show that the FeCZ disappears below a threshold luminosity of about $10^4\,L_\odot$ on the ZAMS at solar metallicity. Third, comparing the two 20 $M_\odot$ models in Fig. 2.2 shows that the extent of the FeCZ, and its presence, depends on the metallicity. We find that for Z=0.001, it is completely absent below 40 $M_\odot$, and at Z=0.00001 it does not occur for $M \leq 60\,M_\odot$. In summary, our models predict an increase of the importance of the FeCZ for cooler surface temperature or lower surface gravity, for higher luminosity, and for higher metallicity.

While in the discussed range of luminosity and effective temperature, the average convective velocity $\langle v_c \rangle$ is on the order of 1 to 10 $\mathrm{km\,s^{-1}}$ for the FeCZ, we found that the average convective velocity $\langle v_c \rangle$ in the He convective zone is always very low ($\lesssim 1\,\mathrm{km\,s^{-1}}$). Convection due to hydrogen recombination is absent; this dominates at lower effective temperatures than the ones studied here.

For our grid of stellar evolution models, we map the average convective velocity of the FeCZ (Eq. 2.6) in the HR diagram for the three different metallicities (see Fig. 2.8, and Sect. 2.4.1). This figure displays the three qualitative trends of the iron zone we have just described.

- For given luminosity and metallicity, the average convective velocity near the upper boundary of the FeCZs increases with decreasing surface temperature. The convection zones are located deeper inside the star (in radius, not in mass), and the resulting larger pressure scale height leads to higher velocities. At solar metallicity and $10^5\,L_\odot$ (i.e.

roughly at 20 $M_\odot$) the velocities increase from just a few km s^{-1} at the ZAMS to more than 10 km s^{-1} in the supergiant regime, where $\langle v_c \rangle = 2.5$ km s^{-1} is achieved at $T_{\rm eff} \simeq 30\,000$ K. At the lowest considered metallicity, the FeCZ is absent at the ZAMS at 10^5 $L_\odot$, and a level of $\langle v_c \rangle = 2.5$ km s^{-1} is only reached at $T_{\rm eff} \simeq 20\,000$ K.

- For fixed effective temperature and metallicity, the iron zone convective velocity increases with increasing luminosity, since a larger flux demanded to be convectively transported requires faster convective motions. Figure 2.8 in Sect. 2.4.1 also shows that there are threshold luminosities below which FeCZs do not occur, i.e., below about $10^{3.2}$ $L_\odot$, $10^{3.9}$ $L_\odot$, and $10^{4.2}$ $L_\odot$ for the Galaxy, LMC and SMC, respectively.

- The FeCZs become weaker for lower metallicities, since due to the lower opacity, more of the flux can be transported by radiation. The threshold luminosity for the occurrence of the FeCZ quoted above for Z=0.02 is ten times lower than that for Z=0.004. And above the threshold, for a given point in the HR diagram, the convective velocities are always higher for higher metallicity.

2.3.1 Rotating models

We considered two 20 $M_\odot$ models with metallicity Z=0.02, one rotating at birth with an equatorial velocity of 250 km s^{-1} (corresponding to about 35% of the critical velocity) and one with 350 km s^{-1} (about 50% of the critical velocity). The evolution of the radial extent of sub-surface convection in the rotating models is very similar to the non-rotating case shown in Fig. 2.2. Also the convective velocities inside the FeCZ change only a few percent between rotating and non-rotating models, even if the rotating models show slightly higher convective velocity peaks (see Fig. 2.4). We conclude that rotation is not significantly affecting the structure and the properties of sub-surface convection in the vast majority of OB stars.

As pointed out by Maeder et al. (2008), the effects of rotation on sub-surface convection become substantial for stars rotating close to critical velocity. While stars rotating with such high velocities exist (e.g. Be stars), their number is modest. The study of sub-surface convection in these very fast rotators is interesting, but may require 2-dimensional stellar models, which is beyond the scope of this paper.

2.4 Comparison with observations

In the following, we investigate the idea that these sub-surface convection zones might be related to observable phenomena at the stellar surface. In particular, we investigate potential connections with microturbulence in massive stars, and discuss whether small scale or large scale clumping in massive star winds, magnetic fields, and non-radial pulsations could be related to sub-surface convection. For each point, we first briefly discuss the theoretical motivation, and then the corresponding observational evidence.

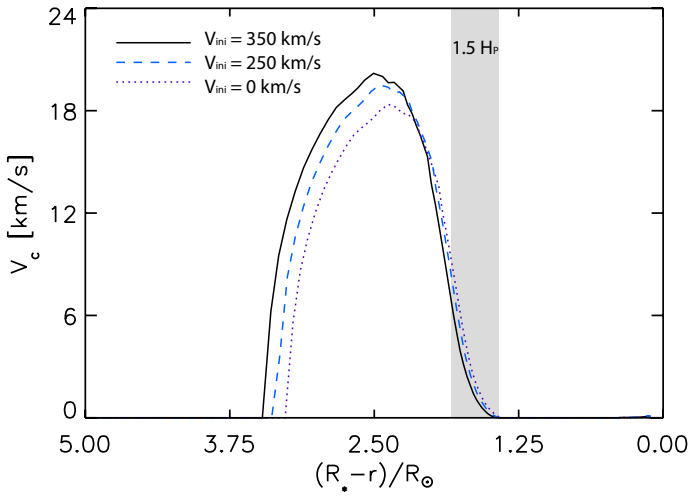

Figure 2.4: Convective velocity in the FeCZ as function of radial distance from the stellar surface. The dotted line corresponds to a non-rotating 20 $M_\odot$ model at Z=0.02, while the dashed and solid lines refer to the same model rotating at birth with 250 km s^{-1} and 350 km s^{-1} respectively. The values correspond to models having the same effective temperature (log $T_{\rm eff}$ = 4.339) and very similar luminosity (log $L/L_\odot$ = 5.04 for the non-rotating model and log $L/L_\odot$ = 5.03 for the rotating ones). The gray band shows the upper 1.5 pressure scale heights of the FeCZ, which is the region considered for the computation of $\langle v_c \rangle$, cf. Eq. 2.6. Convective velocities in the He convection zone are much lower than 1 km s^{-1} and are not visible in this plot.

2.4.1 Microturbulence

Theoretical considerations

The convective cells in the upper part of a convection zone excite acoustic and gravity waves that propagate outward. The generation of sound waves by turbulent motions was first discussed by Lighthill (1952) and extended to a stratified atmosphere by Stein (1967) and Goldreich & Kumar (1990). In a stratified medium, gravity acts as a restoring force and allows the excitation of gravity waves. For both acoustic and gravity waves, the most important parameter determining the emitted kinetic energy flux is the velocity of the convective motions. This is why, in the following, we use the average convective velocity $\langle v_c \rangle$ as the crucial parameter determining the efficiency of sub-surface convection.

Goldreich & Kumar (1990) showed that convection excites acoustic and gravity waves, resulting in maximum emission for those waves with horizontal wave vector $k_h \sim 1/H_{P,c}$ and angular frequency $\omega \sim v_c/H_{P,c}$, where now v_c and $H_{P,c}$ are evaluated at the top of the convective region. They calculated that the amount of convective kinetic energy flux going into acoustic and gravity waves is

$$F_{ac} \sim F_c M_c^{15/2}, \tag{2.7}$$

and

$$F_{\rm g} \sim F_c M_c, \tag{2.8}$$

respectively, where we take $F_c \sim \rho_c \langle v_c \rangle^3$ and M_c is the Mach number in the upper part of the convective region. Since convection in our models is subsonic, gravity waves are expected to extract more energy from the convective region than acoustic waves. These gravity waves can then propagate outward, reach the surface and induce observable density and velocity fluctuations (Fig. 2.5).

The Brunt-Vaisäla frequency in the radiative layer above the FeCZ is about mHz. Molecular viscosity can only damp the highest frequencies, while wavelengths that will be resonant with the scale length of the line forming region should not be affected (see e.g. Lighthill 1967). This is the case for the gravity waves stochastically excited by convective motions: they can easily propagate through the sub-surface radiative layer, steepening and becoming dissipative only in the region of line formation.

Again, multi-dimensional hydrodynamic simulations would be the best way to compute the energy loss of these waves during their propagation through the radiatively stable envelope above the FeCZ, but this is beyond what we can presently do. We can, however, obtain an upper limit to the expected velocity amplitudes at the stellar surface, where we only consider the energy transport through gravity waves. The kinetic energy per unit volume associated with the surface velocity fluctuations $E_{\rm s}$ must be comparable to or lower than the kinetic energy density associated with the waves near the sub-surface convection zone, $E_{\rm g} \sim M_c \rho_c \langle v_c \rangle^2$, or

$$\frac{E_{\rm g}}{E_{\rm s}} \sim M_c \left(\frac{\rho_c}{\rho_s}\right)\left(\frac{\langle v_c \rangle}{v_{\rm s}}\right)^2 \geq 1, \tag{2.9}$$

where ρ_c is the density at the top of the convective region and ρ_s is the surface density, and $v_{\rm s}$ is the surface velocity amplitude. In this ratio we only consider energy density since the volume of the line forming region is comparable to the volume of the upper part of the convective zone. Therefore, we expect

$$v_{\rm s} \leq \langle v_c \rangle \sqrt{M_c \frac{\rho_c}{\rho_s}} \tag{2.10}$$

In our models with well developed FeCZs, $\sqrt{M_c \rho_c / \rho_s} \simeq 1$ (order of magnitude), and thus $v_{\rm s}$ and $\langle v_c \rangle$ should be on the same order of magnitude. It is difficult to estimate the typical correlation length of the induced velocity field at the stellar surface, but a plausible assumption is that it is about one photospheric pressure scale height, $\mathrm{H_{P,s}}$, given the proximity of the FeCZ to the surface and the fact that the horizontal wave vector of the emitted waves is $k_h \sim 1/\mathrm{H_{P,c}}$.

Observations

The microturbulent velocity ξ is defined as the microscale nonthermal component of the gas velocity in the region of spectral line formation:

$$\Delta\lambda_D = \frac{\lambda}{c}\sqrt{\frac{2\mathcal{R}T}{\mu} + \xi^2} \tag{2.11}$$

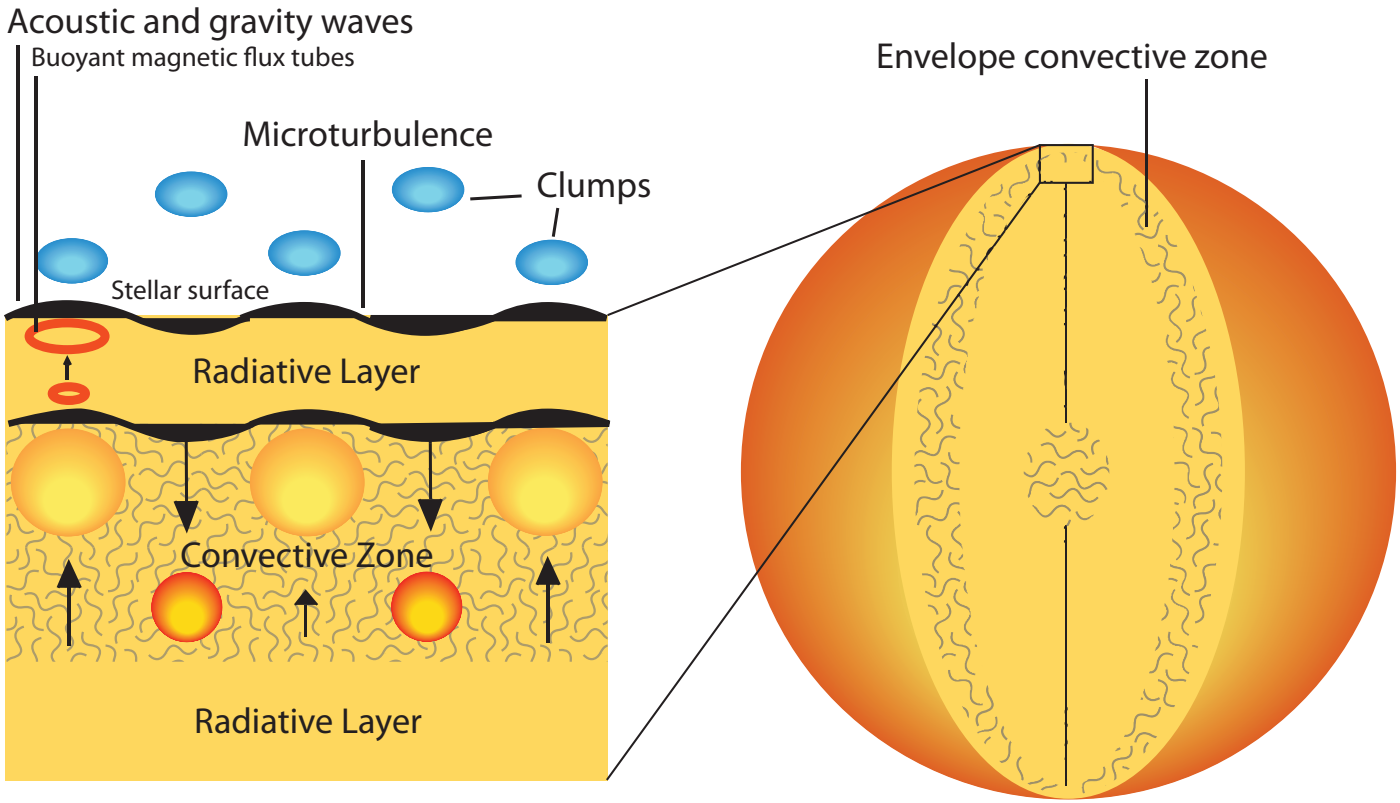

Figure 2.5: Schematic representation of the physical processes connected to sub-surface convection. Acoustic and gravity waves emitted in the convective zone travel through the radiative layer and reach the surface, inducing density and velocity fluctuations. In this picture microturbulence and clumping at the base of the wind are a consequence of the presence of sub-surface convection. Buoyant magnetic flux tubes produced in the convection zone could rise to the stellar surface.

Assuming that the gas in this zone has a temperature only slightly different from the effective temperature, one finds empirically that the observed Doppler widths $\Delta\lambda_D$ cannot be accounted for by the thermal motions alone (e.g. Cowley 1970). Regardless of which physical mechanism causes microturbulence, the process of spectral line fitting yields values of ξ in hot massive stars between 0 and about $20\,\mathrm{km\,s^{-1}}$. In contrast, macroturbulence corresponds to velocity fluctuations which are coherent on a length scale larger than the radial extent of line forming regions. If indeed the length scale of the photospheric velocity fluctuations induced by the iron convection zone are on the order of the photospheric pressure scale height, then this length scale is also comparable to the radial extent of line forming regions, and it is difficult to decide whether the velocity fluctuations would be manifested as micro- or as macroturbulence, or both. Below, we compare our model predictions only to the case of microturbulence since this is the empirical parameter most extensively available in the literature.

Photospheric microturbulence is routinely required, e.g., to derive consistent surface abundances for one element from different photospheric absorption lines through stellar model atmospheres (among many others Rolleston et al. 1996; Hibbins et al. 1998; Vrancken et al. 2000). Unfortunately, differences in physical assumptions or atomic physics can require somewhat different microturbulent velocities for the same star in different studies. Here, we restrict our detailed comparison to the data of Trundle et al. (2007) and Hunter et al. (2008b) from the ESO VLT-FLAMES Survey of Massive Stars (Evans et al. 2005), since it comprises the largest available uniformly analyzed data set. In Fig.2.6, we plot the microturbulent velocities derived for the LMC early B type stars analyzed by Hunter et al. (2008b) versus their projected rotational velocity. The error bar on the derived microturbulent velocities is usually quite big, $\pm 5\,\mathrm{km\,s^{-1}}$, and is often comparable to the measured quantity itself. There seems to be no positive correlation between ξ and the apparent projected rotational velocity $v \sin i$. Though $v \sin i$ is plotted and not v itself, the lack of a correlation in such a large data set (justifying the assumption of random orientation of the sample) argues against rotation as an important effect in triggering microturbulence in hot stars. To compare microturbulent velocities to properties of sub-photospheric convection we use only data obtained for slow rotators (i.e. $v \sin i < 80\,\mathrm{km\,s^{-1}}$) as microturbulent velocities are more difficult to measure for faster rotators.

In Fig.2.6, we show the microturbulent velocities for the LMC stars of Hunter et al. (2008b) versus the stellar surface gravity. Trends of the microturbulent velocity with $\log g$ have been previously reported for hot stars (e.g Gies & Lambert 1992; Hunter et al. 2007). The figure shows that indeed, for $\log g < 3.2$, there is a clear trend. However, the luminosity coding in Fig.2.6 suggests that this trend may be largely produced by the increase in convective velocity with increasing luminosity (Sect. 2.3). This figure displays a detection threshold of about $10\,\mathrm{km\,s^{-1}}$ for the microturbulent velocities so in the following we restrict the comparison to $\xi \geq 10\,\mathrm{km\,s^{-1}}$.

In order to compare these observations to our model predictions, we evaluated the ratio of the kinetic energy in the form of gravity waves at the surface of the FeCZ to the kinetic energy of the surface velocity field, $E_\mathrm{g}/E_\mathrm{s}$ (Eq. 2.9), assuming $v_\mathrm{s} = 10\,\mathrm{km\,s^{-1}}$, in the HR diagram. Fig. 2.7 shows two different iso-contours of this ratio; the stars of the LMC sample shown in Fig. 2.6 are over plotted. Notably, all but one of the LMC stars of Fig. 2.7 with

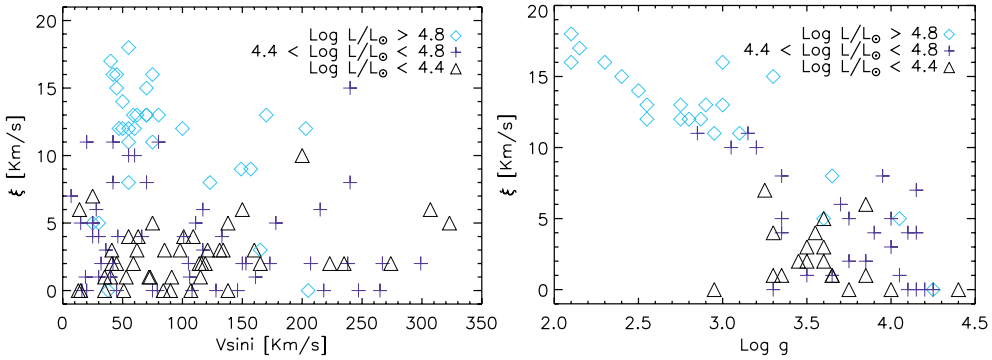

Figure 2.6: The left panel shows projected rotational velocity $v \sin i$ versus photospheric microturbulent velocity ξ for the early B-type stars in the LMC analyzed by Hunter et al. (2008b). Different symbols refer to different luminosity intervals, as explained in the legend. The microturbulent velocities ξ have typical uncertainties of about $\pm 5\,\mathrm{km\,s^{-1}}$. An uncertainty of 10% or $\pm 10\,\mathrm{km\,s^{-1}}$, whichever is the larger, should be considered for the rotational velocity measurements. Right: Logarithm of surface gravity versus microturbulent velocity ξ for the LMC early B-type stars studied by Hunter et al. (2008b); only stars with $v \sin i < 80\,\mathrm{km\,s^{-1}}$ are considered here. For the surface gravity measurements an uncertainty of ±0.1 should be considered

$\xi > 10\,\mathrm{km\,s^{-1}}$ are found in that part of the HR diagram where it is energetically possible that the FeCZ-induced gravity waves trigger a significant surface velocity field ($v_\mathrm{s} > 10\,\mathrm{km\,s^{-1}}$). Thus, a physical connection of the FeCZ with the observed microturbulent velocities appears energetically possible. Moreover, that the iso-contour line of $E_\mathrm{g}/E_\mathrm{s} = 1$ in Fig. 2.7 almost perfectly divides the observed sample in stars with significant ($\xi > 10\,\mathrm{km\,s^{-1}}$) and insignificant ($\xi < 10\,\mathrm{km\,s^{-1}}$) microturbulence is a further indication of such a physical connection.

Figure 2.8 shows the iso-contours in the HR diagram of the average convective velocity from our models in the upper layers of the iron convective zone, $\langle v_c \rangle$ (cf., Sect. 2.4.1), at the three considered metallicities. We have over plotted the microturbulent velocities derived by Trundle et al. (2007) and Hunter et al. (2008b) as filled circles. Again, we distinguish between sample stars with significant ($\xi > 10\,\mathrm{km\,s^{-1}}$; Group A) and insignificant ($\xi < 10\,\mathrm{km\,s^{-1}}$; Group B) microturbulent velocities. Comparing the plot for the LMC in Fig. 2.8 with Fig. 2.7 identifies $\langle v_c \rangle \simeq 2.5\,\mathrm{km\,s^{-1}}$ as a critical convection velocity to be able to trigger microturbulence. Interestingly, the contour of $\langle v_c \rangle = 2.5\,\mathrm{km\,s^{-1}}$ in our stellar models forms an almost perfect dividing line between Groups A and B for all three considered metallicities.

In fact, Fig. 2.8 provides evidence for all three trends found in the average convection velocity as function of stellar parameters (cf., Sect. 2.3) to be present also in the empirical data on microturbulent velocities. The LMC data shows that in the luminosity range $4.5 < \log L/\mathrm{L}_\odot < 5.5$ microturbulence is found only for $T_\mathrm{eff} \lesssim 25\,000\,\mathrm{K}$. The data for all three metallicities clearly suggests a key role of the luminosity, as the stars with $\xi > 10\,\mathrm{km\,s^{-1}}$ are the most luminous ones in each sub sample. And finally, the stars with high microturbulent velocities are all comfortably above our theoretical contour line corresponding to $\langle v_c \rangle = 2.5\,\mathrm{km\,s^{-1}}$. As the latter trends toward the upper right corner of the HR diagram for

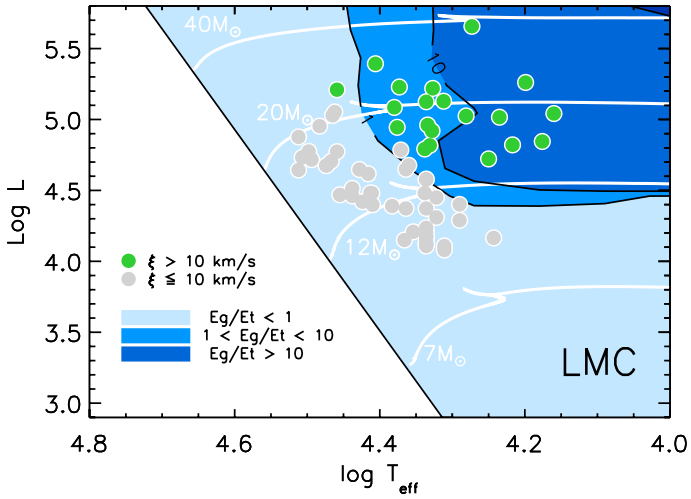

Figure 2.7: Values of the ratio E_g/E_s of the kinetic energy in the form of gravity waves above the iron convection zone, to the kinetic energy of the surface velocity field, as a function of the location in the HR diagram (see color scale). This plot is based on evolutionary models between $5\,M_\odot$ and $100\,M_\odot$ for LMC metallicity. We estimated the ratio E_g/E_s as in Eq. 2.9, using a value $v_s = 10\,\mathrm{km\,s^{-1}}$ for the surface velocity amplitude. Over-plotted as filled circles are stars which have photospheric microturbulent velocities ξ derived in a consistent way by Hunter et al. (2008b). Here, we use only data for stars with an apparent rotational velocity of $v \sin i < 80\,\mathrm{km\,s^{-1}}$. The uncertainty in the determination of ξ is typically $\pm 5\,\mathrm{km\,s^{-1}}$, which justifies our choice of $v_s = 10\,\mathrm{km\,s^{-1}}$. Solid white lines are reference evolutionary tracks. The full drawn black line corresponds to the zero age main sequence.

lower metallicity, the metallicity dependence is also confirmed by the empirical data.

Lyubimkov et al. (2004) studied microturbulence in a sample of 100 Galactic early B stars. Interestingly, they found significant microturbulent velocities (i.e., clearly above $5\,\mathrm{km\,s^{-1}}$) in the mass range 7...11 $M_\odot$ for stars with a relative age on the main sequence of $t/\tau_{\rm MS} > 0.8$, and in the range 12...19 $M_\odot$ for $t/\tau_{\rm MS} > 0.25$, but only insignificant microturbulent velocities for younger or less massive stars. Again, these results appear to agree with Fig. 2.8 up to a remarkable quantitative level.

In summary, our comparison provides evidence for a physical connection of microturbulence in hot star photospheres with the existence and strength of a sub-photospheric FeCZ.

If microturbulence has a physical origin and is not just a fudge factor, the pressure and energy terms associated with such a velocity field should be included in the calculations of atmospheric models of massive stars. Hubeny et al. (1991) have investigated part of these effects by accounting for a constant microturbulent velocity in the pressure term only. They find that for stars with conspicuous ξ values (of $25\,\mathrm{km\,s^{-1}}$) the inclusion of the pressure term leads to higher values of the surface gravity, which can reduce the mass discrepancy for O stars and O-type central stars of planetary nebula. A similar approach was also studied by Smith & Howarth (1998). The impact on gravity discussed by Hubeny et al. (1991) is

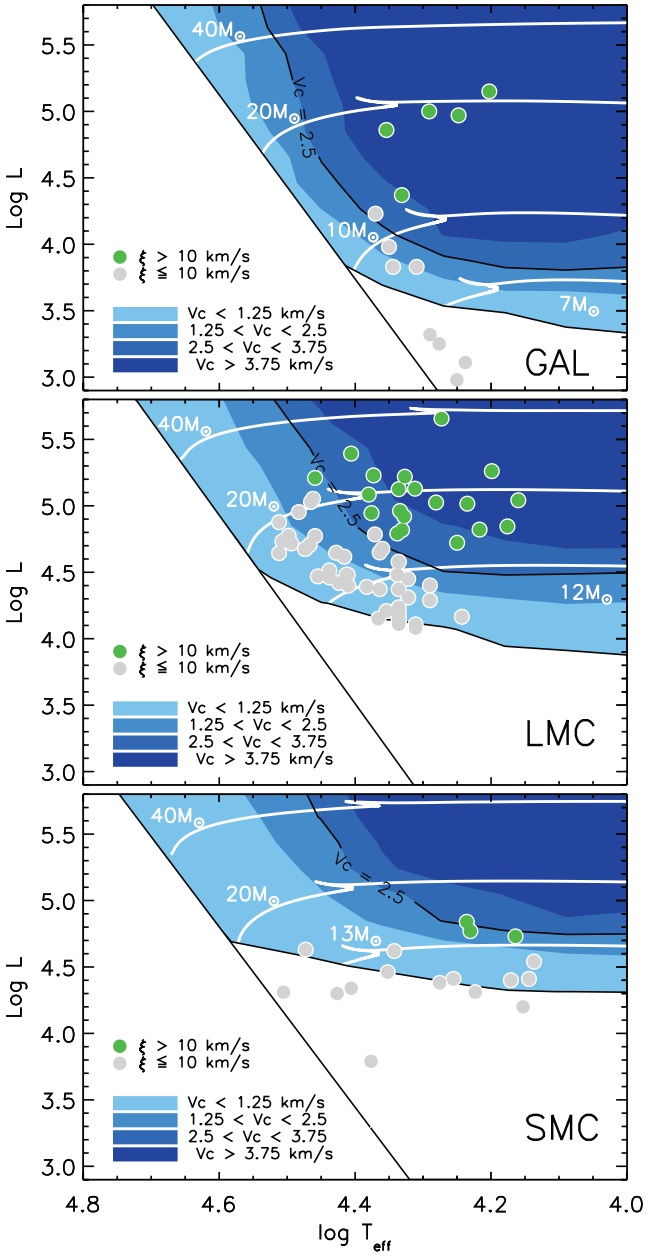

Figure 2.8: Average convective velocity within 1.5 pressure scale heights of the upper border of the iron convection zone in our models, as function of the location in the HR diagram (see color scale), based on evolutionary models between 5 $M_\odot$ and 100 $M_\odot$ (white lines), for three metallicities corresponding to the Galaxy (top panel), the LMC (middle), and the SMC (bottom). The full drawn black line corresponds to the zero age main sequence. Over-plotted as filled circles are photospheric microturbulent velocities ξ derived in a consistent way for hot massive stars by Trundle et al. (2007) and Hunter et al. (2008b). Here, we use only data for stars with an apparent rotational velocity of $v \sin i < 80\,\mathrm{km\,s^{-1}}$. The uncertainty in the determination of ξ is typically $\pm 5\,\mathrm{km\,s^{-1}}$.

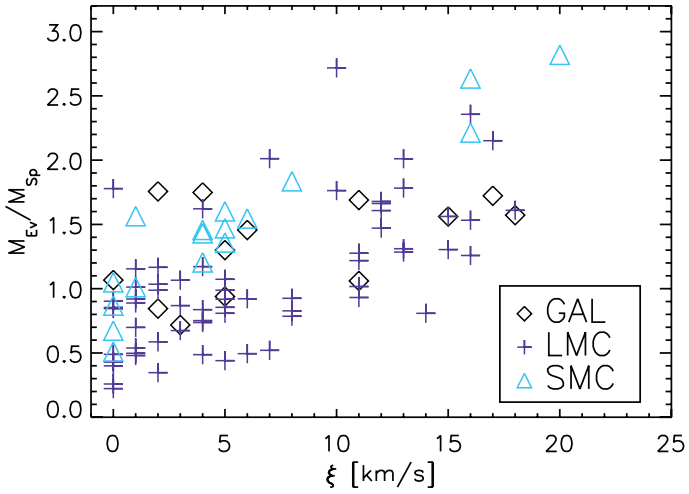

Figure 2.9: Values of the mass discrepancy (evolutionary mass divided by spectroscopic mass) as function of microturbulent velocity in the sample of B stars analysed by Trundle et al. (2007) and Hunter et al. (2008b). Here, we use only data for stars with an apparent rotational velocity of $v \sin i < 80\,\mathrm{km\,s^{-1}}$.

likely an upper limit to the effect as, first, the ξ values are in most cases less than $25\,\mathrm{km\,s^{-1}}$, and, second, a positive gradient in the atmospheric $\xi(r)$ would decrease the pressure gradient due to microturbulence but, to date, the radial stratification of the microturbulent velocity in the atmospheres of hot massive stars has not been studied in detail. From a theoretical perspective, investigating $\xi(r)$ requires hydrodynamic simulations of the stellar atmosphere, including the presence of sub-surface convection.

The mass discrepancy in massive stars is a well documented problem (see for example Herrero et al. 1992; Lennon et al. 2003; Trundle & Lennon 2005; Massey et al. 2005; Mokiem et al. 2007a). It is typically found that the difference between spectroscopic mass and evolutionary mass is most pronounced in supergiants. In main sequence stars it may not be present at all, but see Hunter et al. (2008b). Given that microturbulent velocities are highest in supergiants (see Fig. 2.6) an empirical correlation between mass discrepancy and microturbulent velocity is to be expected and is shown in Fig. 2.9 using data analysed by Trundle et al. (2007) and Hunter et al. (2008b). If indeed microturbulence is related to subsurface convection and supergiants have intrinsically higher microturbulent velocities than dwarfs (see Section 2.3) potentially part of the gradient in Fig. 2.9 may be explained by the effect discussed by Hubeny et al. (1991).

2.4.2 Non-radial pulsation

Theoretical considerations

In our discussion thus far we have considered only the propagation of running waves, it is possible that the stochastic convective motions can also excite standing waves, i.e. high-

order non-radial pulsations. For example, stochastic excitation is thought to be the cause of the Solar oscillations (Ulrich 1970; Leibacher & Stein 1971). It may thus be possible that the FeCZ excites non-radial pulsations in hot early-type stars.

Several classes of OB star models are found to be linearly unstable against non-radial pulsations, among which are the β *Cephei* stars and the slowly pulsating B stars (e.g., Dupret 2001; Pamyatnykh 1999). The key ingredient required for the pulsational instability is the iron opacity peak described in Sect. 2.2. As convection is not required to produce the pulsations in these models, it is not considered in detail as excitation mechanism (Dziembowski 2008). It is conceivable that the convective excitation could modify the predicted pulsation spectrum and/or extend the instability region of certain linear instabilities. The convective kinetic energy flow into waves could be predominantly directed into those modes for which instability is predicted in the models. In certain parts of the HR diagram, one may thus suspect an intricate connection between the occurrence of a sub-photospheric iron convection zone and the properties of non-radial pulsations.

Non-radial pulsations have also been considered as the origin of various observed small scale (e.g., line profile variability, Fullerton et al. 1996, 1997) and large scale phenomena (e.g., so called discrete absorption components, Prinja & Howarth 1988; Massa et al. 1995; Kaper et al. 1997; Prinja et al. 2002) at the surface or in the wind of massive OB stars. Non-radial g-mode pulsations were also recently proposed as the origin of observable macroturbulence in massive B type stars (Aerts et al. 2008). In Fig. 2.10 we compare the regions where strange mode, g-mode, and p-mode pulsations are predicted to occur in the HR diagram with the region where our models predict a strong FeCZ. Pulsations appear to be almost ubiquitous when all types of variables are accounted for. The strange mode pulsators are predicted to cover the HR diagram at high luminosity, where we plotted only the predictions for the radial strange modes of Kiriakidis et al. (1993); high-order non-radial strange modes seem to be omnipresent as well for stars above 40 $M_\odot$ or so (Glatzel & Mehren 1996). Non-radial g-mode pulsators are predicted by Saio et al. (2006) in the B supergiant region. And radial and low order non-radial p-modes are predicted for the β Cephei regime by Deng & Xiong (2001) and by Pamyatnykh (1999) and Saio et al. (2006) for a considerably larger region in the HR diagram. At lower metallicity, many of the predicted areas in the HR diagram are smaller (cf., Kiriakidis et al. 1993; Deng & Xiong 2001) but the general picture is still incomplete.

Observations

Observationally, the classical β Cephei stars are concentrated in the region predicted by Deng & Xiong (Stankov & Handler 2005), while the B supergiant non-radial g-mode pulsators overlap with the prediction of Saio et al. (2006) but extend to an effective temperature of $\sim$ 10 000 K (Lefever et al. 2007). Pulsations are also found for the most luminous stars (e.g., the α Cygni-variables; van Leeuwen et al. 1998), but there is now no clear evidence for strange mode pulsators. Comparing the prediction for the FeCZ with that for pulsational instability (Fig.2.10) shows two things. Firstly, the FeCZ-region is much larger than any region for a particular pulsational instability. Thus, distinguishing whether a certain observational feature is caused by a particular pulsational instability by the FeCZ might, in principle, be possible, since the area in the HR diagram where the latter occurs but the pulsational instability does

not is relatively large. Secondly, some regions exist where (so far) no pulsations are predicted but the FeCZ in our models is strong, or where, vice versa, pulsations are predicted but the FeCZ is weak or absent.

Comparing Fig. 2.10 with Fig. 2.8, where we show the observations of microturbulence and the FeCZ predictions, it is unlikely that microturbulence is associated with a particular pulsational instability. Strong microturbulence is observed at too low a luminosity to be attributable to strange mode pulsations alone, while p-mode pulsators are found where microturbulence seems not to occur. Concerning the g-mode pulsators the situation is less clear. Fig. 2.10 shows that, at solar metallicity, g-mode pulsations for post-main sequence stars are expected only in a rather narrow luminosity interval. Unfortunately, the five Galactic stars shown in Fig. 5 for which strong microturbulence is derived are all inside this luminosity range, so they cannot distinguish between a pulsational or FeCZ origin of microturbulence. However, looking at the LMC data, stars above the g-mode luminosity upper limit with microturbulence are found; whether or not corresponding stellar models are g-mode unstable is currently not known. A connection of microturbulence with non-radial pulsations is thus not impossible, but it is also not very likely.

Comparing Fig. 2.10 with the discrete absorption components (DACs) found in 200 Galactic O stars above $\sim 20\,M_\odot$ by Howarth & Prinja (1989) all the way to the zero age main sequence, seems to argue against non-radial pulsations as the origin of the DACs phenomenon (see also Sect. 2.4.4).

2.4.3 Wind clumping

Theoretical considerations

Observational evidence exists for stellar wind inhomogeneities on small and on large scales. While the latter will be discussed in Sect. 2.4.4, here we consider only small scale wind structure, or wind clumping. In Sect. 2.4.1, we discussed that waves produced by the FeCZ could lead to velocity fluctuations at the stellar surface. In order to induce wind clumping, those waves should induce density fluctuations at the stellar surface. Through the occurrence of porosity or shifts in the ionisation balance of the gas the mass-loss rate may be affected. For this to happen, the amplitude of the velocity fluctuations at the surface should be on the same order of the sound speed. Alternatively, the velocity fluctuations might directly affect the local mass-loss rate through the Doppler effect, if the amplitude of the velocity fluctuations is on the same order as the speed of the wind flow, which, at the base of the wind, is approximately the sound speed. As the sound speed at the surface in our massive main sequence models is on the order of a few times $10\,\mathrm{km\,s^{-1}}$, we consider here those stellar models potentially capable to produce wind clumping for which the convective velocities in the upper part of the FeCZ $\langle v_c \rangle \geq 2.5\,\mathrm{km\,s^{-1}}$, as this allows energetically to have surface velocity amplitudes above $\sim 10\,\mathrm{km\,s^{-1}}$ (cf. Sect. 2.4.1).

Assuming the horizontal extent of the clumps to be comparable to the sub-photospheric pressure scale height H_p, we may estimate the number of convective cells by dividing the stellar surface area by the surface area of a convective cell finding that it scales with $(R/H_\mathrm{P})^2$. For our main sequence O star models in the mass range 20-60 $M_\odot$, we find pressure scale

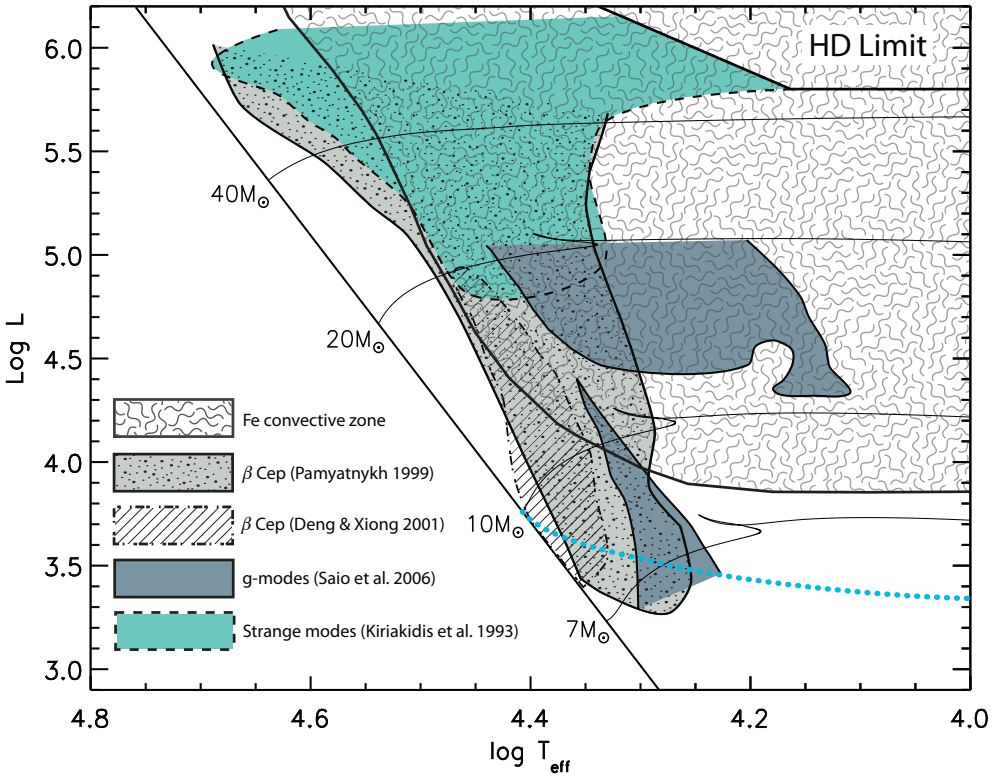

Figure 2.10: The plot shows regions of the HR diagram where pulsational instabilities are predicted, compared to our calculations for the occurrence of iron convection. The cloudy region marks the presence of iron sub-surface convection with $\langle v_c \rangle \geq 2.5\,\mathrm{km\,s^{-1}}$, while the dotted, blue line divides regions of the HR diagram where iron convection is present (above) from regions where it is absent (below). Different modes of instabilities are shown with different colors and different contour line styles, as explained in the legend. Evolutionary tracks between $7\,M_\odot$ and $40\,M_\odot$ are plotted as a reference. The straight, full drawn black line corresponds to the zero age main sequence. The Humphrey-Davidson limit is also plotted for reference (top-right corner).

heights in the range 0.04-0.24 $R_\odot$, corresponding to a total number of clumps in the range $6 \times 10^3 - 6 \times 10^4$. In principle, this might be testable through linear polarization variability measurements, which can probe wind asphericity at the very base of the wind (Davies et al. 2007).

Observations

Evidence has been accumulating that the winds of massive stars may be subject to small scale clumping. So far this is best documented for Wolf-Rayet (WR) stars, where line variability on time scales of minutes to hours is thought to constitute direct evidence of outflows that

are clumped already in the acceleration zone near the base of the wind (Lépine & Moffat 1999). This clumping may be part of the explanation for the wealth of intricate detail seen in nebulae around WR stars (Grosdidier et al. 1998). Recently, Lepine & Moffat (2008) reported spectroscopic variability in the Of supergiants ζ Pup (see also Eversberg et al. 1998) and HD 93129A. The amplitude of the variation (at the 1-3% level) is similar as in WR stars supporting the notion that clumping is not restricted to WR stars.

Indeed, evidence that O star winds are clumped is given by, among others, Puls et al. (2006). These authors investigate the clumping behavior of the inner wind (inside about two stellar radii) relative to the clumping in the outer wind (beyond tens of stellar radii) of a large sample of supergiant and giant stars. They find that in stars that have strong winds, the inner wind is more strongly clumped than the outer wind, whereas those having weak winds have similar clumping properties in the inner and outer regions. Their analysis only allows for such a relative statement. In principle, for weak winds the outer part could be homogeneous. If so, weak winds are not clumped. In any case, strong winds - identified as such if Hα is seen in emission - are clumped near the base of the wind. A measure of the degree of clumping is the clumping factor $f_{\rm cl} = \langle \rho^2 \rangle / \langle \rho \rangle^2 \geq 1$ where angle brackets denote (temporal) average values (e.g. Puls et al. 2006).

Apparently, this type of radial behavior is not consistent with hydrodynamical predictions of the intrinsic, *self-excited* line-driven instability (Runacres & Owocki 2002, 2005). Such models predict a lower clumping in the inner wind than the outer wind. Moreover, if there was any dependence on wind density predicted at all, optically thin winds should be more strongly clumped than optically thick winds (Owocki & Puls 1999; Puls et al. 2006). Therefore, the findings on the radial clumping behavior in O stars may point to an additional excitation mechanism of wind structure.

Fig. 2.11 shows that the O stars investigated by Puls et al. (2006) populate the regime in the HR diagram in which our models predict the average convective velocity in the top part of the FeCZ to change from a few to over $2.5\,{\rm km\,s^{-1}}$, indicating that surface velocity fluctuations on the order of the local sound speed are possible (cf. Sect. 2.4.3). Though the part of the HR diagram that is covered by the sample is limited ($4.46 \lesssim \log T_{\rm eff} \lesssim 4.66$; $5.29 \lesssim \log L/L_\odot \lesssim 6.26$), the trend is such that stars with relatively strong clumping in the inner winds are in a regime where $\langle v_c \rangle$ is higher. A correlation between clumping at the base of the wind and $\langle v_c \rangle$, i.e., between wind clumping and the properties of the FeCZ, appears therefore possible. To further test the idea that the FeCZ produces wind clumping at the wind base for sufficiently luminous and cool stars it would be desirable to derive the radial clumping profiles for cooler (i.e. B-type) stars. If correct, such stars, both the ones with weak and strong winds, should have relatively strong clumping at the base of the wind.

To derive the spatial scale of the wind clumps from linear polarimetry has not yet been possible for main sequence OB stars. A limitation is that this technique requires very high signal-to-noise observations (see discussion in Harries et al. 2002). Luminous Blue Variables (LBVs) however provide a more appropriate category of objects to test wind clump sizes, because of a combination of higher mass-loss rates, and lower wind velocities than for O stars (Davies et al. 2005). Indeed, Davies et al. (2007) show that in order to produce the observed polarization variability of P Cygni, the wind should consist of about ~ 1000 clumps per wind flow-time ($\tau_{fl} \equiv {\rm R}_\star / v_\infty$). To see whether this observational result is compatible with sub-

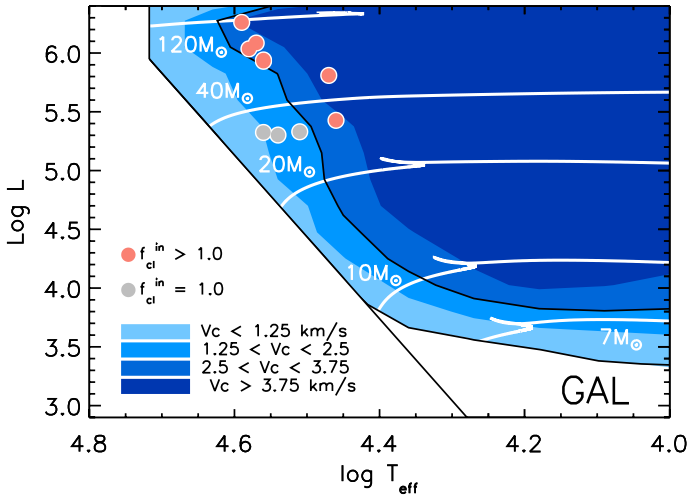

Figure 2.11: Average convective velocity within 1.5 pressure scale heights of the upper border of the iron convection zone in our models, as function of the location in the HR diagram (see color scale), based on evolutionary models between 5 $M_\odot$ and 120 $M_\odot$ (white lines) at solar metallicity. The full drawn black line corresponds to the zero age main sequence. Over-plotted as filled circles are observations of the clumping factor f_{cl}^{in} (see text for definition) in the winds of O stars, according to Puls et al. (2006). The data shown here corresponds to objects with well-constrained clumping parameters. Note the different luminosity range with respect to Fig. 2.8.

surface convection causing wind clumping, we considered the sub-surface convective regions of a massive star model with global properties similar to those of P Cygni (initial mass 60 $M_\odot$, $\log(L/L_\odot = 5.9$, and $\log\ T_{\rm eff}\ = 18\,000$ K). As a result of the lower gravity, the pressure scale height in the FeCZ in this model is about 4 $R_\odot$, which is much bigger than in our O star models. Consequently, the same estimate for the number of clumps as done for the main sequence models in Sect. 2.4.3 yields about 500 clumps per wind flow time, a number which is quite comparable to that derived for P Cygni observationally (about 10^3 clumps per wind flow time).

Finally, Fullerton et al. (1996) have conducted a spectroscopic survey of O stars and observed intrinsic absorption line profile variability (LPVs) for about 77% of their sample. They report an increase of incidence and amplitude of variability with increasing stellar radius and luminosity, as well as no statistically significant line profile variability for dwarfs earlier than O7. While Fullerton et al. attempt to relate their findings to the predictions of strange-mode pulsation in O stars by Kiriakidis et al. (1993), a comparison of their results (see their Fig. 13) with the occurrence of sub-surface convection as depicted in Fig. 2.8 indicates the possibility of a physical connection between line profile variability and sub-surface convection in O stars.

2.4.4 Magnetic fields

Fields from iron convection zones

In solar-type stars, surface convection zones modified by the stellar rotation are thought of being capable of producing a magnetic field through the so called $\alpha\Omega$-dynamo (Parker 1975; Spiegel & Weiss 1980; Spiegel & Zahn 1992). The FeCZ in our massive main sequence stellar models has a spatial extent similar to the Solar convection zone, although its mass is much smaller, and OB stars are rapid rotators, so it is possible that a dynamo may also work in the envelopes of OB stars. If so, the magnetic field may be able to penetrate the radiatively stable layer above the FeCZ, and dynamically significant field strengths might be achievable. To this end, we follow the model by MacGregor & Cassinelli (2003) for the rise of buoyant magnetic flux tubes generated at the edge of the convective core of massive stars through their radiative envelope and apply this model to the FeCZ and the overlying radiative layer. The magnetic field strength B_0 in the iron convection zone is estimated assuming equipartition of kinetic energy density and magnetic energy density inside the convective layers:

$$B_0 \simeq 2 v_c \sqrt{\pi \rho}, \tag{2.12}$$

which, for our 60 $M_\odot$ star at Z=0.02, reaches about $B_0 \simeq 2700$ G inside the iron convective zone. The surface field B_s is then obtained by multiplying this number with the ratio of the surface density ρ_s and the density in the FeCZ ρ_0, i.e. $B_s \simeq B_0 \rho_s / \rho_0 \simeq 60$ G. Similarly, for the 20 $M_\odot$ model at Z=0.02 we obtain $B_0 \simeq 1400$ G and $B_s \simeq 10$ G. Although at the surface, the magnetic pressure in the flux tubes is only on the order of a few percent of the total pressure, it is on the same order as the gas pressure and could thus lead to considerable horizontal density differences. Compared to the situation envisioned by MacGregor & Cassinelli (2003), who found that the rise time of the flux tubes from the edge of the convective core to the stellar surface can be comparable to the main sequence life time (but see also MacDonald & Mullan 2004), the rise time of the flux tubes from the FeCZ to the surface is much shorter. And while the initial magnetic field strength at the edge of the convective core can be considerably higher than our values of B_0, the surface fields obtainable from the sub-surface convection zones are higher, due to the much lower density contrast between convection zone and surface in this case.

As a consequence, even though we are far from a detailed picture, it seems conceivable that the FeCZs in massive main sequence stars produce localized magnetic fields at their surface. The interaction of the stellar wind with the localized surface magnetic fields could enhance the rate at which the wind induces a loss of stellar angular momentum. Furthermore, co-rotating density patterns in the outflowing wind could be produced by these local magnetic spots.

Rotation may play an important role in the dynamo process, possibly resulting in the appearance of stronger fields at the surface for faster rotating stars. To estimate this effect, a dynamo model accounting for the differential rotation needs to be implemented in the stellar evolution calculations. This will be the discussed in a subsequent paper.

Observations

Surface magnetic fields have been linked to several observed phenomena in OB stars, e.g. discrete absorption components (DACs) in UV resonance lines (e.g., Prinja & Howarth 1988; Massa et al. 1995; Kaper et al. 1997; Prinja et al. 2002), which are thought to diagnose large scale coherent wind anisotropies (Cranmer & Owocki 1996; Lobel & Blomme 2008), or the less coherent line profile variability mentioned above (Fullerton et al. 1996, 1997). Also non-thermal X-ray emission of OB main sequence stars has been proposed to relate to surface magnetic fields (e.g., Babel & Montmerle 1997; ud-Doula & Owocki 2002).

A connection of the FeCZ in massive stars with the phenomena mentioned above has not yet been considered. However, such a connection becomes testable through our results. While in our comparison to observed microturbulence presented above we discussed when sub-surface convection may lead to detectable surface velocity fluctuations, the presence of surface magnetic fields may simply depend on whether an FeCZ is present in the star or not. Looking at Fig. 2.8, we see that in our models the FeCZ is absent for luminosities below about $10^{3.2}\,L_\odot$, $10^{3.9}\,L_\odot$, and $10^{4.2}\,L_\odot$ for the Galaxy, LMC and SMC, respectively. If DACs or line profile variability were produced by magnetic flux tubes generated in the FeCZ, those phenomena would not be expected for OB stars below those luminosities. Howarth & Prinja (1989) find DACs in nearly all O stars (97%) in a large Galactic sample, with $\log L/L_\odot > 4.5$ and with effective temperatures as high as the zero-age main sequence values of stars above $\sim 20\,M_\odot$. Since those stars are well above the luminosity threshold for the occurrence of the iron convection at Galactic metallicity, these observations do not exclude DACs being due to FeCZ induced B-fields. Also, all eleven early B supergiants with DACs in the sample of Prinja et al. (2002) are predicted to have strong FeCZ by our results. Notably, between about $20\,M_\odot$ and $40\,M_\odot$, stars close to the zero-age main sequence are not predicted to be pulsationally unstable (cf. Fig. 2.10), which may be in conflict with pulsations as the origin for DACs.

Other types of fields

It may be interesting to briefly compare the expectation from surface magnetic fields produced via the FeCZ to that for fields produced by other means. Surface fields produced by convective cores (Schuessler & Paehler 1978; Charbonneau & MacGregor 2001; MacGregor & Cassinelli 2003) have been proposed to relate to the same phenomena as those mentioned above, even if for massive stars the buoyant rise of magnetic fields from the convective core seems to be unlikely (MacDonald & Mullan 2004). In contrast to the sub-surface FeCZ, convective cores are prevalent in all stars above about $1.2\,M_\odot$. It has been found that the longer lifetime of stars of lower mass may favor the drift of fields produced in the core to the surface (Schuessler & Paehler 1978; MacGregor & Cassinelli 2003). Therefore, the expected trend is opposite to that found for fields produced by the FeCZ, where surface fields may occur only for stars above a critical mass (or luminosity), and stronger fields are found for more massive stars.

On the other hand, in contrast to fields from the FeCZ, magnetic flux tubes produced in the core may carry CNO-processed material to the surface. This might thus constitute a

mechanism to explaining nitrogen enrichment in slowly rotating early B stars (Morel et al. 2006, 2008; Hunter et al. 2008a). Strong fossil magnetic fields are thought to persist in only a fraction of massive stars (Ferrario & Wickramasinghe 2005; Braithwaite & Spruit 2004), and may lead to, among other phenomena, highly anomalous surface chemical compositions, wind confinement, and variable X-ray emission (e.g., Wade et al. 2006; Townsend et al. 2005). Those strong features can clearly not be produced by fields originating from the FeCZs.

Finally, magnetic fields produced in differentially rotating massive stars by the Spruit-Taylor dynamo (Spruit 2002) may transport angular momentum and chemical species (cf., Heger et al. 2005). These fields are predominantly of toroidal geometry and would quickly decay near the stellar surface, and are thus not thought to lead to observable fields at the stellar surface (but see also Mullan & MacDonald (2005)).

2.5 Concluding remarks

Hot luminous stars show a variety of phenomena at their photosphere and in their winds which still lack a clear physical interpretation at this time. Among these phenomena are photospheric turbulence, spectral line variability (DACs and LPVs; see Sect. 2.4), wind clumping, variable or constant non-thermal X-ray and radio emission, chemical composition anomalies, and intrinsic slow rotation. In the previous section, we argued that the iron convection zone could be responsible for various of these phenomena.

We proposed in Sect. 2.4.1 that a physical connection may exist between microturbulence in hot star atmospheres and a sub-surface FeCZ. The strength of the FeCZ is predicted to increase with increasing metallicity Z, decreasing effective temperature T and increasing luminosity L (Sect. 2.3), and all three predicted trends are reflected in the observational data. This suggests that microturbulence corresponds to a physical motion of the gas in hot star atmospheres. This motion may then be connected to wind clumping (Sect. 2.4.3), since the empirical microturbulent velocities are comparable to the local sound speed at the stellar surface. In order to verify such a picture, multi-dimensional calculations of the FeCZ and the radiative layers above, including the stellar atmosphere, are required — similar to the recent generation of atmosphere models for cool stars (e.g., Asplund et al. 1999; Wedemeyer et al. 2004).

In Sect. 2.4.4, we proposed that the FeCZ in hot stars might also produce localized surface magnetic fields, in Galactic stars for luminosities above $\sim 10^{3.2}\,L_{\odot}$. This could explain the occurrence of DACs (discrete absorption components in UV absorption lines), also in very hot main sequence stars for which pulsational instabilities are not predicted. We further argued that there may be regions of the upper HR diagram for which the presence of the FeCZ influences, or even excites, non-radial stellar pulsations (Sect. 2.4.2).

The FeCZ could also turn out to directly affect the evolution of hot massive stars. If it induces wind clumping, it may alter the stellar wind mass-loss rate. Such a change would also influence the angular momentum loss. In addition magnetic fields produced by the iron convection zone could lead to an enhanced rate of angular momentum loss. These effects become weaker for lower metallicity, where the FeCZ is less prominent or absent (see Sect. 2.3).

Finally, we note that the consequences of the FeCZ might be strongest in Wolf-Rayet stars. These stars are so hot that the iron opacity peak, and therefore the FeCZ, can be directly at the stellar surface, or — to be more precise — at the sonic point of the wind flow (Heger & Langer 1996). This may relate to the very strong clumping found observationally in Wolf-Rayet winds (Lépine & Moffat 1999; Marchenko et al. 2006), and may be required for an understanding of the very high mass-loss rates of Wolf-Rayet stars (Eichler et al. 1995; Kato & Iben 1992; Heger & Langer 1996).

Acknowledgments The authors would like to thank Myron Smith, Alex Fullerton, Derk Massa and the members of the VLT-FLAMES consortium. MC wants to thank the STScI for kind hospitality and the Leids Kerkhoven-Bosscha Fonds for financial support. S.-C. Y. is supported by the DOE SciDAC Program (DOE DE-FC02-06ER41438).

CHAPTER 3

Rotational mixing in massive binaries: detached short-period systems

S. E. de Mink, **M. Cantiello**, N. Langer, O. R. Pols, I. Brott, S.-Ch. Yoon

Astronomy & Astrophysics, 2009, **497**, 243-253

Abstract Models of rotating single stars can successfully account for a wide variety of observed stellar phenomena, such as the surface enhancements of N and He observed in massive main-sequence stars. However, recent observations have questioned the idea that rotational mixing is the main process responsible for the surface enhancements, emphasizing the need for a strong and conclusive test for rotational mixing.

We investigate the consequences of rotational mixing for massive main-sequence stars in short-period binaries. In these systems the tides are thought to spin up the stars to rapid rotation, synchronous with their orbital revolution. We use a state-of-the-art stellar evolution code including the effect of rotational mixing, tides, and magnetic fields. We adopt a rotational mixing efficiency that has been calibrated against observations of rotating stars under the assumption that rotational mixing is the main process responsible for the observed surface abundances.

We find that the primaries of massive close binaries ($M_1 \approx 20\,\mathrm{M}_\odot$, $P_{\rm orb} \lesssim 3$ days) are expected to show significant enhancements in nitrogen (up to 0.6 dex in the Small Magellanic Cloud) for a significant fraction of their core hydrogen-burning lifetime. We propose using such systems to test the concept of rotational mixing. As these short-period binaries often show eclipses, their parameters can be determined with high accuracy.

For the primary stars of more massive and very close systems ($M_1 \approx 50\,\mathrm{M}_\odot$, $P_{\rm orb} \lesssim 2$ days) we find that centrally produced helium is efficiently mixed throughout the envelope. The star remains blue and compact during the main sequence evolution and stays within

its Roche lobe. It is the less massive star, in which the effects of rotational mixing are less pronounced, which fills its Roche lobe first, contrary to what standard binary evolution theory predicts. The primaries will appear as "Wolf-Rayet stars in disguise": core hydrogen-burning stars with strongly enhanced He and N at the surface. We propose that this evolution path provides an alternative channel for the formation of tight Wolf-Rayet binaries with a main-sequence companion and might explain massive black hole binaries such as the intriguing system M33 X-7.

3.1 Introduction

The rotation rate is considered as one of the main initial stellar parameters, along with mass and metallicity, which determine the fate of single stars. Rotation deforms the star to an oblate shape (of which Achernar is an extreme example, see Domiciano de Souza et al. 2003), it interplays with the mass loss from the star (e.g. Friend & Abbott 1986; Langer 1998; Maeder & Meynet 2000a) and it induces instabilities in the interior leading to turbulent mixing in otherwise stable layers (e.g. Meynet & Maeder 1997). As rotationally induced mixing can bring processed material from the core to the surface, it has been proposed as explanation for observed surface abundance anomalies, such as a nitrogen enrichment found in several massive main-sequence stars (e.g. Walborn 1976; Maeder & Meynet 2000b; Heger & Langer 2000). In models of rapidly rotating massive stars, rotational mixing can efficiently mix the centrally produced helium throughout the stellar envelope. Instead of expanding during core H burning as non-rotating models do, they stay compact, become more luminous and move blue-wards in the Hertzsprung-Russell diagram. This type of evolution is commonly referred to as (quasi-)chemically homogeneous evolution (Maeder 1987; Yoon & Langer 2005). Some over-luminous O and WNh[1] in the Magellanic Clouds in the Magellanic Clouds have been put forward as examples pf this type of evolution (Bouret et al. 2003; Walborn et al. 2004; Mokiem et al. 2007a; Martins et al. 2008). This alternative evolutionary scenario has been proposed as a way to create rapidly rotating massive helium stars as the possible progenitors of long gamma-ray bursts within the collapsar scenario (Yoon & Langer 2005; Woosley & Heger 2006; Cantiello et al. 2007).

Multiple attempts have been made to constrain the efficiency of rotational mixing (e.g. Gies & Lambert 1992; Fliegner et al. 1996; Daflon et al. 2001; Venn et al. 2002; Korn et al. 2002; Huang & Gies 2006; Mendel et al. 2006), but often these attempts remained inconclusive due to limited sample sizes or a strong bias towards stars with low projected velocities. The VLT-FLAMES survey provided, for the first time, a large sample of massive stars with accurate abundance determinations, covering a wide range of projected rotational velocities (Evans et al. 2005; Hunter et al. 2008a). This sample was used to calibrate the efficiency of rotational mixing, under the assumption that rotational mixing is the main process responsible for the observed enhancements (Brott et al. 2009).

These authors performed a population synthesis, based on detailed models of rotating single stars, to reproduce the properties of the VLT-FLAMES sample. They find that their

[1] Wolf-Rayet stars with evidence of enhanced nitrogen and hydrogen in their spectra (e.g. Schnurr et al. 2008)

models cannot account for a large number (20% of the sample) of highly nitrogen-enriched, slow rotators and a group of evolved fast rotators which are relatively non-enriched (a further 20% of the sample). This raises the question whether other processes play an important role in explaining the nitrogen enhancements of massive main-sequence stars, such as mass transfer in binaries (Langer et al. 2008).

Regardless of the successes of rotating stellar models to explain a variety of stellar phenomena (Maeder & Meynet 2000b), rotational mixing is still a matter of debate. Clearly a conclusive observational test for the concept of rotational mixing is needed. In this paper we propose to use eclipsing binaries for this purpose.

Eclipsing binaries have frequently been used to test stellar evolution models as they provide accurate stellar masses, radii and effective temperatures. Even beyond our own Galaxy, in the Magellanic Clouds, stellar parameters of O and early B stars have been determined with accuracies of 10% (Harries et al. 2003; Hilditch et al. 2005), which have been used to test binary evolution models (e.g. De Mink et al. 2007). As rotational mixing is more important in more massive stars (e.g. Heger et al. 2000), it is a major advantage to know the stellar masses for quantitative testing of the efficiency of rotational mixing.

In close binaries with orbital periods $P_{\rm orbit}$ less than a few days, the tides are so strong that the stars rotate synchronously with the orbital motion: $P_{\rm spin} = P_{\rm orbit}$. With stellar radii known from eclipse measurements, this enables us to determine the rotational velocity directly from the orbital period. This is the second important advantage of using binaries for testing rotational mixing with respect to single stars. For single stars fitting of spectral lines allows only for the determination of $v \sin i$, where v is the rotational velocity at the equator and i the inclination of the rotation axis, which is generally not known.

Here, we propose to use eclipsing binaries, consisting of two detached main-sequence stars. Detailed calculations of binary evolution show that if one of the stars fills its Roche lobe during the main sequence, it does not detach again before hydrogen is exhausted in the core, except maybe for a very short thermal timescale (Wellstein et al. 2001; De Mink et al. 2007). Turning this around we find that, in a binary with two detached main-sequence stars, we can safely exclude the occurrence of previous mass transfer. In other words, the fact that a system consists of two detached main-sequence stars, constrains the evolutionary history. In contrast, for a fast rotating apparently single star we do not know whether the star was born as a rapidly rotating single star, or whether the rapid rotation is the result of mass transfer in a binary or of a binary merger. The companion, if still present, may be very hard to detect, being a faint low-mass star in a wide orbit[2].

If the spectra of a binary are of high quality, one can determine the surface abundances of the two components (e.g. Leushin 1988; Pavlovski & Hensberge 2005; Rauw et al. 2005). These surface abundances, together with accurate determinations of the stellar parameters and the orbital period have the potential of strongly constraining the efficiency of rotational mixing.

The evolution of close massive binaries has been modeled by various groups (e.g. Podsiadlowski et al. 1992; Pols 1994; Wellstein et al. 2001; Wellstein & Langer 1999; Nelson & Eggleton 2001; Belczynski et al. 2002; Petrovic et al. 2005a; Vanbeveren et al. 2007; De

[2]Abundance determinations of boron, if available, may be used to distinguish between binary effects and pure rotational mixing, see Fliegner et al. (1996)

Mink et al. 2007, and references therein). In this work we use a detailed binary evolution code to predict the surface abundances for massive detached close binaries. In addition we discuss models of very massive close binaries, in which rotational mixing can be so efficient that the change in chemical profile leads to changes in the stellar structure.

3.2 Stellar evolution code

We model the evolution of rotating massive stars using the 1D hydrodynamic stellar evolution code described by Yoon et al. (2006) and Petrovic et al. (2005b), which includes the effects of rotation on the stellar structure and the transport of angular momentum and chemical species via rotationally induced hydrodynamic instabilities (Heger et al. 2000). The rotational instabilities considered are: dynamical shear, secular shear, Eddington-Sweet circulation and the Goldreich-Schubert-Fricke instability (Heger et al. 2000). Two processes dominate rotational mixing in massive stars: Eddington-Sweet circulation, large-scale meridional currents resulting from the thermal imbalance between pole and equator characteristic of rotating stars (von Zeipel 1924; Eddington 1925, 1926; Vogt 1925) and shear mixing, eddies, that can form between two layers of the star rotating at different angular velocity (e.g. Zahn 1974). We take into account angular momentum transport by magnetic torques as proposed by Spruit (2002) as these can successfully provide the coupling between the stellar core and envelope necessary to explain the observed spins in young compact stellar remnants (Heger et al. 2005; Petrovic et al. 2005b; Suijs et al. 2008).

Mixing of chemical species and the transport of angular momentum are implemented as diffusion processes. For convection we assume a mixing length parameter $\alpha_{\rm MLT} = 1.5$. In semi-convective regions we assume efficient mixing ($\alpha_{\rm SEM} = 1.0$, as defined in Langer 1991). The turbulent viscosity is determined as the sum of the convective and semi-convective diffusion coefficients and those that arise from the rotationally induced instabilities. The inhibiting effect of gradients in the mean molecular weight on rotational mixing is decreased by a factor $f_\mu = 0.1$ (Yoon et al. 2006).

Brott et al. (2009) calibrated the efficiency of rotationally induced mixing using data from the VLT-FLAMES survey of massive stars, assuming that rotational mixing is the main process responsible for the observed enhancements. To reproduce the extension of the main sequence in the Hertzsprung-Russell diagram, they assumed overshooting of 0.355 times the pressure scale height. The main parameter responsible for the efficiency of rotational mixing is f_c, defined as the contribution of rotationally induced instabilities to the diffusion of chemical species (Heger et al. 2000). Brott et al. (2009) found that $f_c = 0.0228$ is needed to reproduce the spread in N abundances observed in the VLT-FLAMES data (Hunter et al. 2008a). We do not consider possible mixing by instabilities related to magnetic buoyancy due to winding up of the magnetic field lines through differential rotation (Spruit 2002) as this leads to too efficient mixing (Hunter et al. 2008a).

Metallicity-dependent mass loss in the form of stellar winds has been included as in Yoon et al. (2006); Brott et al. (2009). For the associated angular momentum loss we assume that mass is lost with the specific angular momentum equal to the latitudinally averaged specific

angular momentum of the surface layer. The mass loss is thus assumed to be independent of latitude.

The effect of mass and angular momentum loss on the binary orbit is computed according to Podsiadlowski et al. (1992), with the specific angular momentum of the wind calculated according to Brookshaw & Tavani (1993). We assume that the orbit is circular and that the spins of the stars are perpendicular to the orbital plane. Tidal interaction is modeled as described in Detmers et al. (2008) using the timescale for synchronization by turbulent viscosity (Zahn 1977), see also Section 3.3. Angular momentum is transported between the surface layers and the inner regions by magnetic torques and rotational instabilities. At the onset of central H burning, we assume that the rotation of the stars is rigid and synchronized with the orbital motion.

Initial Composition

We discuss single stellar models starting with three different initial compositions, representing the composition of the Small and Large Magellanic Cloud (abbreviated as SMC and LMC) and the Galaxy (GAL) following the approach by Brott et al. (2009) to which we refer for details. For C, O, Mg and Si we use the average abundances determined for stars in the VLT-FLAMES survey (Hunter et al. 2007). For the Magellanic Clouds we adopt the N abundance measured for HII regions which is in agreement with the lowest observed N abundances in the VLT-FLAMES sample (Hunter et al. 2007, and references therein). For the remaining heavy elements we adopt solar abundances by Asplund et al. (2005) scaled down by 0.7 dex for the SMC and 0.4 dex for the LMC. For our binary models we have assumed the SMC composition. The opacity tables of OPAL (Iglesias & Rogers 1996) are adopted, where the Fe abundance is used to interpolate between the tables of different metallicity.

3.3 Stellar rotation under the influence of tides

n a close binary, angular momentum and kinetic energy can be exchanged between the two stars and their orbit through tides. The system tends to evolve towards a state of minimum mechanical energy due to dissipative processes. This is an equilibrium state, where the orbit is circular, the spins of the stars are aligned and perpendicular to the orbital plane and the stars are in synchronous rotation with the orbital motion, such that $P_{\rm spin} = P_{\rm orbit}$. How quickly this equilibrium state is approached depends on the efficiency of the processes responsible for the energy dissipation.

The most efficient form of energy dissipation takes place in turbulent regions of the star, such as convective layers, where the kinetic energy of the large-scale flow induced by the tides cascades down to smaller and smaller scales, until it is dissipated into heat. Zahn (1977, 1989) estimated the timescale for synchronization due to this “turbulent viscosity” as a function of the ratio q of the mass of the companion star to the mass of the star under consideration and on the ratio of the stellar radius R over the separation a between the two stars:

$$\tau_{\rm sync,turb} = f_{\rm turb}\, q^{-2} \left(\frac{R}{a}\right)^{-6} \text{ year.} \tag{3.1}$$

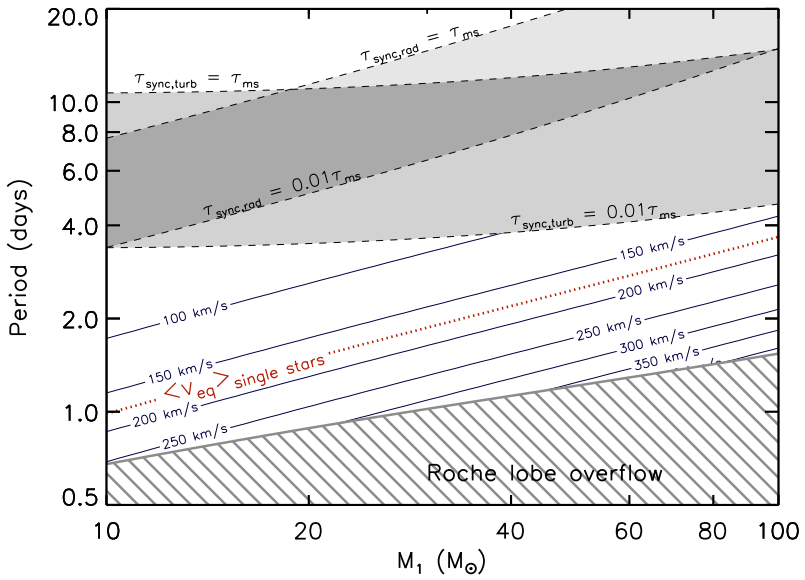

Figure 3.1: Timescales for tidal synchronization. The four dashed lines indicate where the timescales for tidal synchronization by turbulent viscosity $\tau_{\rm sync,turb}$ and radiative dissipation $\tau_{\rm sync,rad}$ for zero-age main-sequence stars are equal to (one percent of) the main-sequence lifetime $\tau_{\rm ms}$ of the most massive star of a binary system, see Sect. 3.3 for details. In the region below the gray-shaded bands, tides quickly synchronize the stellar rotation with the orbit. The resulting equatorial velocity in kms^{-1} for the primary star is indicated with contour levels, assuming the radius at the onset of hydrogen burning. We have assumed a metallicity of Z=0.004 and a mass ratio $\mathrm{M}_2/\mathrm{M}_1 = 0.75$, to be consistent with the models presented in Sect. 3.4. The average velocity measured for apparently single stars in the SMC, $\langle v_{\rm eq}\rangle = 175\mathrm{kms}^{-1}$, is plotted with a dotted line. Very small orbital periods are excluded (hashed region) as the stars fill their Roche lobe at zero-age.

The proportionality factor $f_{\rm turb}$ depends on the structure of the star, on the location of the turbulent layers and on the timescale for dissipation of kinetic energy, which is uncertain. Nevertheless, the dependence of the time scale on R/a is so steep that, approximating $f_{\rm turb} \approx 1$, Zahn (1977) showed that this expression adequately explains the observed orbital period below which tides lead to synchronization.

In the absence of turbulent viscosity, another dissipative process is required in order to have efficient tides. If the star does not rotate synchronously, it experiences a varying gravitational potential, which triggers a large range of oscillations in the star. These oscillations are damped near the stellar surface by radiative dissipation. Zahn (1975) derived the corresponding timescale for synchronization:

$$\tau_{\rm sync,rad} = f_{\rm rad}\, q^{-2}\,(1+q)^{-5/6}\left(\frac{R}{a}\right)^{-17/2} \text{ year}, \tag{3.2}$$

$$\text{where } f_{\rm rad} = 52^{-5/3}\, E_2 \left(\frac{I}{MR^2}\right)\left(\frac{GM}{R^3}\right)^{-1/2}.$$

Here, M denotes the mass of the star under consideration, I its moment of inertia and E_2 the tidal coefficient, which is sensitive to the structure of the star, in particular to the size of the convective core: $E_2 \propto (R_{\rm core}/R)^8$ (Zahn 1977).

The early-type massive stars considered in this work have radiative envelopes (except for convective zones just below the surface which contain almost no mass, e.g. Cantiello et al. 2009) and synchronization by radiative damping has been proposed to be the most efficient dissipation mechanism. However, in fast rotating stars turbulence is induced by rotational instabilities and one may argue that the first timescale applies also to these stars (Toledano et al. 2007). In addition Witte & Savonije (1999) show that in some cases resonance locking can contribute to even more efficient tidal dissipation.

In Figure 3.1 we compare both synchronization timescales with the main-sequence lifetime of the more massive star in a binary. For this plot we have used the radii of non-rotating zero-age main sequence stars assuming a metallicity of Z = 0.004 and a mass ratio of $M_2/M_1 = 0.75$. For E_2 we use an analytic approximation by Hurley et al. (2002), for the Roche-lobe radius we use the analytic expression by Eggleton (1983). The diagram shows that in binaries with orbital periods shorter than approximately 3-5 days, the timescale for synchronization is less than one percent of the main-sequence lifetime $\tau_{\rm MS}$, regardless of the actual process responsible for the synchronization. The resulting equatorial velocity of the primary star, assuming synchronous rotation, is given in kms^{-1} along contour lines.

For comparison: the average equatorial velocity for apparently single stars in the VLT-FLAMES survey with masses between 7 and 25 $M_\odot$ is 150 kms^{-1} for the LMC and 175 kms^{-1} for the SMC (Hunter et al. 2008a). In most binaries tides will slow down the rotation of the star, but in the tightest binaries the rotation rate is higher than that for average single stars. Note that the binary systems of interest in this work, for which the components have high enough equatorial velocities to show significant surface abundance changes by rotational mixing ($\gtrsim$100-150 kms^{-1}, see Sect. 3.4), are in the region where tides are very efficient, according to both prescriptions for the synchronization timescale.

3.4 Rotational mixing in single star models

Any element produced or destroyed in the hot interior of the star can in principle be used as a tracer of rotational mixing. The amount by which the surface abundance of a particular element changes depends on the location in the star where the element is processed.

Helium is the most important element synthesized during core hydrogen burning. By the time a substantial amount of helium has been formed in the stellar core, a gradient in mean molecular weight has been established at the interface between the core and the envelope, which has an inhibiting effect on rotationally induced mixing. Models of moderately fast rotating stars (with an equatorial velocity of about 170 kms^{-1} and a mass of about 20 $M_\odot$) show that helium will only appear at the surface towards the very end of the main-sequence evolution. In more massive stars, the helium surface abundance may be significantly enhanced but

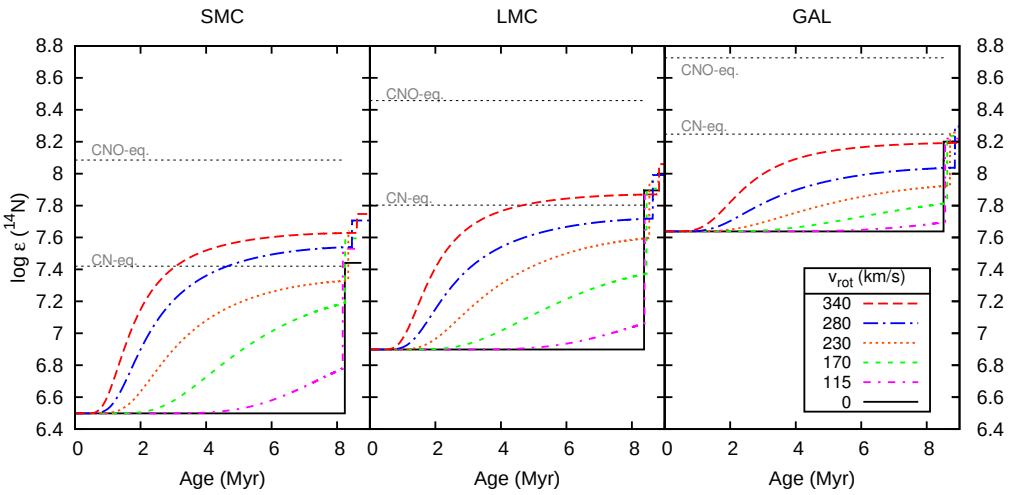

Figure 3.2: Surface nitrogen abundance versus time for single stellar models of 20 $M_\odot$ with different (approximate) initial equatorial rotational velocities starting with the initial composition of the SMC (left panel), LMC (center panel) and GAL (right panel). The nitrogen abundance is given in the conventional units: the logarithm of the number fraction of nitrogen n_N with respect to hydrogen n_H, where the hydrogen abundance is fixed at 10^{12}, i.e. $\log \epsilon(N) = \log_{10}[n_N/n_H] + 12$.

this is partly due to the strong stellar winds. This makes helium not very suitable for testing the effect of rotational mixing.

A better tracer for rotational mixing during the main-sequence evolution is nitrogen, which is produced in the hot interior layers on a very short time scale when carbon is converted into nitrogen by CN-cycling. On a longer timescale (about 1-2 Myr in the center of a 20 $M_\odot$ star) the CNO cycle comes into equilibrium, leading to additional N at the expense of both carbon and oxygen. Rotational mixing can bring nitrogen to the surface, resulting in a gradual increase of the nitrogen surface abundance over the main-sequence lifetime (Fig. 3.2). Nitrogen can be measured in rotating B-type stars in the Magellanic Clouds with accuracies of 0.2-0.25 dex (Hunter et al. 2008a). Carbon decreases accordingly, but cannot be measured as accurately and is therefore less suitable as a tracer of rotational mixing. Other elements such as boron can be used, but these are less abundant and may be hard to detect, especially in metal-poor environments such as the Magellanic Clouds.

Rotational mixing becomes more efficient in higher-mass stars since radiation pressure becomes more important, which helps to overcome the entropy barrier at the interface between the core and the envelope. Also, the ratio of the timescale for meridional circulation with respect to the main-sequence lifetime decreases with increasing mass (Yoon et al. 2006).

Table 3.1: Key properties of the massive binary evolution models (20 $M_\odot$+15 $M_\odot$) as defined and discussed in Sect. 3.5.1.

$P_{\rm orb}$ (d)	$t_{\rm RL}$ (Myr)	$t_{\rm delay}$ (Myr)	$t_{\rm RL} - t_{\rm enh}$ (Myr)	$R/R_{\rm RL}$ ($t = t_{\rm enh}$)	$X_{\rm He,center}$ ($t = t_{\rm RL}$)	$\log \epsilon(N^{14})$ ($t = t_{\rm RL}$)	$B_{\rm RL}/B^{a}_{\rm init}$	$C_{\rm RL}/C^{a}_{\rm init}$	$N_{\rm RL}/N^{a}_{\rm init}$	$\langle v_{\rm eq}\rangle^{b}$ (kms^{-1})	$v^{b}_{\rm eq,RL}$ (kms^{-1})
1.1	3.3	1.3	1.0	0.92	0.42	7.12	0.11	0.87	4.17	243	267
1.2	3.9	1.6	1.2	0.90	0.47	7.07	0.08	0.85	3.71	228	260
1.4	5.0	2.1	1.5	0.86	0.55	6.98	0.06	0.82	3.04	203	248
1.6	5.5	2.7	1.0	0.86	0.61	6.89	0.07	0.83	2.45	181	234
1.8	6.0	3.2	0.9	0.86	0.65	6.85	0.07	0.83	2.27	166	228
2.0	6.3	3.7	0.6	0.87	0.69	6.81	0.09	0.86	2.05	152	216
2.2	6.7	4.1	0.5	0.89	0.73	6.79	0.10	0.87	1.96	141	212
2.4	6.9	4.5	0.4	0.90	0.75	6.77	0.11	0.88	1.87	131	207
2.6	7.1	4.9	0.2	0.93	0.78	6.74	0.13	0.90	1.74	123	199
2.8	7.2	5.2	0.1	0.96	0.79	6.73	0.14	0.91	1.69	116	196
3.0	7.3	5.6	0.0	0.99	0.81	6.70	0.15	0.92	1.59	110	190

[b] The surface mass fraction at the onset of Roche-lobe overflow divided by the initial mass fraction of resp. boron (^{10}B + ^{11}B), carbon (^{12}C) and nitrogen (^{14}N).

[b] The equatorial rotational velocity for the primary star, averaged over time from the onset of hydrogen burning until the start of mass transfer (one before last column) and at the onset of Roche-lobe overflow (last column).

The disadvantage of using very massive stars as test cases for rotational mixing is the uncertainty in their mass-loss rates. As mass loss exposes deeper layers of the star, enriched in N and He, it has qualitatively the same effect on the surface composition as rotational mixing. At lower metallicity mass loss in the form of a radiatively driven stellar wind is reduced. Therefore, also the uncertainty in the mass-loss rate is less important.

Figure 3.2 shows the nitrogen surface abundance as a function of time for rotating single stellar models of 20 $M_\odot$ with three different initial compositions, representative for the relatively metal-poor composition of the Small and Large Magellanic Cloud, and for a mixture representing stars in the Galaxy. The equilibrium abundances for N in the center for CN- and CNO-cycling are plotted as horizontal lines. The Galactic model with an equatorial velocity of 230 kms^{-1} shows nitrogen enhancements up to about 0.3 dex, while in the SMC model the N abundance increases by up to approximately 0.8 dex. The high C/N ratio in the Magellanic clouds is partly responsible for this effect as it leads to a strong increase of N during CN-cycling (Brott et al. 2009). Indeed, in the VLT-FLAMES survey, Hunter et al. (2008a) find a larger spread in N abundances for the stars in the Magellanic Clouds than for ones in the Galactic stars. We conclude that the Magellanic Clouds are the most promising location for testing rotational mixing, as the effect of rotational mixing is most pronounced in the N surface abundances.

3.5 Binary models

In this section we present binary evolution models calculated with the same set of input physics as the single stellar models presented in Section 3.4, taking into account the effects of mass and angular momentum loss on the orbit and spin-orbit coupling by tides. We assume

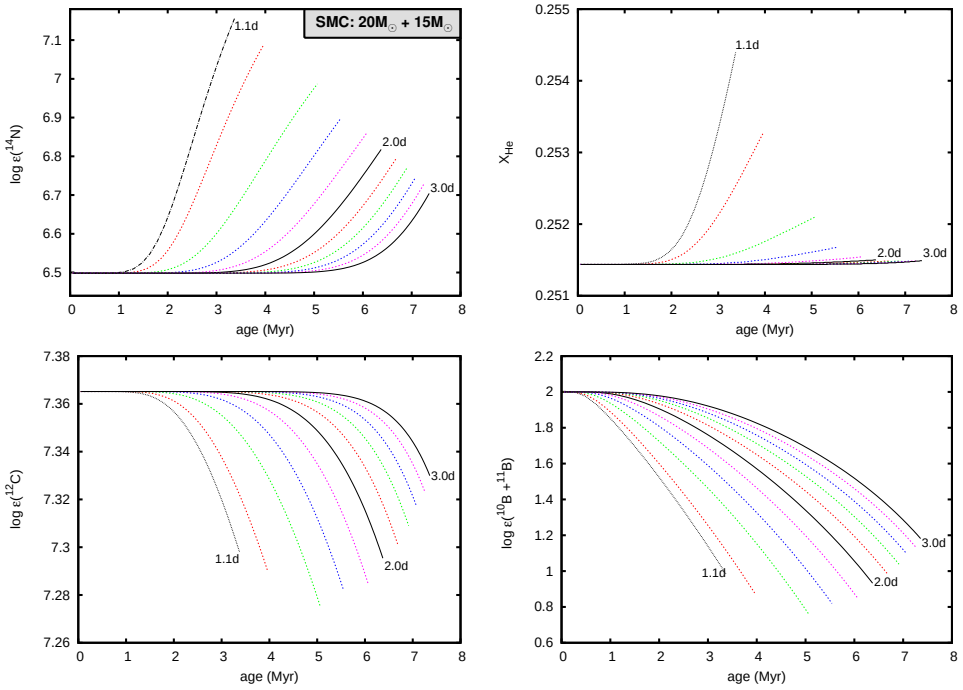

Figure 3.3: Surface abundances of nitrogen (^{14}N), carbon (^{12}C), boron (^{10}B+^{11}B) and the mass fraction of helium at the surface versus time for a 20 $M_\odot$ star with a 15 $M_\odot$ close companion. Note the different vertical scales. The abundance of an element X is given relative to hydrogen in the conventional units: $\log \epsilon(\mathrm{X}) = \log_{10}(n_\mathrm{X}/n_\mathrm{H}) + 12$, where n_X and n_H refer to the number fractions. The different lines show the evolution assuming initial orbital periods of 1.1 days and between 1.2 and 3 days, with a spacing of 0.2 days. The tracks are plotted from the onset of central H burning until the onset of Roche-lobe overflow. See also Table 3.1.

a composition representative of the Small Magellanic Cloud, which is relatively metal-poor and has a high carbon to nitrogen ratio. We discuss two specific model sets: systems with a massive primary, $M_1 = 20\ \mathrm{M}_\odot$, in Sect. 3.5.1 and systems with a very massive primary, $M_1 = 50\ \mathrm{M}_\odot$, in Sect. 3.5.2.

3.5.1 Massive binaries (20 $M_\odot$+15 $M_\odot$)

With the Small Magellanic Cloud sample of double-lined eclipsing binaries by Harries et al. (2003) and Hilditch et al. (2005) in mind, which contains 21 detached systems[3] with orbital periods ranging from 1–4 days and primary masses ranging from 7–23 $M_\odot$, we chose to

[3]Possibly only 20 systems are detached. For two of the systems an alternative semi-detached solution exists. For one of these systems a comparison to binary evolution models including the effects of mass transfer showed that the semi-detached solution was more consistent than the detached solution (De Mink et al. 2007).

model the following binary systems. For the mass of the primary component we adopt 20 $M_\odot$, for the secondary component 15 $M_\odot$. The evolution of both stars is followed starting at the onset of central hydrogen burning, at $t = 0$, until the primary star fills its Roche lobe, at $t = t_{\rm RL}$. We adopt orbital periods up to 3 days. In these systems the tides are efficient enough to keep both stars in synchronous rotation with the orbit (Sect. 3.3).

Surface abundances

The abundances of nitrogen, carbon, helium and boron at the surface of the primary star are shown as a function of time in Fig. 3.3, see also Tab. 3.1. The nitrogen abundances at the surface starts to increase after about 1 Myr for the 1.1 day binary, and after about 5 Myr for the 3.0 day binary. This time delay $t_{\rm delay}$ is the time it takes to transport the nitrogen from the deeper layers, where it is produced, to the surface[4]. The largest enhancement, 0.6 dex, is achieved in the 1.1 day binary. The shorter the orbital period, the faster the rotation of the stars, the more efficient rotational mixing and the faster the surface abundances change with time. On the other hand in the systems with short orbital periods the stars fill their Roche lobe at an earlier stage, leaving less time to modify their surface abundances.

The typical uncertainty in the nitrogen abundance determinations for stars in the VLT-FLAMES survey is about 0.2 dex. Therefore, to be able to detect whether nitrogen is enhanced, it should exceed the initial nitrogen abundance by 0.2 dex. The age at which this lower limit for detecting a surface nitrogen enhancement is exceeded is denoted as $t_{\rm enh}$ in Table 3.1. Systems with orbital periods shorter than 3 days all reach surface enhancements of 0.2 dex, at the latest just before they fill their Roche lobe. The time span during which the primary can be observed with a surface nitrogen abundance exceeding 6.7 dex, listed as $t_{\rm RL} - t_{\rm enh}$ in Table 3.1, is highest for the 1.4 day system, 1.5 Myr. For detached tidally locked main-sequence binaries with initial orbital periods greater than about 3 days we do not expect detectable N enhancements on the basis of these models: their rotation rates and therefore the efficiency of rotational mixing is too low.

While the nitrogen abundance increases, the carbon abundance decreases accordingly, see Fig. 3.3. It decreases by less than 0.1 dex in our models. The changes in the mass fraction of helium at the surface are very small, just over 1% at maximum for the tightest system. An element that is a very sensitive tracer of rotational mixing is boron. It is easily destroyed in the hotter layers just below the surface. Therefore the time delay for boron, after which the boron surface abundance starts to change, is very short. The change in the boron surface abundance is considerable, up to 1.2 dex in the 1.4 day model. In practice it may be hard to measure boron due to its low overall abundance.

The closer the stars are to filling their Roche lobe, the higher is their surface N abundance. This can be turned around and may be used to predict which binary systems are likely to show nitrogen surface enhancements. In Tab. 3.1 we indicate the Roche-lobe filling factor $R/R_{\rm RL}$, defined as the radius of the primary star over the Roche-lobe radius, at the moment when the surface N enhancement exceeds the initial abundance by 0.2 dex. Based on these models, we predict that the observed systems with masses close to 20 and 15 $M_\odot$ have to fill their Roche lobes by about 86% or more before they show detectable surface N enhancements

[4]We define $t_{\rm delay}$ as the age at which the surface nitrogen abundance is enhanced by 0.01 dex.

(see Table 3.1 col. 5). We do note that the radii predicted by our models are sensitive to the assumed amount of overshooting.

In the last two columns of Table 3.1 we indicate the rotational velocity at the equator, averaged over time and at the onset of Roche-lobe overflow. Whereas a single star at this metallicity slows down its rotation rate due to its evolutionary expansion, the spin periods of the stars in tidally locked binaries are nearly constant because the orbit acts as an angular momentum reservoir. Therefore rotationally induced mixing is more important in a star in a tidally locked binary than in a single star that started with the same initial rotation rate. The effect is small, however, as the expansion mainly takes place after about 5–6 Myr for a 20 $M_\odot$ star. Binaries with orbital periods shorter than 2 days fill their Roche lobe before the expansion sets in. The effect is stronger at higher metallicity, where angular momentum loss by the stellar wind becomes important, see Sect. 3.6.

Expected trends with system mass and mass ratio

For an ideal comparison between models and observations one would prefer a model in which the binary parameters match the observed parameters. In the above, we discussed models with a specific choice for the primary mass and mass ratio and we only varied the initial orbital period. Here we discuss how our findings are expected to change for systems with slightly different system masses and mass ratios.

In more massive binaries rotational mixing is more efficient, such that they will show a shorter time delay, even when measured in units of the core hydrogen-burning lifetime. Detectable surface enhancements are expected to occur at an earlier stage, while the stars are further away from filling their Roche lobe. At very high masses additional effects can play a role, which are discussed in Sect. 3.5.2. The secondary star in the models discussed above does not show significant surface abundance changes for C, N and He. The surface boron abundance does decrease by up to 0.6 dex for the 1.4 day model. In systems with mass ratios closer to 1, the time scale for rotational mixing becomes similar in both stars and nitrogen enhancements are expected for both stars.

Another effect of changing the mass ratio is that the size of the Roche lobe changes. A more extreme mass ratio results in a wider Roche lobe for the primary, if the primary mass and orbital period are kept constant. The efficiency of rotational mixing does not change, as it depends on the rotational period which is fixed by the orbital period. However, the star has more space to expand before it fills its Roche lobe. We noted above that the primary stars fill their Roche lobes by at least 86% before they show detectable surface N enhancements (see also Sect 3.6). This changes to approximately 83% and 76% for mass ratios of $q = 0.5$ and $q = 0.25$ respectively. A bigger Roche lobe also leaves more time to enhance the surface abundance. This implies a greater chance of catching the system in a stage where the surface abundance is significantly enhanced.

To summarize: the biggest surface N enhancements are expected for systems with a high-mass primary, which is close to filling its Roche lobe, with a companion which has a significantly lower mass in an orbit of no more than a few days.

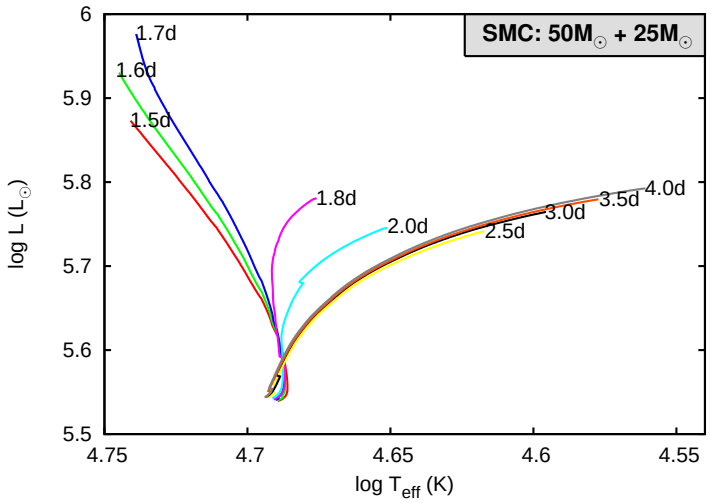

Figure 3.4: The evolution from the onset of central H burning until the moment of Roche-lobe overflow for a 50 $M_\odot$ star in a binary with a 25 $M_\odot$ companion (not plotted) with initial orbital periods between 1.5 and 4 days.

3.5.2 Very massive binaries (50 $M_\odot$+25 $M_\odot$)

In more massive binaries, rotational mixing can be so efficient that the change in chemical profile leads to significant structural changes. In this model set we adopt a primary mass of 50 $M_\odot$, a secondary mass of 25 $M_\odot$ and orbital periods varying from 1.5 to 4 days, assuming an SMC composition to be consistent with the models presented in Sect. 3.5.1. Although such massive close systems are rare, observational counterparts do exist, for example two of the four massive binaries presented by Massey et al. (2002) which are located in the R136 cluster at the center of the 30 Doradus nebula in the Large Magellanic Cloud: R136-38[5] and R136-42[6]. Another example with an even closer orbit is [L72] LH 54-425[7] located in the LH 54 OB association in the Large Magellanic Cloud (Williams et al. 2008). All three binary systems have O-type main-sequence components, which reside well within their Roche lobes.

Figure 3.4 shows the evolution of the primary stars in the Hertzsprung-Russell diagram, until one of the stars in the binary fills its Roche lobe (not necessarily the primary, see below). At the onset of hydrogen burning their location in the diagram is very similar, although the stars in tighter binaries, which rotate faster, are slightly cooler and bigger: a direct consequence of the centrifugal force. As they evolve their tracks start to deviate. The wider systems ($P_{\rm orb} > 2.0$d) evolve similarly to non-rotating stars: they expand during core hydrogen burning, evolving towards cooler temperatures until they fill their Roche lobe. Their

[5] $M_1 = 56.9 \pm 0.6$ $M_\odot$, $M_2 = 23.4 \pm 0.2$ $M_\odot$ and $P_{\rm orb} = 3.39$d
[6] $M_1 = 40.3 \pm 0.1$ $M_\odot$, $M_2 = 32.6 \pm 0.1$ $M_\odot$ and $P_{\rm orb} = 2.89$d
[7] $M_1 = 47 \pm 2$ $M_\odot$, $M_2 = 28 \pm 1$ $M_\odot$ and $P_{\rm orb} = 2.25$d

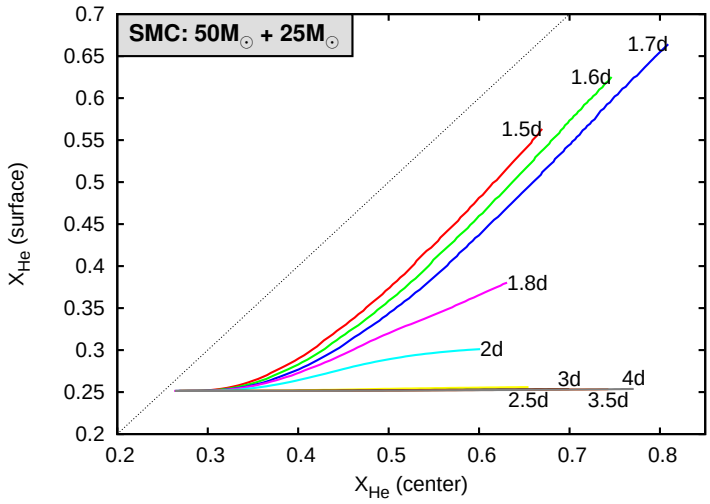

Figure 3.5: Helium abundance at the surface as a function of the helium abundance in the center for the same systems as plotted in Figure 3.4.

evolutionary tracks overlap in the Hertzsprung-Russell diagram.

The primaries in the tighter systems ($P_{\rm orb} < 2.0$d) behave very differently: they evolve left- and up-ward in the HR-diagram, becoming hotter and more luminous while they stay relatively compact. The transition in the morphology of the tracks around $P_{\rm orb} \approx 2$ days is similar to the bifurcation found for fast rotating single stars (Maeder 1987; Yoon & Langer 2005).

Surface abundances

Rotational mixing is so efficient in these systems that even a large amount of helium can be transported to the surface. Figure 3.5 depicts the helium mass fraction at the surface as a function of the helium mass fraction in the center. In the hypothetical case that mixing would be extremely efficient throughout the whole star, the surface helium abundance would be equal to the central helium abundance at all time. This is indicated by the dotted line. For the widest systems, the surface helium mass fraction is not affected by rotational mixing at all, while for the tighter systems $X_{\rm He}$ reaches up to 65%. They follow the evolution of chemically homogeneous stars. Figure 3.5 also shows that for each system, mass transfer starts before all hydrogen is converted into helium in the center. Note that the highest central He mass fraction when mass transfer starts is reached in the 1.7 day system (more than 80%), whereas on the basis of standard binary evolution theory (e.g. Kippenhahn & Weigert 1967) one would expect this to occur in the widest system. This anomalous behavior is connected to the evolution of the radius, as discussed below.

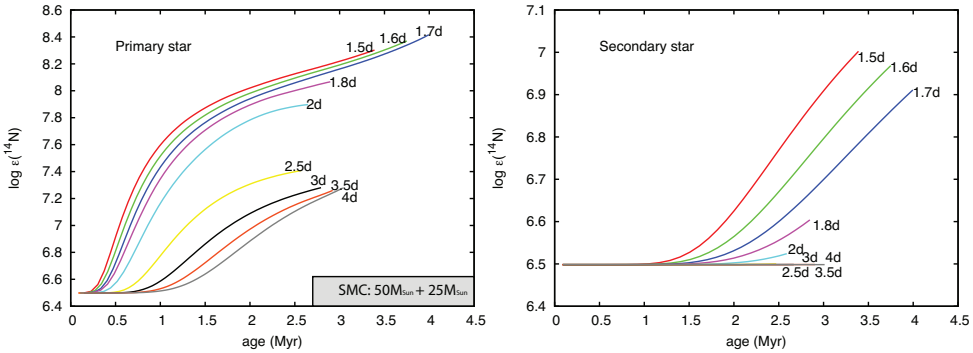

Figure 3.6: Nitrogen abundance as a function of age at the surface for the primary and secondary star of the same systems as plotted in Figure 3.4. Note the different scales.

All systems show big enhancements of nitrogen at the surface of the primary, see Fig. 3.6. The wider systems are enhanced by up to 0.9 dex. In the tight systems the enhancement reaches almost 2 dex. This extreme increase is partly due to the fact that abundance is measured relative to hydrogen, which is significantly depleted at the surface of the primaries in the tightest systems (cf. Table. 3.2). Also the secondary stars show nitrogen surface enhancements, of up to 0.5 dex.

Evolution of the radius

The increase of helium in the envelopes of the primary stars in the tightest binaries leads to a decrease of the opacity and an increase in mean molecular weight in the outer layers, resulting in more luminous and more compact stars. In Figure 3.7 we plot the stellar radii as a fraction of their Roche-lobe radii. The primary stars in the wider systems expand and fill their Roche lobe after about 2.5-3 Myr. Contrary to what one might expect, we find that Roche-lobe overflow is delayed in tighter binaries. Whereas classical binary evolution theory predicts that the primary star is the first to fill its Roche lobe, we find instead that for systems with $P_{\rm orb} \leq 1.7$ days it is the less massive secondary star that starts to transfer mass towards the primary. During this phase of reverse mass transfer from the less massive to the more massive star, the orbit widens. Nevertheless we find that, if we continue our calculations, the two stars come into contact shortly after the onset of mass transfer and the stars are likely to merge.

Expected trends with system mass and mass ratio

In more massive systems the effect of rotational mixing becomes stronger in both components. This may allow for chemically homogeneous evolution to occur in binary systems with wider orbits. If the mass ratio is closer to one, $M_2 \approx M_1$, the effect of rotational mixing becomes comparable in both stars, and they may both evolve along an almost chemically ho-

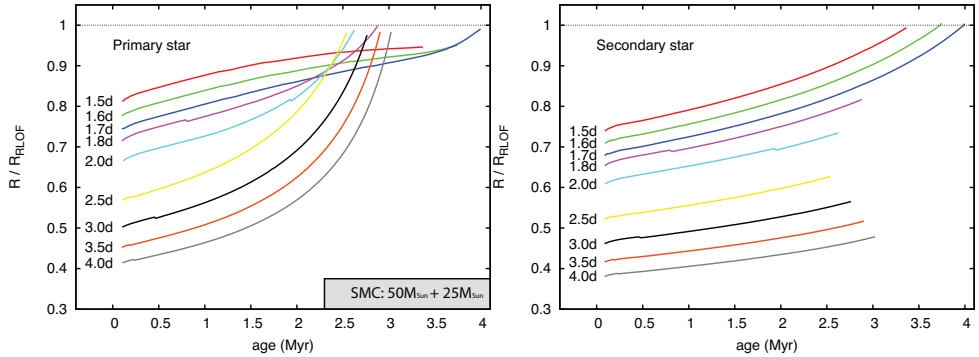

Figure 3.7: Radius as fraction of the Roche-lobe radius for the primary (left panel) and secondary star (right panel) of the same systems as plotted in Figure 3.4.

Table 3.2: Key properties of very massive binaries (50 $M_\odot$+25 $M_\odot$) as described in Sect. 3.5.2 (see also Table 3.1 and Sect. 3.5.1). In the last column we indicate which component fills its Roche lobe first. Velocities are given in $\mathrm{km\,s^{-1}}$.

$P_{\rm orb}(d)$	$t_{\rm RL}$(Myr)	$X_{\rm He,center}$	$X_{\rm He,surface}$	$\log\epsilon(N^{14})$	$B_{\rm RL}/B_{\rm init}$	$C_{\rm RL}/C_{\rm init}$	$N_{\rm RL}/N_{\rm init}$	$\langle v_{\rm eq}\rangle$	$v_{\rm eq,RL}$)	RLOF
1.5	3.4	0.68	0.56	8.30	2.0×10^{-6}	9.0×10^{-2}	37	304	315	Sec.
1.6	3.7	0.75	0.63	8.37	6.6×10^{-7}	9.1×10^{-2}	37	289	307	Sec.
1.7	4.0	0.81	0.66	8.41	4.7×10^{-7}	9.5×10^{-2}	37	277	310	Sec.
1.8	2.9	0.64	0.38	8.06	2.8×10^{-4}	2.3×10^{-1}	30	262	315	Prim.
2.0	2.6	0.61	0.30	7.90	2.4×10^{-3}	4.0×10^{-1}	23	240	305	Prim.
2.5	2.6	0.66	0.26	7.41	8.1×10^{-3}	7.4×10^{-1}	8.0	200	279	Prim.
3.0	2.8	0.71	0.25	7.28	1.3×10^{-2}	7.8×10^{-1}	6.0	172	261	Prim.
3.5	2.9	0.75	0.25	7.26	1.8×10^{-2}	8.0×10^{-1}	5.7	152	248	Prim.
4.0	3.0	0.78	0.25	7.27	2.4×10^{-2}	7.9×10^{-1}	6.0	137	236	Prim.

mogeneous evolution track. In that case both stars can stay within their Roche lobe and gradually become two compact WR stars in a tight orbit. In a system with a more extreme mass ratio, $M_2 \ll M_1$, the secondary star will hardly evolve or expand during the core hydrogen-burning lifetime of the primary. Also in this case Roche-lobe overflow may be avoided during the core hydrogen-burning lifetime of the primary component, leading to the formation of a Wolf-Rayet star with a main-sequence companion in a tight orbit. The parameter space in which this type of evolution can occur will be examined in a subsequent paper.

3.6 Discussion

We have shown that rotational mixing can have important effects in close massive binaries. The mixing parameters in our code have been calibrated against observations of rotating massive stars in the VLT-FLAMES survey under the assumption that rotational mixing is

the main process responsible for the observed surface N enhancements (see Sect. 3.2). The predictions we present for close binaries can be used to test the validity of this assumption.

In Sect. 3.4 we conclude that eclipsing binaries in the Magellanic Clouds are the most promising test cases for rotational mixing. In these systems we expect the biggest enhancements of N at the surface. Also, the uncertainty in the mass-loss rates plays a less important role, as radiatively driven winds are reduced at low metallicity. A disadvantage of Magellanic Cloud binaries with respect to Galactic systems is the greater distance. Long integration times may be needed to obtain spectra with high enough quality to determine the stellar parameters and abundances. The advantage of using eclipsing binaries is that we can compare directly to evolution models with corresponding masses and orbital periods. Therefore, just a few well-studied systems may be enough to put constraints on the efficiency of rotational mixing. However, ideally one would prefer a large sample to enable a statistical comparison.

The main parameter in our code that affects the efficiency of mixing due to rotational instabilities is f_c (see Sect 3.2) which has been calibrated directly against the surface N abundances in the VLT-FLAMES survey. However, the calibration involves multiple parameters, such as f_μ which is a measure of how effectively a gradient in mean molecular weight can inhibit rotational mixing. We expect that uncertainties in this parameter are not important for our predictions for nitrogen, as this element is mainly produced and transported to the envelope early in the evolution, before a strong mean molecular-weight gradient has been established at the interface between the core and the envelope. However, a lower value of f_μ may lead to higher helium surface abundances, which may facilitate the possibility of chemically homogeneous evolution in close binaries, but this remains to be investigated.

We use a large amount of overshooting in our models (0.355 times the pressure scale height H_p), to reproduce the extension of the main sequence observed in the VLT-FLAMES data. However, the amount of overshooting is an uncertain parameter and some authors quote lower values for the amount of overshooting, for example Schroder et al. (1997) who find 0.24-0.32H_p based on eclipsing binaries with stellar masses between 2.5 and 6.5 $M_\odot$, (see also Stothers & Chin 1992; Alongi et al. 1993). We recomputed one of our models (20+15 $M_\odot$, 3 days) without overshooting we find that, although the stars are less luminous as expected, the surface nitrogen abundance and the radius at a given time are very similar (deviations of less 0.01 dex in the N abundance at a given age, and less than 4% in the radius for a given nitrogen surface abundance). For tighter binaries we expect an even smaller effect on the radius. We conclude that our predictions are not very sensitive to the uncertainties in the overshooting parameter.

In our models we assume that mixing processes in binaries operate in the same way as in single stars. For both single stars and binary members we find that the stellar interior rotates nearly rigidly (at least during the early phase of evolution of interest here) as a result of efficient internal angular momentum transport by magnetic torques. Having very similar internal rotational profiles, the only difference in our models arises from the evolution of the rotation rate, which in single stars is governed by angular momentum loss and evolutionary expansion, while in binaries the tides play a major role. However, in the binary models we consider the stars are close to filling their Roche lobe. They are slightly deformed in a lobsided way, no longer being symmetric around the rotation axis. In addition, one side of the star is irradiated by the companion and may be heated. Although the system is synchronized,

the tides continue to extract or deposit angular momentum from or onto the stars. How such effects, induced by the presence of the companion star, interact with the different rotational instabilities is not well understood and poses an additional uncertainty on our predictions. If such effects are important and lead to additional mixing, our predictions for the N surface abundance can still be used as a test for rotational mixing if they are considered as lower limits to the expected N abundance.

Avoiding mass transfer in short-period binaries

We have shown that rotational mixing, if it is as efficient as assumed in our models, can lead to chemically homogeneous evolution for tight binaries with a 50 $M_\odot$ primary. In these models the primary star stays so compact that the secondary star is the first to fill its Roche lobe.

This peculiar behavior of the radius of stars, which are efficiently mixed, has been noted in models of rapidly rotating massive single stars (Maeder 1987) and has been suggested as an evolutionary channel for the progenitors of long gamma-ray bursts (Yoon et al. 2006; Woosley & Heger 2006) in the collapsar scenario Woosley (1993). In single stars this type of evolution only occurs at low metallicity, because at solar metallicity mass and angular momentum loss in the form of a stellar wind spins down the stars and prevents initially rapidly rotating stars from evolving chemically homogeneously (Yoon et al. 2006; Brott et al. 2009). In a close binary tides can replenish the angular momentum, opening the possibility for chemically homogeneous evolution in the solar neighborhood.

The binary models presented here all evolve into contact, but (as we discussed briefly in Sect 3.5.2) Roche-lobe overflow may be avoided altogether in systems in which the secondary stays compact, either because it also evolves chemically homogeneously, which may occur if $M_1 \approx M_2$, or because it evolves on a much longer timescale than the primary, when $M_2 \ll M_1$. Whereas standard binary evolution theory predicts that the shorter the orbital period, the earlier mass transfer sets in, we find that binaries with the lowest orbital periods may avoid the onset of mass transfer altogether. This evolution scenario does not fit in the traditional classification of interacting binaries into Case *A*, *B* and *C*, based on the evolutionary stage of the primary component at the onset of mass transfer (Kippenhahn & Weigert 1967; Lauterborn 1970). In the remainder of this paper we will refer to this new case of binary evolution, in which mass transfer is delayed or avoided altogether as a result of very efficient internal mixing, as Case *M*.

The massive and tight systems in which Case *M* can occur are rare. Additional mixing processes induced by the presence of the companion star, which may be important in such systems, will widen the parameter space in which Case *M* can occur: it would lower the minimum mass for the primary star and increase the orbital period below which this type of evolution occurs. The massive LMC binary [L72] LH 54-425, with an orbital period of 2.25 d (Williams et al. 2008, see also Sec. 3.5.2) may be a candidate for this type of evolution. Another interesting case is the galactic binary WR20a, which consists of two core hydrogen burning stars of 82.7 ± 5.5 and 81.9 ± 5.5 $M_\odot$ in an orbit of 3.69 d. Both stars are so compact that they are detached. The surface abundance show evidence of rotational mixing: a nitrogen

abundance of six times solar is observed and carbon is depleted (Bonanos et al. 2004; Rauw et al. 2005).

Short-period Wolf-Rayet and black-hole binaries

If Roche-lobe overflow is avoided throughout the core hydrogen-burning phase of the primary star, both stars will stay compact while the primary gradually becomes a helium star and can be observed as a Wolf-Rayet star. Initially the Wolf-Rayet star will be more massive than its main sequence companion, but mass loss due to the strong stellar wind may reverse the mass ratio, especially in systems which started with nearly equal masses. Examples of observed short-period Wolf-Rayet binaries with a main-sequence companion are CQ Cep[8], CX Cep[9], HD 193576[10] and the very massive system HD 311884[11] (van der Hucht 2001). Such systems are thought to be the result of very non-conservative mass transfer or a common envelope phase (e.g. Petrovic et al. 2005a). Case M constitutes an alternative formation scenario which does not involve mass transfer.

Case *M* is also interesting in the light of massive black-hole binaries. Orosz et al. (2007) recently published the stellar parameters of M33 X-7, located in the nearby galaxy Messier 33 which harbors one of the most massive stellar black holes known to date, $M_{bh} = 15.7 \pm 1.5\ M_\odot$, orbiting a massive O star, $M_O = 70 \pm 7\ M_\odot$, which resides inside its Roche lobe in spite of the fact that the orbit is very tight, $P_{orb} = 3.45$ d. The explanation for the formation of this system with standard binary evolutionary models involves a common-envelope phase that sets in after the end of core helium burning (Case *C*), as the progenitor of the black hole must have had a radius much greater than the current orbital separation. This scenario is problematic as it requires that the black-hole progenitor lost roughly ten times less mass before the onset of Roche-lobe overflow than what is currently predicted by stellar evolution models (Orosz et al. 2007). An additional problem is that the most likely outcome of the common envelope phase would be a merger, as the envelopes of massive stars are tightly bound (Podsiadlowski et al. 2003). In the Case *M* scenario the black-hole progenitor can stay compact and avoid Roche-lobe overflow at least until the end of core helium burning, such that it retains its envelope.

There are examples of stellar mass black-hole binaries with short periods and a massive main-sequence companion, in which nearly chemically homogeneous evolution may be important. IC 10 X-1 is a system harboring the most massive stellar mass black hole known to date with a mass of at least 21 $M_\odot$, orbiting a Wolf-Rayet star of approximately 25 $M_\odot$ in an orbit of 1.45 days (Silverman & Filippenko 2008). Homogeneous evolution helps to explain the high mass of the black hole, but the short orbital period poses a difficulty, also for Case *M*: strong mass loss during the Wolf-Rayet life time will widen the orbit. Other examples of high mass black hole binaries with short orbital periods are the famous systems

[8]CQ Cep: $M_{WR} = 24\ M_\odot$, $M_O = 30\ M_\odot$, $P_{orb} = 1.6$ d
[9]CX Cep: $M_{WR} = 20\ M_\odot$, $M_O = 28\ M_\odot$, $P_{orb} = 2.1$ d
[10]HD 193576: $M_{WR} = 9\ M_\odot$, $M_O = 29\ M_\odot$, $P_{orb} = 4.2$ d
[11]HD 311884: $M_{WR} = 51\ M_\odot$, $M_O = 60\ M_\odot$, $P_{orb} = 6.2$ d

Cyg X-1[12] (Herrero et al. 1995), LMC X-1[13] (Orosz et al. 2008) and LMC X-3[14] (Yao et al. 2005, and references therein).

The subsequent evolution of tight rapidly rotating Wolf-Rayet binaries remains to be investigated. If one or both members of the system can retain enough angular momentum to fulfill the collapsar scenario (Woosley 1993), which may be hard as the tides can slow down the stars (e.g. Detmers et al. 2008), it may lead to the production of one or even two long gamma-ray bursts.

Although promising, the importance of this channel may be small due to the limited binary parameter space in which Case *M* can occur. To make any strong statements about this new evolutionary scenario, further modeling is needed, which we will undertake in the near future.

3.7 Conclusion

We investigated the effect of rotational mixing on the evolution of detached short-period massive binaries using a state of the art stellar evolution code. The efficiency of rotational mixing was calibrated under the assumption that rotational mixing is the main process responsible for the observed N enhancements in rotating stars.

We find nitrogen surface enhancements of up to 0.6 dex for massive binaries in the SMC. The largest enhancements can be reached in systems with orbital periods less than about 2 days, in which the primary is massive (about 20 $M_\odot$ or more) and evolved (filling its Roche lobe by about 80% or more) and the secondary is significantly less massive, which leads to a more spacious Roche lobe for the primary (preferably $M_2/M_1 \lesssim 0.75$).

We propose to use such systems as test cases for rotational mixing. These systems often show eclipses and big radial velocity variations, such that their stellar parameters, the rotation rate and possibly their surface abundances can be determined with high accuracy. This enables a direct comparison between an observed system and models computed with the appropriate stellar and binary parameters. An additional major advantage of using detached main-sequence binaries is the constraint on the evolutionary history. For a fast spinning apparently single star we do not know whether it was born as a fast rotator or whether its rotation rate is the result of mass transfer or merger event. In a detached main-sequence binary we can exclude the occurrence of any mass transfer phase since the onset of core-hydrogen burning (see Sect 3.1).

In the most massive binaries we find that rotational instabilities can efficiently mix centrally produced helium throughout the stellar envelope of the primary. They follow the evolution for chemically homogeneous stars: they stay within their Roche lobe, being overluminous and blue compared to normal stars. Due to large amount of nitrogen and helium at the surface these stars can be observed as Wolf-Rayet stars with hydrogen in their spectra. In contrast to standard binary evolution, we find that it is the less massive star in these systems that fills its Roche lobe first.

[12]Cyg X-1: $M_{bh} \approx 10\ M_\odot$, $M_O \approx 18\ M_\odot$, $P_{orb} = 5.6$ d
[13]LMC X-1: $M_{bh} \approx 10\ M_\odot$, $M_O \approx 30\ M_\odot$, $P_{orb} = 3.9$ d
[14]LMC X-3: $M_{bh} \approx 4$–$10\ M_\odot$, $M_O \approx 40\ M_\odot$, $P_{orb} = 4.2$ d

There may be regions in the binary parameter space in which Roche-lobe overflow can be avoided completely during the core hydrogen-burning phase of the primary. The parameter space for this new evolutionary scheme, which we denote Case *M* to emphasize the important role of mixing, increases if additional mixing processes play a role in such massive systems. It may provide an alternative channel for the formation or tight Wolf-Rayet binaries with a main-sequence companion, without the need for a mass transfer and common envelope phase to bring the stars close together. This scenario is also potentially interesting for tight massive black hole binaries, such as M33 X-7 (Orosz et al. 2007), for which no satisfactory evolutionary scenario exists to date.

Acknowledgments The authors would like to thank G. Meynet (referee), E. Glebbeek, M, Verkoulen, K. Belzcinski, Z. Han, J.-P. Zahn and the members of the VLT-FLAMES consortium. The authors acknowledge NOVA and LKBF for financial support. S.-Ch. Y. is supported by the DOE SciDAC Program (DOE DE-FC02-06ER41438).

CHAPTER 4

Binary star progenitors of long gamma-ray bursts

M. Cantiello, S.-C.Yoon, N. Langer & M.Livio
Astronomy & Astrophysics, 2007, **465**, L29-L33

Abstract The collapsar model for long gamma-ray bursts requires a rapidly rotating Wolf-Rayet star as progenitor. We test the idea of producing rapidly rotating Wolf-Rayet stars in massive close binaries through mass accretion and consecutive quasi-chemically homogeneous evolution — the latter had previously been shown to provide collapsars below a certain metallicity threshold. We use a 1-D hydrodynamic binary evolution code to simulate the evolution of a 16+15 $M_\odot$ binary model with an initial orbital period of 5 days and SMC metallicity (Z=0.004). Internal differential rotation, rotationally induced mixing and magnetic fields are included in both components, as well as non-conservative mass and angular momentum transfer, and tidal spin-orbit coupling. The considered binary system undergoes early Case B mass transfer. The mass donor becomes a helium star and dies as a Type Ib/c supernova. The mass gainer is spun-up, and internal magnetic fields efficiently transport accreted angular momentum into the stellar core. The orbital widening prevents subsequent tidal synchronization, and the mass gainer rejuvenates and evolves quasi-chemically homogeneously thereafter. The mass donor explodes 7 Myr before the collapse of the mass gainer. Assuming the binary to be broken-up by the supernova kick, the potential gamma-ray burst progenitor would become a runaway star with a space velocity of $27\,\mathrm{km\,s^{-1}}$, traveling about 200 pc during its remaining lifetime. The binary channel presented here does not, as such, provide a new physical model for collapsar production, as the resulting stellar models are almost identical to quasi-chemically homogeneously evolving rapidly rotating single stars. However, it may provide a means for massive stars to obtain the required high rotation rates. Moreover, it suggests that a possibly large fraction of long gamma-ray bursts occurs in runaway stars.

4.1 Introduction

Long gamma-ray bursts are thought to be produced by a subset of dying massive and possibly metal-poor stars (Jakobsson et al. 2005; Langer & Norman 2006; Modjaz et al. 2007). Within the currently favored collapsar scenario (Woosley 1993), the burst is produced by a rapidly rotating massive Wolf-Rayet (WR) star whose core collapses into a black hole (MacFadyen & Woosley 1999). While single star evolution models without internal magnetic fields can produce such configurations (Petrovic et al. 2005b; Hirschi et al. 2005), only models including magnetic fields are capable of reproducing the slow spins of young Galactic neutron stars (Heger et al. 2005; Ott et al. 2006) and white dwarfs (Suijs et al. 2008), due to the magnetic core-envelope coupling during the giant stage.

Various rather exotic binary evolution channels have been proposed to lead to long gamma-ray bursts (Fryer et al. 1999; Fryer & Heger 2005), supported by the idea that long gamma-ray bursts are very rare events (cf. Podsiadlowski et al. 2004). The recent realization that long gamma-ray bursts may have a bias towards low metallicity (e.g., Fynbo et al. 2003; Fruchter et al. 2006) may change the situation: rather than being exotic, GRBs may simply represent massive low-metallicity stars — which locally are much rarer than O stars of solar metallicity (Langer & Norman 2006).

Yoon & Langer (2005), Yoon et al. (2006) and Woosley & Heger (2006) recently showed that below a certain metallicity threshold, very rapidly rotating single stars avoid the magnetic braking of the core through the so-called quasi-chemically homogeneous evolution: rotationally induced mixing processes keep the star close to chemical homogeneity, and thus the giant stage is avoided altogether. While these models are successful in producing models which fulfill all constraints of the collapsar model, they require very rapid initial rotation. The resulting number of long GRBs thus depends critically on the initial distribution of rotational velocities (IRF) of massive stars (Yoon et al. 2006).

The question thus arises whether the quasi-chemically homogeneous of massive stars can also be obtained in mass transferring massive binary systems (Vanbeveren & de Loore 1994), since in such systems the mass gainer can be spun-up to close to critical rotation (see Petrovic et al. 2005a,b), independent of its initial rotation rate. While Petrovic et al. (2005b) addressed this question and obtained a negative result, they used restrictive semiconvective mixing. As discussed in Yoon et al. (2006), the semiconvective mixing efficiency is still weakly constrained, but most recent stellar evolution models apply efficient semiconvective mixing. Thus, here we readdress the question, using models with efficient semiconvective mixing, as in Yoon et al. (2006).

4.2 Method

Our stellar model is calculated with the same hydrodynamic stellar evolution code as in Yoon et al. (2006). This includes the effect of rotation on the stellar structure, transport of angular momentum and chemical species via magnetic torques and rotationally induced hydrodynamic instabilities. Stellar wind mass loss, in particular metallicity dependent Wolf-Rayet

Table 4.1: Major evolutionary phases of the computed 16 $M_\odot$ + 15 $M_\odot$ early Case B binary sequence. The binary calculation ends after core carbon exhaustion of the mass loser (the primary), and the mass gainer (the secondary) is then evolved as a single star. We show evolutionary time, masses of both stars, mass lost from the system, orbital period, surface rotational velocities, central and surface helium mass fraction of the mass gainer, and orbital velocites of both stars. The abbreviations for the evolutionary phases are: ZAMS = zero age main sequence; ECHB = end core hydrogen burning; ICB= ignition of carbon burning; ECCB = end core carbon burning. The numbered evolutionary stages correspond to those given in Fig. 4.1 and Fig. 4.2

Phase	Time	M_1	M_2	ΔM	P	$v_{\rm rot,1}$	$v_{\rm rot,2}$	$Y_{\rm c,2}$	$Y_{\rm s,2}$	$v_{\rm orbit,1}$	$v_{\rm orbit,2}$
	Myr	$M_\odot$	$M_\odot$	$M_\odot$	d	km s^{-1}	km s^{-1}			km s^{-1}	km s^{-1}
1 ZAMS	0	16	15	–	5.0	230	230	0.248	0.248	188	201
2 begin Case B	9.89	15.92	14.94	0.14	5.1	96	85	0.879	0.248	186	198
3 end Case B	9.90	3.93	20.77	6.30	38.2	27	719	0.434	0.348	153	29
4 ECCB primary	11.30	3.71	20.86	6.44	42.7	40	767	0.457	0.441	149	27
5 ECHB secondary	18.10	–	16.76	–	–	–	202	0.996	0.956	–	–
6 ICB secondary	18.56	–	12.85	–	–	–	191	0.000	0.996	–	–
7 ECCB secondary	18.56	–	12.83	–	–	–	258	0.000	0.996	–	–

mass loss, and enhancement of mass loss due to rapid rotation, have been included as in Yoon et al. (2006).

The binary evolution physics of our code is described in Petrovic et al. (2005a,b). It includes tidal coupling, mass and angular momentum transfer, and thermohaline mixing. The mass transfer efficiency is determined by the angular momentum balance of the accreting star: The amount of accreted matter is limited by the constraint that the angular momentum which it carries does not drive the rotation of the star beyond critical rotation (Petrovic et al. 2005a). To determine the accreted angular momentum, the code solves the equation of motion of test particles leaving the mass donor into a Roche potential (cf. also Dessart et al. 2003).

Here, we apply efficient semiconvective mixing; i.e., a value of $\alpha_{\rm SM} = 1.0$ (cf. Langer et al. 1985) is used in the calculations discussed below. However, the same binary model as discussed below was also computed with $\alpha_{\rm SM} = 0.1$ and $\alpha_{\rm SM} = 0.01$.

4.3 Results

We compute the evolution of a binary system with rotating and magnetic components of 16 $M_\odot$ and 15 $M_\odot$, and an initial orbital period of 5 days. We chose an early Case B system with an initial mass ratio close to one for two reasons. Firstly, the expected mass transfer efficiency for this case was about 60% (meaning that 60% of the transfered matter can be retained by the mass gainer), based on the calculations by Wellstein (2001), Langer et al. (2004), and Petrovic et al. (2005a). Secondly, a Case B rather than Case A system was chosen to avoid synchronization *after* the major mass transfer phase.

The evolution of the binary system proceeded as follows (cf. Table 1). The initial rotational velocity of both stars has been set to 230 km s^{-1}, but both stars synchronize with the

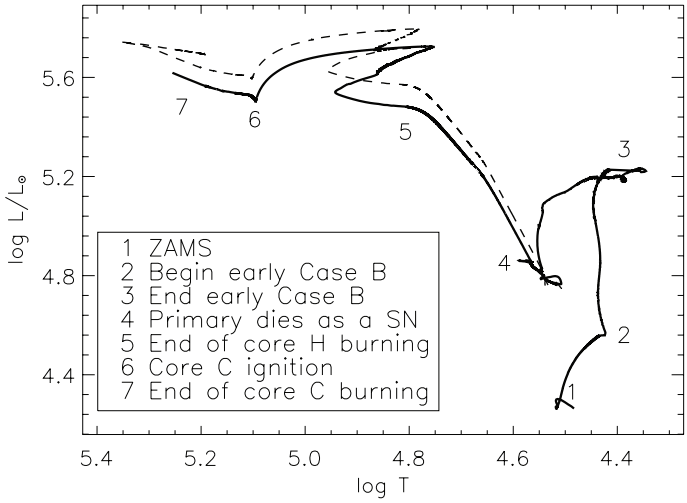

Figure 4.1: Evolutionary track of the mass gainer in our 16 $M_\odot$ + 15 $M_\odot$ early Case B binary model (5 d initial orbital period) in the HR diagram (solid line), from the zero age main sequence up to core carbon exhaustion. The main evolutionary phases are labeled by numbers (see legend). The dashed line shows the evolutionary track of a very rapidly rotating ($v_{\rm init}/v_{\rm K} = 0.9$) 24 $M_\odot$ single star. Both stars have SMC metallicity, and undergo quasi-chemically homogeneous evolution (see text).

orbital rotation within about 1 Myr, to equatorial rotational velocities of only about 50 km s^{-1} (cf. Fig.4.2). Rotationally induced mixing before the onset of mass transfer is thus negligible — in contrast to typical O stars evolving in isolation (Heger & Langer 2000; Meynet & Maeder 2000). The initially more massive star ends core hydrogen burning after $\sim$ 9.89 Myr, and Case B mass transfer begins shortly thereafter. It sheds about 12 $M_\odot$ evolving into a $\sim$ 4 $M_\odot$ helium star. About 1.5 Myr later, it sheds another $\sim$ 0.2 $M_\odot$ as a helium giant, before exploding as Type Ib/c supernova.

The mass gainer keeps about 6 $M_\odot$ of the overflowing matter, rendering the mass accretion efficiency to roughly 50%. Thereafter, it enters a phase of close-to-critical rotation, which induces rejuvenation and quasi-chemically homogeneous evolution (Figs. 4.2 and 4.3). Its mass loss is enhanced by rotation. About 5 Myr after the onset of accretion, the surface helium mass fraction of the mass gainer is increased to values above 60%, and Wolf-Rayet mass loss is assumed from then on. The star finishes core hydrogen burning after another 3 Myr, at an age of 18.1 Myr, with a mass of 16.8 $M_\odot$, a surface helium mass fraction of 95%, and rotating with $\sim$ 200 km s^{-1}.

After core hydrogen exhaustion, the mass gainer contracts and spins-up to critical rotation, which leads to a mass shedding of almost 2 $M_\odot$. During its remaining lifetime of less than 0.5 Myr, it loses about another 2 $M_\odot$ to a Wolf-Rayet wind. It ends its life as a rapidly rotating Wolf-Rayet star with a final mass of about 13 $M_\odot$, ready to form a collapsar. Assuming the binary broke up upon the explosion of the mass loser, the mass gainer would have traveled for about 7 Myr with its final orbital velocity of 27 km s^{-1} a distance of about 200 pc.

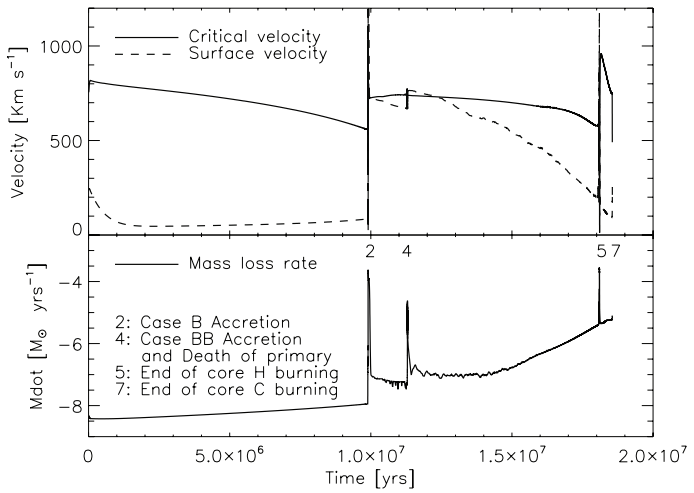

Figure 4.2: **Upper panel:** Equatorial rotation velocity (dashed line) and critical rotation velocity (solid line) of the mass gainer of the computed $16\,M_\odot$ + $15\,M_\odot$ early Case B binary sequence, as function of time, from the zero-age main sequence until core carbon exhaustion. **Lower panel:** Mass loss rate of the same stellar model, as function of time. The numbered evolutionary stages correspond to those given in Fig. 4.1 and Tab. 4.1

Following Brandt & Podsiadlowski (1995) we calculate the kick velocity necessary to unbind the binary system, under the hypothesis of instantaneous removal of the SN ejecta. Two extreme values correspond to the most and to the least efficient geometrical configuration for the supernova kick to break up the system. The minimum kick velocity is $52\,\mathrm{km\,s^{-1}}$ and corresponds to the case where the kick is aligned with the orbital velocity vector of the supernova progenitor. The maximum kick velocity necessary to unbind the system is $350\,\mathrm{km\,s^{-1}}$, which is required if the kick is aligned to the orbital velocity vector, but directed backward. According to the observed velocity distribution of radio pulsars, about 55% of pulsars have a space velocity larger than $350\,\mathrm{km\,s^{-1}}$, while more than 98% have a velocity above $52\,\mathrm{km\,s^{-1}}$ (Arzoumanian et al. 2002). In order to estimate the chance of obtaining a runaway star out of our system we performed a Monte Carlo simulation for a randomly oriented supernova kick. According to the observed velocity distribution of radio pulsars (Arzoumanian et al. 2002) the probability for the binary system to break up by the first supernova explosion is about 80%.

The same binary model as discussed above was also computed with $\alpha_{\rm SM} = 0.1$ and $\alpha_{\rm SM} = 0.01$. The first case mentioned practically reproduces the results outlined above, even if the CO core angular momentum content of the GRB progenitor is lower in this case (see Tab. 4.2). The second case confirmed the finding of Petrovic et al. (2005b) that chemically homogeneous evolution does not occur for restrictive semiconvective mixing.

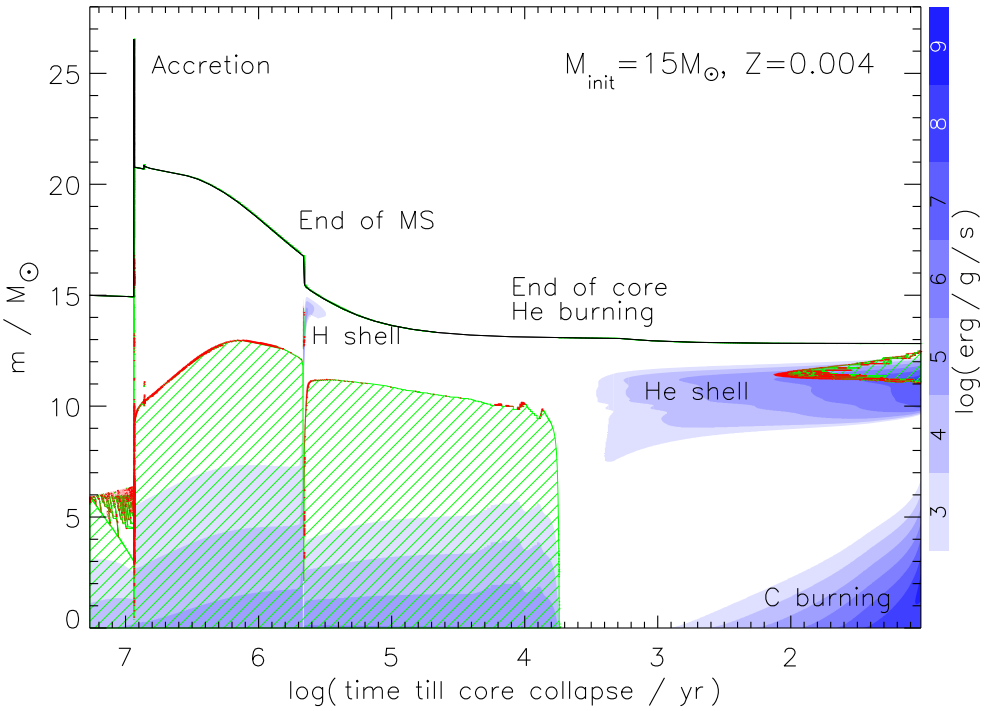

Figure 4.3: Evolution of the internal structure of the mass gainer of the computed 16 $M_\odot$ + 15 $M_\odot$ early Case B binary sequence, as function of time, from the zero-age main sequence to core carbon exhaustion. The time axis is logarithmic, with the time of core collapse as zero point. Convective layers are hatched. Semiconvective layers are marked by dots (red dots in the electronic version). Gray (blue) shading indicates nuclear energy generation (color bar to the right of the figure). The topmost solid line denotes the surface of the star.

4.4 Comparison to single star model

It is instructive to compare the evolution of the mass gainer of the binary model described above with that of a rapidly rotating single star of similar mass. Fig. 4.4 shows the Kippenhahn diagram of a 24 $M_\odot$ single star with SMC metallicity with an initial rotation rate of 700 km s^{-1}, corresponding to 90% of Keplerian rotation ($v_{\rm init}/v_{\rm K}$ = 0.9). Modeling details are as in Yoon et al. (2006). A comparison with Fig.4.3 reveals that its evolution is almost identical to that of the mass gainer after accretion in the binary model described above. This similarity is underpinned by a comparison of the evolutionary tracks of both stars in the HR diagram (Fig.4.1). Table 2 shows that also the final core angular momentum of the binary model is not significantly different from that of corresponding single stars.

As a consequence, one may conclude that the binary model does not, from the point of view of the internal stellar evolution, provide anything new or different from what is already obtained in rapidly rotating single stars. In particular, it can not be expected that the metallic-

Table 4.2: Average specific angular momentum in the CO core ($< j_{\rm CO} >$) for six different stellar evolution models, at the end of carbon core burning. The first three (labeled 'binary') correspond to the mass gainers of the computed $16\,M_\odot + 15\,M_\odot$ early Case B binary sequence, for three different values of the semiconvection parameter. The fourth corresponds to the computed $24\,M_\odot$ single star with initially 90% of Keplerian velocity ($v_{\rm init}/v_{\rm K} = 0.9$). The last two correspond to the $20\,M_\odot$ single star models with Z=0.004 and initially 60% and 30% of Keplerian rotation of Yoon et al. (2006). Models in bold face are evolving quasi-chemically homogeneous. The specific angular momentum of the least stable orbit around a $3\,M_\odot$ Kerr black hole for these models is about 30×10^{15} cm^2 s^{-1}.

Model	$M_{\rm i}$ $M_\odot$	$\alpha_{\rm SM}$	$v_{\rm init}/v_{\rm K}$	$< j_{\rm CO} >$ 10^{15} cm^{2}s^{-1}	$M_{\rm CO}$ $M_\odot$
binary	**15**	**1.0**	**–**	**18.15**	**10.0**
binary	**15**	**0.1**	**–**	**8.90**	**8.4**
binary	15	0.01	–	1.09	2.8
single	**24**	**1.0**	**0.9**	**23.42**	**11.4**
single	**20**	**1.0**	**0.6**	**11.62**	**9.9**
single	20	1.0	0.3	2.09	4.2

ity threshold for obtaining a long gamma-ray burst (cf. Yoon et al. 2006) can be significantly increased through the type of binary evolution considered here. While a rejuvenated accretion star is somewhat more evolved than a zero-age main sequence star, this difference is small and leads only to the avoidance of a small fraction of the mass loss induced spin-down during core hydrogen burning. However, it is to be said that single stars which rotate initially with 90% of their break-up velocity might not form in nature (cf. Mokiem et al. 2006, and see below). Thus, perhaps the main benefit of the massive close binaries is just to produce very rapidly rotating O stars.

4.5 Discussion

The binary evolution model presented above shows that quasi-chemically homogeneous evolution may occur in mass gainers of low-metallicity massive early Case B binaries. The comparison of the mass gainer with a corresponding single star model made it clear that such binary components evolve in the same way as extremely rapidly rotating single stars. This confirms that the scenario of quasi-chemically homogeneous evolution might not be restricted to single stars, but may apply to the accreting component of massive close binaries as well.

While we provide only one example, it seems likely that this scenario applies to most massive close binary components which accrete or gain an appreciable amount of mass; this may encompass Case A binaries and early Case B binaries (Podsiadlowski et al. 1992; Wellstein & Langer 1999; Wellstein et al. 2001). Case A merger are also likely contributing to this scenario. While the merged object will have more mass than the initially more massive star in the binary, the product will be extremely rapidly rotating due to the orbital angular momentum, as in the case of some blue stragglers (Livio 1993).

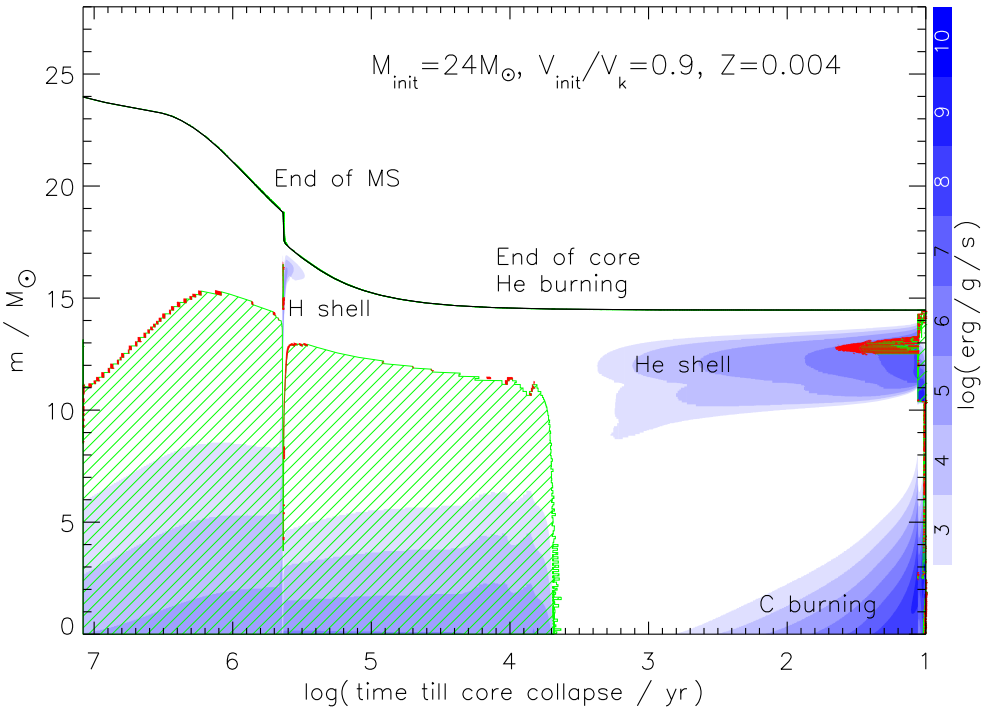

Figure 4.4: Evolution of the internal structure of a single star model with initial mass of 24 $M_\odot$ and initial rotation close to Keplerian ($v_{\rm init}/v_{\rm K}$=0.9). The evolution is shown from the zero-age main sequence to the end of O burning. Convective layers are hatched. Semi-convective layers are marked by dots (red dots in the electronic version). The gray (blue) shading gives nuclear energy generation rates in log scale, as indicated on the right side. The topmost solid line denotes the surface of the star.

4.5.1 Binaries and the distribution of rotational velocities

The best constraint so far on the distribution of initial rotational velocities (IRF) comes from the recent study of young O stars in the SMC, mostly from the cluster NGC 346 (Mokiem et al. 2006). According to Yoon et al. (2006), the three most rapid rotators from the sample of 21 O stars would qualify for the quasi-chemically homogeneous evolution scenario, and remarkably, all three stars are found to be helium-enhanced. The simplest approach to understand those stars is to assume that they correspond to the tip of the IRF.

However, that data of Mokiem et al. (2006) reveals another interesting feature: two of the the three mentioned stars are runaway stars, with radial velocities deviating from the average cluster radial velocity by 30 to 70 km s^{-1}. While dealing with low number statistics, this information opens another possibility: that the most rapidly rotating young O stars in the SMC are products of binary evolution. A closer examination of the IRF derived by Mokiem et al. (2006) appears to support this idea: While the three rapid rotators show $v \sin i \gtrsim 290$ km s^{-1}, all other stars have $v \sin i \lesssim 210$ km s^{-1}.

The following hypothesis therefore seems conceivable: The IRF of single O stars in the SMC ends at about 210 km s^{-1} — too early to allow quasi-chemically homogeneous evolution and collapsar formation. However, massive close binary evolution enhances the IRF to what we may call the apparent IRF as measured by Mokiem et al. (2006), which leads to the redshift dependent GRB rate as worked out by Yoon et al. (2006). According to the binary population synthesis model of Podsiadlowski et al. (1992), about 10% of all massive binaries might lead to a Case A merger or early Case B mass transfer, which is sufficient to populate the rapidly rotating part of the IRF of Mokiem et al. In that context, the rapidly rotating O star in the sample of Mokiem et al. (2006) which does not appear as runaway star could either have an undetected high proper motion, or it could be the result of a Case A merger — where no runaway is produced.

4.5.2 Effects from runaway GRBs

The runaway nature of a GRB progenitor, as obtained in our example, has important observational consequences for both the positions of GRBs, and their afterglow properties. Concerning the afterglow, it is relevant that the medium close to a WR star has the density profile of a free-streaming wind, and analytical and numerical calculations both suggest that the free wind of a single WR typically extends over many parsec (van Marle et al. 2006). However, from the analysis of GRB afterglows, a constant circumstellar medium density has been inferred in many cases (Chevalier & Li 2000; Panaitescu & Kumar 2001, 2002; Chevalier et al. 2004). A possible explanation has been proposed by van Marle et al. (2006), who simulated the circumstellar medium around a moving WR star. As the GRB jet axis is likely perpendicular to the space velocity vector, the jet escapes through a region of the bow-shock where the wind termination shock is very close to the star. Therefore, the jet may enter a constant density medium quickly in this situation.

Concerning the GRB positions, since the spin axis of the stars in a close binary system are likely orthogonal to the orbital plane, the observation of a GRB produced by the proposed binary channel is possible only if the binary orbit is seen nearly face on. Then the direction of motion of the runaway GRB progenitor must be orthogonal to the line of sight, allowing the progenitor, for the given space velocity, to obtain the maximum possible apparent separation from its formation region. The finding of Hammer et al. (2006), that the nearest three long gamma-ray bursts may be due to runaway stars is in remarkable agreement with our scenario. While the collapsar progenitor in our binary model travels only 200 pc before it dies, compared to the 400...800 pc deduced by Hammer et al. (2006), binary evolution resulting in higher runaway velocities are certainly possible (Petrovic et al. 2005a). It remains to be analyzed whether the runaway scenario is compatible with the finding that long GRBs are more concentrated in the brightest regions of their host galaxies than core collapse supernovae (Fruchter et al. 2006).

Acknowledgements We are grateful to the referee Stan Woosley, for his criticism which helped to significantly improve this paper.

CHAPTER 5

Pair creation supernovae at low and high redshift

N. Langer, C. A. Norman, A. de Koter, J.S. Vink, **M. Cantiello** & S.-C.Yoon
Astronomy & Astrophysics, 2007, **475**, L19-L23

Abstract Pair creation supernovae (PCSN) are thought to be produced from very massive low metallicity stars. The spectacularly bright SN 2006gy does show several signatures expected from PCSNe. Here, we investigate the metallicity threshold below which PCSN can form and estimate their occurrence rate. We perform stellar evolution calculations for stars of 150 $M_\odot$ and 250 $M_\odot$ of low metallicity ($Z_\odot/5$ and $Z_\odot/20$), and analyze their mass loss rates. We find that the bifurcation between quasi-chemically homogeneous evolution for fast rotation and conventional evolution for slower rotation, which has been found earlier for massive low metallicity stars, persists in the mass range considered here. Consequently, there are two separate PCSN progenitor types: (I) Fast rotators produce PCSNe from very massive Wolf-Rayet stars, and (II) Slower rotators that generate PCSNe in hydrogen-rich massive yellow hypergiants. We find that hydrogen-rich PCSNe could occur at metallicities as high as $Z_\odot/3$, which — assuming standard IMFs are still valid to estimate their birth rates — results in a rate of about one PCSN per 1000 supernovae in the local universe, and one PCSN per 100 supernovae at a redshift of $z = 5$. PCSNe from WC-type Wolf-Rayet stars are restricted to much lower metallicity.

5.1 Introduction

Pair creation supernovae (PCSNe) are thought to be produced by stars which are, and remain throughout their lives, very massive. As they are radiation pressure dominated, the electron-positron pair production occurring in their cores for temperatures in excess of $\sim 10^9\,K$ can decrease the adiabatic index below 4/3 and destabilize the core (Fowler & Hoyle 1964; Kippenhahn & Weigert 1990). While the most massive stars ($\gtrsim 260\,M_\odot$) are thought to collapse into black holes (Bond et al. 1984; Heger & Woosley 2002), the ensuing explosive oxygen burning may disrupt stars with initial masses in the range of $\sim 100\,M_\odot$...$260\,M_\odot$ and thus produce a pair creation supernova (Ober et al. 1983; Langer & El Eid 1986; Heger & Woosley 2002).

PCSNe have mostly been considered in the context of pre-galactic (Pop III) stars (Ober et al. 1983; Heger & Woosley 2002), since locally very massive stars are thought to lose mass at a high rate: a Galactic $120\,M_\odot$ star is expected to end as a Wolf-Rayet star with a mass of the order of $10\,M_\odot$ (Meynet & Maeder 2005). Heger et al. (2003) pointed out that there is a finite metallicity threshold below which PCSNe would occur, due to the strong metallicity dependence of massive star winds. However, this metallicity threshold has not been investigated in detail. The interest in this has been triggered by the recent supernova 2006gy, the brightest supernova which was ever found. Its properties might well correspond to a PCSN: its extreme brightness could relate to a large radius in combination with a high nickel mass (Smith et al. 2007; Scannapieco et al. 2005), and its slow evolution and expansion velocity correspond well to PCSN explosion models (Heger & Woosley 2002; Scannapieco et al. 2005). This raises the question of the likelihood of PCSNe occurring in the local universe. This question is intrinsically interesting, independent of the particular event of SN 2006gy.

To this end, we investigate the metallicity threshold for the occurrence of PCSNe. We perform stellar evolution calculations into the PCSN regime, to investigate the possible range of properties of PCSN progenitor stars. As the fate of potential PCSN progenitors depends mostly on stellar mass loss rates, we then discuss the relevant mass loss rates and derive metallicity thresholds for the main branches of PCSNe. Finally, we estimate the occurrence rate of PCSNe, and their progenitor stars, in the local universe and at high redshift.

5.2 Stellar evolution models

We have computed several stellar evolution sequences for initial masses of $150\,M_\odot$ and $250\,M_\odot$ at low-metallicity (Table 5.1). All physical ingredients and assumptions in these calculations are identical to the ones by Yoon et al. (2006, hereafter YLN06). In particular, the mass loss recipe of Kudritzki et al. (1989) with a metallicity scaling proportional to $(Z/Z_\odot)^{0.69}$ (Vink et al. 2001) was used to compute the mass loss rate of main sequence stars. This scaling is consistent with the empirically derived scaling law (Mokiem et al. 2007b). For Wolf-Rayet phases, mass loss was computed according to Eq. (1) of YLN06, which includes mass loss enhancement for metal-enriched surfaces, and a metallicity scaling as proposed by Vink & de Koter (2005). For cool stars, we used the mass loss rate of Nieuwenhuijzen & de Jager (1990) with a metallicity scaling of $(Z/Z_\odot)^{0.50}$. The scaling relations and the com-

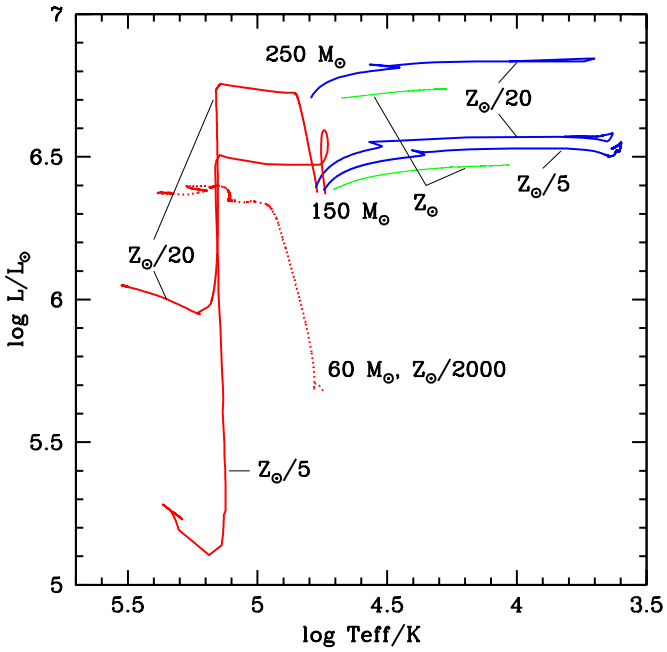

Figure 5.1: Evolutionary tracks of the computed sequences (Tab. 5.1) in the HR diagram, from the zero age main sequence to their pre-SN position. The two sequences which rotate rapidly initially (150 $M_\odot$; red lines) evolve quasi-chemically homogeneously, i.e. blueward, and end their evolution with an iron core collapse. The slow rotators (150 $M_\odot$ and 250 $M_\odot$; blue lines) become yellow hypergiants after the main sequence evolution. Additionally, the 60 $M_\odot$ rapid rotator ($v_{\rm rot,i}/v_{\rm Kepler} = 0.3$) for $Z/Z_\odot = 5\,10^{-4}$ from YLN06 is shown (red). Furthermore, solar metallicity tracks for 150 $M_\odot$ and 250 $M_\odot$ from Figer et al. (1998) are shown (green lines); they end during core hydrogen burning, when their surfaces become unstable.

puted stellar models are based on the Anders & Grevesse (1989) solar system heavy element distribution.

All sequences have been computed including the physics of rotation and rotationally induced mixing and magnetic fields, as in YLN06. We computed models for slow rotation, i.e. with an initial equatorial rotation rate of 10 km s^{-1}, and for fast rotation, adopting rotation at 500 km s^{-1} or about 40% of Kelperian rotation (Tab. 5.1). As for the low-metallicity stars of lower mass computed by YLN06, we find the rapid rotators to evolve quasi-chemically homogeneous. This is to be expected, since rotationally induced mixing is faster in more massive stars, where gas pressure becomes less and radiation pressure more important. YLN06 found quasi-chemically homogeneous evolution for $v_{\rm rot,i}/v_{\rm Kepler} > 0.2$ at 60 $M_\odot$, which was their largest considered mass. Our fast rotating 150 $M_\odot$ models (Sequences No. 2 and 4; Tab. 5.1) evolve quickly into Wolf-Rayet stars (Fig. 5.1), and lose large amounts of mass and angular momentum; they end at 7 $M_\odot$ ($Z/Z_\odot$=0.2) and 23 $M_\odot$ ($Z/Z_\odot$=0.05). Due to their

Table 5.1: Key properties of the computed sequences: initial mass, metallicity and rotation rate, total main sequence and post main sequence mass loss, final total, He-core and CO-core mass, pre-SN luminosity, effective temperature, and radius, and central temperature of last computed model, and fate (cc=iron core collapse, PCSN=pair creation supernova).

#	M_i	Z	$v_{\rm rot,i}$	$\Delta M_{\rm MS}$	$\Delta M_{\rm PMS}$	$M_{\rm f}$	$M_{\rm He,f}$	$M_{\rm CO,f}$	$L_{\rm f}$	$T_{\rm eff,f}$	$R_{\rm f}$	$T_{\rm c,end}$	fate
	$M_\odot$	$Z_\odot$	km s^{-1}	$M_\odot$	$M_\odot$	$M_\odot$	$M_\odot$	$M_\odot$	log $L/L_\odot$	K	$R_\odot$	10^8 K	
1	150	0.2	10	14	~ 90	~ 45	-	-	-	-	-	2.27	?
2	150	0.2	500	74	69	7	6.8	5.4	5.2	202 000	0.3	22.7	cc
3	150	0.05	10	4	53	93	71	64	6.5	4 200	3300	22.7	PCSN
4	150	0.05	500	31	96	23	23	22	6.0	315 000	0.4	50.1	cc
5	250	0.05	10	10	71	169	121	109	6.8	10 700	760	14.1	PCSN
	60	0.0005	400	0.02	8.5	51	51	46	6.4	219 000	1.1	20.6	cc

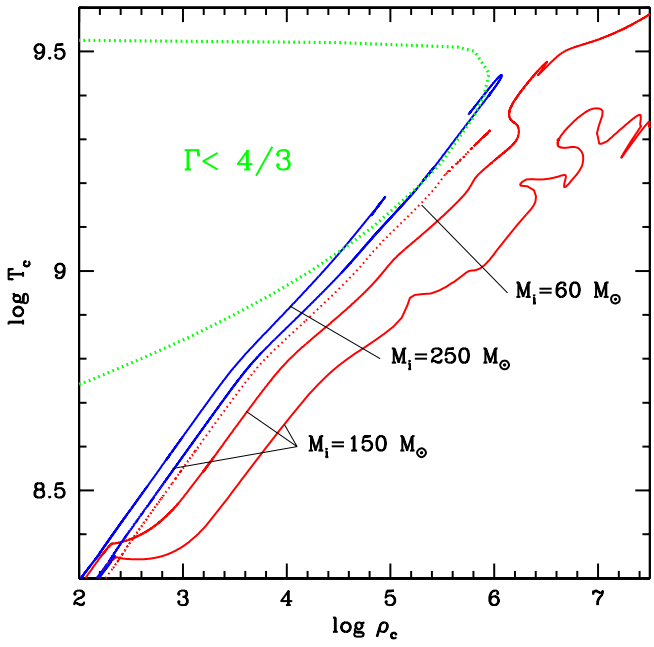

Figure 5.2: Evolutionary tracks of our stars in the $\log\rho_{\rm c} - \log T_{\rm c}$-diagram. The region of pair-instability is indicated ($\Gamma < 4/3$). The red lines correspond to our initially rapidly rotating 150 $M_\odot$ models for $Z=Z_\odot/5$ (lower curve) and $Z=Z_\odot/20$ (upper curve), and to the 60 $M_\odot$ model at $Z/Z_\odot = 5\,10^{-4}$ from YLN06 (dotted line). Shown in blue are the slowly rotating 150 $M_\odot$ model at $Z=Z_\odot/20$, and the 250 $M_\odot$ model at $Z=Z_\odot/20$.

reduced mass, they avoid the pair creation instability regime and undergo stable oxygen burning (Fig. 5.2), evolving towards iron core collapse. We also show the trajectory of a rapidly rotating ($v_{\rm rot,i}/v_{\rm Kepler} = 0.3$) 60 $M_\odot$ model at $Z/Z_\odot = 5\,10^{-4}$ of YLN06 in Figs. 5.1 and 5.2, to illustrate that, if strong mass loss is avoided — i.e. for low enough metallicity —, the chemically homogeneous models may also develop into PCSNe (Sect. 3.2). This model ends with a total mass of about 51 $M_\odot$ and will likely undergo iron core collapse, but Fig. 5.2 shows that it evolves very close to the PCSN regime.

As shown in Fig. 5.1, our slowly rotating models (Seq. No. 1, 3, 5) pursue more conventional tracks in the HR diagram and evolve redward after core hydrogen burning. The total amount of mass lost during core hydrogen burning is rather moderate for those models (Tab. 5.1); their surfaces do not become enriched by hydrogen burning products. After core hydrogen exhaustion, these stars evolve into cool supergiants. None of the models becomes cool enough to form dust; their effective temperatures remain higher than 4 200 K (see also Maeder & Meynet 2001). The lower metallicity models of 150 $M_\odot$ and 250 $M_\odot$ (Seq. No. 3 and 5) suffer significant mass loss during core helium burning. However, the helium core of both stars is not affected by the mass loss, and both models evolve into the pair creation instability and start collapsing before core oxygen ignition (Fig. 5.2)

According to our mass loss prescription, the 150 $M_\odot$ sequence at $Z/Z_\odot$=0.2 loses about all of its hydrogen-rich envelope during core helium burning. Numerical problems prevented us from computing this model to core helium exhaustion. An extrapolation of the mass loss rate during the core helium burning stage up to core helium exhaustion leads to expect a total mass loss during core helium burning of the order of 90 $M_\odot$; this would bring the star onto the Wolf-Rayet branch and into the core collapse regime. However, we can not exclude that this star would settle in the blue supergiant regime where mass loss is smaller. Therefore, the fate of this model remains uncertain.

5.3 PCSN metallicity thresholds

Most important for estimating the metallicity thresholds for PCSNe are the mass loss rates of very massive stars during their evolution. From the evolutionary models shown above, it is clear that for the rapid rotators, the Wolf-Rayet mass loss is detrimental. For slow rotators it is the mass loss on the main sequence, and in the cool supergiant stage. A problem in evaluating this quantitatively is that the required mass loss rates are not accessible observationally, and that theoretical estimates have to be stretched quite far to yield numbers in the required luminosity and metallicity range. In the following, we discuss mass loss for slowly and fast rotating models, separately.

5.3.1 Slow rotation

Our slowly-rotating 150 $M_\odot$ model at $Z/Z_\odot = 0.2$ has a main-sequence mass loss of only about 14 $M_\odot$. Ignoring, for the moment, mass loss in post-main sequence phases, this would be sufficiently low to allow for a PCSN. To estimate the critical metallicity $Z_{\rm PCSN,MS}$ above which already the main sequence mass loss in itself is such that a PCSN is no longer possible

Table 5.2: Estimated main sequence mass loss according to Vink et al. (2001), using $T_{\rm eff}$ = 40 000 K and $v_\infty/v_{\rm esc}$ = 2.6. For the 150 $M_\odot$ case, we adopted log $L/L_\odot$ = 6.5 and τ = 2.8 Myr, while for the 250 $M_\odot$ case log $L/L_\odot$ = 6.8 and τ = 2.5 Myr.

	150 $M_\odot$		250 $M_\odot$	
Z	log $\dot{M}$	ΔM	log $\dot{M}$	ΔM
$Z_\odot$	-4.46	96	-4.10	200
$Z_\odot/3$	-4.87	38	-4.51	77
$Z_\odot/10$	-5.32	13	-4.96	27
$Z_\odot/30$	-5.73	5	-5.37	11

— i.e. when it exceeds, say, a third of the initial stellar mass — we use the Vink et al. (2001) mass-loss recipe. Note that the predicted absolute mass loss rates following from this recipe are on average some 50 percent higher than those from the Kudritzki et al. (1989) prescription which we used in computing our models. Also, the estimates given in Tab. 5.2 are based on a representative mass-loss rate for the entire main sequence (see Table caption). Keeping these uncertainties in mind, we find that $Z_{\rm PCSN,MS}/Z_\odot$ is about 1/3.

Currently, the main sequence mass-loss rates of O and early-B type stars are under debate (Bouret et al. 2005; Fullerton et al. 2006). Empirical rates may have been overestimated because of the neglect of density inhomogeneities (or clumping) in the spectroscopic analysis of wind sensitive lines. Mokiem et al. (2007b) show that if the clumping is modest, observations will match with the Vink et al. predictions. If, however, clumping in the outflows of these stars is severe, theoretical mass-loss rates may be significantly overestimated. In that case, the critical metallicity $Z_{\rm PCSN,MS}$ may be even be super-solar. Here, we do not consider this possibility.

Baraffe et al. (2001) investigated the pulsational instabilities of PCSN progenitors of various metallicities, in order to estimate pulsation driven mass loss rates for those stars. While they found the ε-mechanism to be unimportant, the κ-mechanism was found to occur in 120 $M_\odot$ main sequence models of solar and half-solar metallicity, but not at $Z_\odot/100$ or below. However, the local character of the stability analysis did not allow Baraffe et al. to estimate mass loss rates from pulsations driven by the κ-mechanism.

The post main sequence mass loss of slowly rotating potential PCSN progenitors, i.e. for yellow supergiants, is more difficult to assess. None of our models evolves into the red supergiant regime, where dust formation might boost the mass loss rate. However, one important question is whether the stars, on their way to cool temperatures, would become Luminous Blue Variables (LBVs) and suffer from eruptive mass loss. While a good theoretical understanding of the LBV phenomenon is still lacking, metal-rich models of very massive stars do become unstable for effective temperatures significantly below 20 000 K, as these models have high enough Rosseland-mean opacities in their outermost layers to hit the Eddington limit (Figer et al. 1998, Fig. 1). Our low metallicity models here do not encounter this problem (see also Maeder & Meynet 2001). We take this as an indication that an LBV-type mass loss can be avoided at the metallicities considered here.

The yellow supergiant mass loss rate is very uncertain. The metallicity-scaled rate of

Nieuwenhuijzen & de Jager (1990) as used in our models implies a post-main sequence wind induced metallicity threshold for PCSN between $Z/Z_\odot$=0.2 and $Z/Z_\odot$=0.05: The post main sequence mass loss of sequences #1 and #3 is $\sim 90\,M_\odot$ and $53\,M_\odot$, which certainly in the latter case leaves a massive enough CO-core to undergo PCSN (see Tab. 5.1 and Fig. 5.2). However, the physics of the winds from yellow supergiants is not well understood, and the applied metallicity scaling might be inappropriate for cool stars. Schröder & Cuntz (2005) work out a mass loss rate based on the physics of thermally driven winds, in which case no metallicity dependence is expected. Schröder & Cuntz (2007) show that this mass loss rate fits observations well over the whole observationally accessible dwarf, giant and supergiant regime (up to $\log L/L_\odot \simeq 5$). If we extrapolate it to our $150\,M_\odot$ models at $T_{\rm eff} = 4000\,$K, we obtain a mass loss rate of $1.9\,10^{-5}\ M_\odot\ {\rm yr}^{-1}$, or a total mass loss of $5.2\,M_\odot$ over the post main sequence life time. Interestingly, the pre-SN mass loss rate of SN 2006gy is constrained by the soft X-ray measurements to $1...5\,10^{-4}\ M_\odot\ {\rm yr}^{-1}$, which, extrapolated over $3\,10^5\,$yr would result in a mass loss of $30...140\,M_\odot$. We conclude that, while there is a large uncertainty, the consideration of post main sequence mass loss can currently not be used to exclude PCSNe from slowly rotating massive stars with metallicities below the value of $Z_{\rm PCSN,MS}/Z_\odot = 1/3$.

5.3.2 Fast rotation

The fast rotating PCSN progenitor candidates undergo quasi-chemically homogeneous evolution (Yoon & Langer 2005; Yoon et al. 2006; Woosley & Heger 2006). This will lead to a smaller minimum initial mass for PCSN formation if mass loss is negligible (see below). The quasi-chemically homogeneous models evolve into Wolf-Rayet stars already during core hydrogen burning. As the mass loss rates during the core hydrogen burning Wolf-Rayet stage is significantly higher than the mass loss rate of the slowly rotating counterparts (Tab. 5.1), our rapidly rotating $150\,M_\odot$ star at $Z/Z_\odot$=0.2 loses already $74\,M_\odot$ during core hydrogen burning, which disqualifies it as a PCSN progenitor (Fig. 5.2). However, during the core hydrogen burning Wolf-Rayet stage, photon scattering with iron ions provides the main force to drive the stellar wind, which is strongly decreasing at least down to metallicities of $Z/Z_\odot = 10^{-4}$ (Vink & de Koter 2005). Consequently, looking at our rapidly rotating models (Tab. 5.1), rapid rotators may only evolve into a PCSN if their metallicity is below $Z/Z_\odot$=0.05.

During the post-main sequence evolution, the surfaces of the rapid rotators are quickly enriched with carbon and oxygen, transforming them into WC-type Wolf-Rayet stars. This enhances the mass loss rate, especially for $Z/Z_\odot < 0.1$ (Vink & de Koter 2005). The final masses of our rapidly rotating $150\,M_\odot$ sequences are $7\,M_\odot$ and $23\,M_\odot$, indicating that the metallicity limit to allow for PCSNe from initially rapidly rotating stars is much smaller than $Z/Z_\odot$=0.05. Vink & de Koter (2005) predict that the WC-type mass loss rate reaches a lower limit at about $Z/Z_\odot = 10^{-4}$, and extrapolating their results to $150\,M_\odot$ and $250\,M_\odot$ predicts only about $4\,M_\odot$ and $9\,M_\odot$ being lost during the WC stage at $Z/Z_\odot = 10^{-4}$. Therefore, PCSNe are likely to occur from the lowest metallicity rapid rotators. This agrees with the fact that the rapidly rotating $60\,M_\odot$ models at $Z/Z_\odot = 5\,10^{-4}$ of YLN06 lose only about $10\,M_\odot$ and are actually very close to the pair-instability (Figs. 5.1 and 5.2). We conclude that the metallicity threshold for PCSN from the rapidly rotating branch is roughly at $Z/Z_\odot = 10^{-3}$.

Table 5.3: PCSN-to-SN ratios at various redshifts z, for two different PCSN-metallicity thresholds $Z_{\rm PCSN}$ (first 2 lines), and for PCSNe from rapid rotators with a metallicity threshold of $Z_\odot/1000$. Here $f_{\rm r}$ is the fraction of rapid rotators; according to YLN06 (their Fig. 5), it might be $f_{\rm r} \simeq 0.25$.

$Z_{\rm PCSN}$	$z = 0$	$z = 2$	$z = 5$
$Z_\odot/3$	0.001	0.004	0.01
$Z_\odot/10$	0.0001	0.001	0.004
$Z_\odot/1000$	$4\,10^{-7} f_{\rm r}$	$10^{-6} f_{\rm r}$	$10^{-5} f_{\rm r}$

5.4 Observational consequences

In the following, we want to discuss occurrence and detection rates of PCSNe at various redshifts. For this purpose, we assume that slowly rotating massive stars produce PCSNe for initial masses in the range $140\,M_\odot$ to $260\,M_\odot$ (Heger & Woosley 2002) and for $Z/Z_\odot < 1/3$, while rapid rotators do so for initial masses above $80\,M_\odot$ and for $Z/Z_\odot < 1/1000$. The uncertainties in the post-main sequence mass loss rates discussed above imply that this way we derive upper limits to the occurrence and detection rates.

The occurrence rate of PCSNe depends decisively on the formation rate of stars with masses above the mentioned limits. Not much is known about that, due to the strong decline of the initial mass function (IMF) with mass. Figer (2005) finds that in the Arches cluster close the the Galactic center, there is a firm upper limit to the IMF at $150\,M_\odot$. On the other hand, Kudritzki et al. (1996) give evidence for stars with masses of up to $200\,M_\odot$ in the LMC. In any case, PCSN initial masses could be lower than the numbers suggested by Heger & Woosley (2002), either due to rotational mixing (Sect. 3.2) or due to efficient convective core overshooting (Langer & El Eid 1986) which is not well constrained at the considered masses. In lieu of more meaningful constraints especially at low metallicity, we simply use the Salpeter IMF to estimate the birth rate of PCSN progenitors. This results in stars above $140\,M_\odot$ making up for about 1% of all stars above the supernova threshold of $8\,M_\odot$, while stars above $80\,M_\odot$ amount to about 3.6%.

5.4.1 Local universe

In the local universe, the ratio of the birth rate of massive stars with $Z/Z_\odot < 1/3$ to that of all massive stars is about $1/10$ (Langer & Norman 2006), which then results in a local PCSN/SN-ratio of about 1/1000 (Tab. 5.3). Most PCSNe locally are expected to occur in yellow hypergiants with massive hydrogen-rich envelopes, since PCSNe produced from initially rapidly rotating stars are expected to be negligible in the local universe. The large radii of these PCSN progenitors (Tab. 5.2) will lead to very bright events (Young 2004; Scannapieco et al. 2005). The large ejecta mass and slow expansion velocity of PCSNe (Heger & Woosley 2002; Scannapieco et al. 2005) implies a supernova light curve with a broad maximum. All this appears to be consistent with SN2006gy (Ofek et al. 2007; Smith et al. 2007).

If SN2006gy were a typical PCSN, it being about 10 times brighter, and shining about twice as long as an average supernova (Fig. 2 in Smith et al. 2007) would imply an increased

detection probability of $2 \times 10^{3/2} \simeq 60$ for PCSNe. I.e., the ratio of the detection probability of a PCSN to that of an average supernova in a local magnitude-limited search would work out to be 0.06, a number which appears too high to account for only one observed case. Thus, either SN2006gy is not a typical PCSN, or the PCSN metallicity threshold is lower than $Z_\odot/3$.

In fact, Herzig et al. (1990) derived realistic light curves for PCSNe, and considering compact progenitor models for PCSNe at the lower mass limit. They found a maximum bolometric brightness of only $M_{\rm bol} \simeq -14.6$ mag, compared to $M_{\rm bol} \simeq -22$ mag for SN2006gy (Smith et al. 2007). This is consistent with only small amounts of ^{56}Ni being produced in the lower third or so of the PCSN progenitor mass range according to Heger & Woosley (2002), while the nickel mass implied for SN2006gy is of the order of $20\,M_\odot$ (Smith et al. 2007), which would require a progenitor mass in the upper part of the PCSN progenitor mass range. On the other hand, our slowly rotating $150\,M_\odot$ model at $Z_\odot/20$ (Seq. #3) explodes with a very large radius ($3300\,R_\odot$; Table 5.1), which may lead to a high peak brightness even without a large amount of radioactive energy input (Young 2004).

Scannapieco et al. (2005) compute light curves of population III PCSNe, and find a wide range of peak luminosities and light curve peak widths. Furthermore, the fraction of stars which rotates rapidly enough to undergo chemically homogeneous evolution (YLN06) does not contribute significantly to the number of PCSN in the local universe. Additionally, supernova searches are not optimally designed to find bright, rare objects with long ($\sim 1yr$) time variations. Thus, for a PCSN metallicity threshold of $Z_\odot/3$, the detection PCSN probability may be of the order 0.001/SN if their progenitors form according to a Salpeter IMF. Adopting a star formation rate in the local universe of $0.0063\,M_\odot\,{\rm yr}^{-1}\,{\rm Mpc}^{-1}$ (Bouwens et al. 2004) results in about one PCSN per year within a radius of 100 Mpc for $Z_{\rm PCSN} = Z_\odot/3$, and one per 10 years for $Z_{\rm PCSN} = Z_\odot/10$. We note that the metallicity of NGC 1260, the S0/Sa peculiar host of SN 2006gy, is estimated from the Mg_2 index to be $\gtrsim Z_\odot/2$ (Ofek et al. 2007). Given the theoretical and observational uncertainties, we do not consider this as evidence against SN 2006gy being a PCSN.

We want to point out that also the progenitors of PCSNe might be detectable in the local universe. They have luminosities in the range $\log L/L_\odot \simeq 6.4...6.9$ and since they have only small bolometric corrections this translates into $M_{\rm bol} \simeq M_{\rm V} \simeq -11.2... - 12.5$ mag. This makes them 13^{th} magnitude stars at 1 Mpc distance. Even the progenitor of SN 2006gy at a distance of 73 Mpc (Smith et al. 2006) might have been visible with $m_{\rm V} \simeq 22$ mag, or with $m_{\rm V} \simeq 24$ mag including two magnitudes extinction (Smith et al. 2007). For the local star formation rate quoted above, we expect about 200 000 yellow hypergiant progenitors for $Z_{\rm PCSN} = Z_\odot/3$, and ten times less for $Z_{\rm PCSN} = Z_\odot/10$, within a radius of 100 Mpc.

The Small Magellanic Cloud may be a local test case for the PCSN metallicity threshold. If its metallicity ($\sim Z_\odot/5$) is below the threshold, then from the number ratio of O to WR stars of 0.015 (with O stars being stars more massive than about $15\,M_\odot$), and about 10 WR stars (Azzopardi et al. 1988), we expect about 14 O stars stars above $140\,M_\odot$, and about one PCSN progenitor in the YSG phase, and a PCSN rate of the order of $10^{-6}\,{\rm yr}^{-1}$. We believe that none of these numbers can exclude that the SMC metallicity is indeed below the PCSN threshold.

5.4.2 High z, low Z universe.

The formalism of Langer & Norman (2006) allows to compute the occurrence rates of PCSNe in the high redshift universe for different metallicity thresholds. Tab. 5.3 shows that at redshift $z = 2$, the PCSN/SN ratio is 4 or 10 times higher than locally, for $Z_{\rm PCSN} = Z_\odot/3$ and $Z_{\rm PCSN} = Z_\odot/10$, respectively. In the first case, the metallicity bias for PCSNe has vanished at redshift $z = 5$. The fraction of PCSNe from rapid rotators remains negligible even out to a redshift of $z = 5$. However, PCSNe from rapid rotators may be more numerous in the Pop III era.

In environments with $Z < Z_{\rm PCSN}$, PCSNe may also significantly contribute to the nucleosynthesis. Even though PCSNe constitute only 1% of the supernovae in that case, they encompass 10% of the mass which star formation incorporates into supernova progenitors. And while core collapse supernovae produce from zero up to a few solar masses, a PCSN liberates 50...120 $M_\odot$ of metals; i.e., PCSNe might produce about half of all metals (Heger & Woosley 2002; Umeda & Nomoto 2002). Thus, the consideration of their yields may significantly constrain the number of PCSNe. Extensive PCSN yields have been computed so far only for $Z = 0$, and the lack of an odd-even pattern in intermediate mass elements of extremely metal-poor halo stars appears to question the existence of Population III PCSNe (Heger & Woosley 2002; Umeda & Nomoto 2002, 2005). Detailed nucleosynthesis calculations for PCSNe at $Z \simeq Z_\odot/3$ are presently not available, but Heger & Woosley's zero metallicity PCSN models show a "surprising overall approximate agreement" with solar system abundances in the range oxygen to nickel. Ballero et al. (2006) find that the nucleosynthesis signature of Pop III PCSNe can not affect the predicted abundance ratios for the evolution of the Milky Way, even in its earliest evolutionary phase. Therefore, it may be difficult to rule out a PCSN metallicity threshold as high as $Z \simeq Z_\odot/3$ on nucleosynthesis reasons at present. Metallicity dependent PCSN yields and subsequent chemical evolution modeling is needed to obtain more stringent constraints on $Z_{\rm PCSN}$ from nucleosynthesis.

In general, detecting low redshift PCSNe and understanding their physical properties will be a significant help in designing observational studies to observe PCSNe with JWST at high redshift and very low metallicity.

Acknowledgments This work largely benefited from discussions during the Lorentz-Center workshop "From massive stars to supernova remnants" in Leiden held in Aug. 2007. Support for this work was provided by the National Aeronautics and Space Administration through Chandra Award Number GO6-7130X, and by the National Aeronautics and Space Administration under Grant NNG04GQ04G.

CHAPTER 6

Thermohaline mixing in evolved low mass stars

M. Cantiello & N. Langer

Astronomy & Astrophysics, submitted

Abstract Thermohaline mixing has recently been proposed to occur in low mass red giants, with large consequence for the chemical yields of low mass stars. We investigate the role of thermohaline mixing during the evolution of stars between $1\,M_\odot$ and $3\,M_\odot$, in comparison to other mixing processes acting in these stars. We use a stellar evolution code which includes rotational mixing, internal magnetic fields and thermohaline mixing. We confirm that during the red giant stage, thermohaline mixing has the potential to decrease the abundance of ^{3}He which is produced earlier on the main sequence. In our models we find that this process is working on the RGB only in stars with initial mass $M \lesssim 1.5\,M_\odot$. Moreover we report that thermohaline mixing is present also during core helium burning and beyond, and has the potential to change the surface abundances of AGB stars. While rotational and magnetic mixing is negligible compared to the thermohaline mixing in the relevant layers, the interaction of thermohaline motions with the differential rotation may be essential to establish the time scale of thermohaline mixing in red giants. To explain the surface abundances observed at the bump in the luminosity function, the speed of the mixing process needs to be more than two orders of magnitude higher than in our models. We argue that such a mixing efficiency is unlikely, due to the fact that blobs, and not fingers, are the most probable geometrical configuration for thermohaline mixing in stellar interiors. Therefore it is not possible at this stage to firmly identify thermohaline mixing as the cause of the anomalies in the surface abundances of low-mass giants. In particular the long standing ^{3}He problem can not be considered solved. In agreement with the work of Charbonnel & Zahn (2007), we claim that to clarify the picture it would be desiderable to have realistic hydrodynamic simulations of thermohaline mixing.

6.1 Introduction

Stars are rotating, self-gravitating balls of hot plasma. Due to thermonuclear reactions in the deep stellar interior, stars, which presumably start out chemically homogeneous, develope chemical inhomogeneities. At the densities typically achieved in stars, thermal diffusion, or Brownian motion, is not able to lead to chemical mixing. However, various turbulent mixing processes are thought to act inside stars, leading to transport of chemical species, heat, angular momentum, and magnetic fields (Pinsonneault 1997; Heger et al. 2000, 2005).

Thermohaline mixing is usually not considered as an important mixing process in single stars, since the ashes of thermonuclear fusion consists of heavier nuclei than its fuel, and stars usually burn from the inside out. The condition for thermohaline mixing, however, is that the mean molecular weight (μ) decreases inward. This can occur in accreting binaries, and the importance of thermohaline mixing has been long recognized by the binary community (e.g., de Greve & Cugier 1989; Sarna 1992; Wellstein et al. 2001). Recently Charbonnel & Zahn (2007, CZ07) identified thermohaline mixing as an important mixing process which significantly modifies the surface composition of red giants after the first dredge-up. The work by CZ07 was triggered by the paper of Eggleton et al. (2006, EDL06), who found an mean molecular weight (μ) inversion — i.e., $\left(\frac{d\log\mu}{d\log P}\right) < 0$ — below the red giant convective envelope in a 1D-stellar evolution calculation. While EDL06 then investigated the stability of the zone containing the μ-inversion with a 3D hydro-code and found these layers to be Rayleigh-Taylor-unstable, CZ07 could not confirm this, but found the layers to be unstable due to thermohaline mixing.

EDL06 found a μ-inversion in their 1 $M_\odot$ stellar evolution model, occurring after the so-called luminosity bump on the red giant branch, which is produced after the first dredge-up, when the hydrogen burning shell source enters the chemically homogeneous part of the envelope. The μ-inversion is produced by the reaction ^{3}He(^{3}He,2p)^{4}He, as predicted by Ulrich (1972). It does not occur earlier, since the magnitude of the μ-inversion is small, and negligible compared to a stabilizing μ-stratification.

Mixing processes below the convective envelope in models of low mass stars turns out to be essential for the prediction of their chemical yield of ^{3}He (EDL06), and are essential to understand the surface abundances of red giants — in particular the ^{12}C/^{13}C ratio, ^{7}Li and the carbon and nitrogen abundances (CZ07). This may also be important for other occurrences of thermohaline mixing in stars, i.e., in single stars when a μ-inversion is produced by off-center ignition in semi-degenerate cores (Siess 2009), or in stars which accrete chemically enriched matter from a companion in a close binary (e.g., Stancliffe et al. 2007). Accreted metal-rich matter during the phases of planetary formation also leads to thermohaline mixing, which can reconcile the observed metallicity distribution of the central stars of planetary systems (Vauclair 2004).

In the present paper, we investigate the evolution of solar metallicity stars between 1 $M_\odot$ and 3 $M_\odot$ from the ZAMS up to the thermally-pulsing AGB stage, based on models computed during the last years. We show for which initial mass range, and during which evolutionary phase thermohaline mixing occurs, and with which consequences. Besides thermohaline mixing, our models include convection, rotation-induced mixing, and internal magnetic fields, and we compare the significance of these processes in relation to the thermohaline mixing.

6.2 The speed of thermoaline mixing

6.2.1 Thermohaline mixing VS Rayleigh-Taylor

As pointed out by CZ07, a μ-inversion inside a star should give rise to thermohaline mixing, which is a slow mixing process acting on the local thermal time scale. Could a Rayleigh-Taylor instability be present in these layers? In fact, EDL06 interprete the origin of the instability which they find in their 3D models as due to the buyoncy $g\left(\frac{\Delta\mu}{\mu}\right)$ produced by the μ-inversion, i.e. a dynamical effect. But a dynamical instability should only occur if the μ-inversion would lead to a density inversion. However, this would only be possible if the considered layers were convectively unstable in the hydrostatic 1D stellar evolution models. As pointed out by CZ07, and as confirmed by our models, the μ-inversion produced by the ^{3}He(^{3}He,2p)^{4}He reaction does not induce convection. We conclude that the Rayleigh-Taylor instability may not be a likely explanation of the hydrodynamic motions found by EDL06. A similar conclusion was also reached by Denissenkov & Pinsonneault (2008), who studied in details the instability driven by the μ-inversion in both the adiabatic and the radiative limit.

Since smaller blobs have a smaller thermal time scale (Kippenhahn et al. 1980), could EDL06 have found the high wavenumber tail of the thermohaline instability? ELD06 found the instability to occur within 2000 s. The size of a blob with such a short thermal timescale above the hydrogen burning shell of a red giant is of the order of 50 km. This is too small to be resolved in the 3D model shown by ELD06. Furthermore, inspection of their Fig. 5 reveals that the length scale of the instability they found is of the order of 10^3...10^4 km, which corresponds to thermal time scales of about 1 yr. Therefore, it seems unlikely that EDL06 actually picked up the thermohaline instability in their 3D hydrodynamic model, unless its non-linear manifestation involves a much shorter than the thermal time scale.

6.2.2 The efficiency of thermohaline mixing

In Section 6.3 we explain the details of the implementation of thermohaline mixing in 1D stellar evolution calculations. The diffusion coefficient for the mixing process contains a parameter, which depends on the geometrical configuration of the fluid elements. This parameter ($\alpha_{\rm th}$) is very important to understand the role of thermohaline mixing. It determines the timescale of the mixing (the velocity of the fingers/blobs) that we show in Section 6.4 and 6.5 plays a role not only in determining how fast the surface abundances of red giants can change, but also if thermohaline mixing is present in stars of different mass and at different evolutionary phases.

Charbonnel & Zahn (2007) showed that a high value of $\alpha_{\rm th}$ is needed to match the surface abundances of field stars after the luminosity bump (Gratton et al. 2000). Similar to the value adopted by Ulrich (1972) they use an efficiency factor corresponding to $\alpha_{\rm th} = 667$ in our diffusion coefficient. This value corresponds to the diffusion process involving fingers with an aspect ratio (length/width) of 5. In their work Denissenkov & Pinsonneault (2008) claim that to explain the observed mixing pattern in low mass RGB stars, fluid elements have to travel over length scales exceeding their diameters by a factor of 10 or more.

On the other hand, the order of magnitude of our efficiency parameter $\alpha_{\rm th} = 2.0$ corresponds to the prescription of Kippenhahn et al. (1980), where the diffusion process involves blobs of size L traveling a mean free path L before dissolving. The same prescription has been used recently by Stancliffe et al. (2007), who dealt with the problem of thermohaline mixing in accreting binaries. The sensitivity of thermohaline mixing to a change of the efficiency parameter is shown in Fig. 6.1, where the change of the surface abundance of ^{3}He at the luminosity bump is shown for different values of $\alpha_{\rm th}$.

The fact that a prescription can reproduce the observed surface abundances may not be sufficient to prefer it over others. It is possible that other mixing processes are at work. The resulting observed abundances could still be mainly due to thermohaline mixing, as proposed by CZ07, but at this stage is not possible to exclude that magnetic buoyancy (Busso et al. 2007; Nordhaus et al. 2008), or the interaction of different mixing processes (e.g., thermohaline mixing and magnetic buoyancy, Denissenkov et al. 2009), could play an even more important role.

To clarify the picture we discuss here the main differences between the two physical prescriptions for thermohaline mixing, trying to evaluate which one is more adequate to stellar interiors. Experiments of thermohaline mixing show slender fingers in the linear regime (e.g., Krishnamurti 2003), supporting the picture of Ulrich (1972). On the other hand the physical conditions inside a star are quite different than in the laboratory. In particular the Prandtl number σ, defined as the ratio of the kinematic viscosity ν to the thermal diffusivity κ_T, is very small in stars ($\sigma \sim 10^{-6}$). This number is about 7 in water, where most of thermohaline mixing experiments have been performed. The question arise if for such small values of σ a finger-like structure can be stable, especially in layers where shear and horizontal turbulence is present. 2D hydrodynamic simulations of double-diffusive phenomena, in the absence of external perturbations, have been performed in the past (e.g., Merryfield 1995; Bascoul 2007b). While the resolution required by the physical conditions in stellar interiors is computationally not accessible, lowering the Prandtl number down to values of about 10^{-2} always results in increasingly unstable structures (Merryfield 1995; Bascoul 2007a). Therefore it seems unlikely that the same configuration of thermohaline mixing, as observed in water, is occurring in stars.

As we will show in Section 6.6, the radiative buffer between the H-burning shell and the convective envelope is a region of the star where the angular velocity is rapidly changing. Even if the order of magnitude of the rotationally-induced instabilities is much lower than the one from thermohaline mixing (cf. Fig 6.8), it is possible that the interaction of the shear motions with the thermohaline diffusion is preventing a relatively ordered flow to be stable, contrary to Ulrich's assumption. The fact that shear can decrease the efficiency of thermohaline mixing was already pointed out by Canuto (1999). The effect of strong horizontal turbulence in stellar layers has also been discussed by Denissenkov & Pinsonneault (2008), and we conclude in Section 6.6 that this effect could work against the fingers and in favor of blobs.

All these considerations seem to point toward the thermohaline mixing prescription proposed by Kippenhahn et al. (1980), which therefore has been used for the calculations presented in this work.

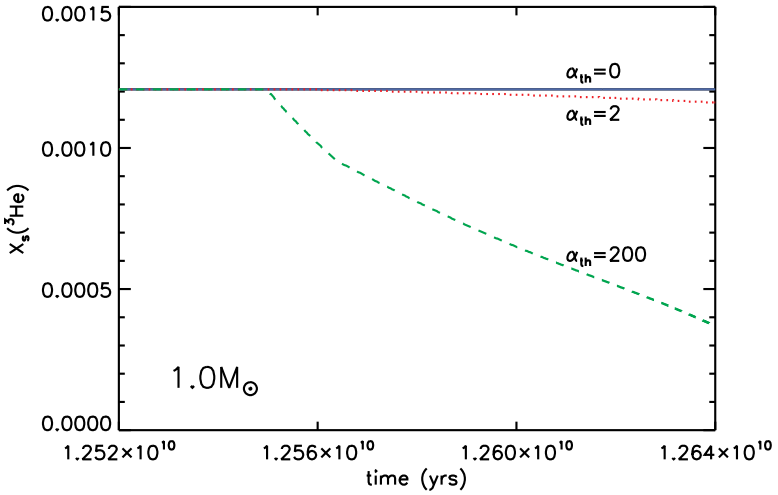

Figure 6.1: Evolution of the surface abundance of ^{3}He for $\alpha_{th} = 0$ (blue solid line), $\alpha_{th} = 2$ (red dotted line) and $\alpha_{th} = 200$ (green dashed line) from before the onset of thermohaline mixing to core He-flash in a 1.0 $M_\odot$ star.

6.3 Method

We use a 1-D hydrodynamic stellar evolution code (Yoon et al. 2006, and references therein). Mixing is treated as a diffusive process and is implemented by solving the diffusion equation

$$\left(\frac{\partial X_n}{\partial t}\right)_m = \left(\frac{\partial}{\partial m}\right)_t \left[(4\pi r^2 \rho)^2 \, D \left(\frac{\partial X_n}{\partial m}\right)_t\right] + \left(\frac{\mathrm{d}X_n}{\mathrm{d}t}\right)_{\mathrm{nuc}} \tag{6.1}$$

where D is the diffusion coefficient constructed from the sum of individual mixing processes and X_n, the mass fraction of species n. The second term on the right hand side accounts for nuclear reactions. The contributions to the diffusion coefficient are convection, semiconvection, thermohaline mixing, rotationally induced mixing and magnetic diffusion. The code includes the effect of centrifugal force on the stellar structure and the transport of angular momentum is also treated as a diffusive process (Endal & Sofia 1978; Pinsonneault et al. 1989).

The condition for the occurrance of thermohaline mixing is

$$\frac{\varphi}{\delta} \nabla_\mu \leq \nabla - \nabla_{\mathrm{ad}} \leq 0 \tag{6.2}$$

i.e. the instability operates in regions that are stable against convection (according to the Ledoux criterion) and where an inversion in the mean molecular weight is present. Here $\varphi = (\partial \ln \rho / \partial \ln \mu)_{P,T}$, $\delta = -(\partial \ln \rho / \partial \ln T)_{P,\mu}$, $\nabla_\mu = d \ln \mu / d \ln P$, $\nabla_{ad} = (\partial \ln T / \partial \ln P)_{ad}$, and $\nabla = d \ln T / d \ln P$. Numerically, we treat thermohaline mixing through a diffusion scheme

(Braun 1997; Wellstein et al. 2001). The corresponding diffusion coefficient is based on the work of Stern (1960), Ulrich (1972), and Kippenhahn et al. (1980); it reads

$$D_{th} = -\alpha_{\rm th} \frac{3K}{2\rho c_P} \frac{\frac{\varphi}{\delta}\nabla_\mu}{(\nabla_{\rm ad} - \nabla)} \tag{6.3}$$

where ρ is the density, $K = 4acT^3/(3\kappa\rho)$ the thermal conductivity and $c_P = (dq/dT)_P$ the specific heat capacity. The quantity $\alpha_{\rm th}$ is a efficiency parameter for the thermohaline mixing. The value of this parameter depends on the geometry of the fingers arising from the instability and is still a matter of debate (Ulrich 1972; Kippenhahn et al. 1980; Charbonnel & Zahn 2007; Denissenkov & Pinsonneault 2008). As explained in Section 6.2.2, in this paper, unless otherwise specified, a value $\alpha_{\rm th} = 2.0$ is assumed for the efficiency of thermohaline mixing. This value corresponds roughly to the prescription of Kippenhahn et al. (1980), in which fluid elements (blobs) travel over length scales comparable to their diameter.
For rotational mixing, four different diffusion coefficients are calculated for dynamical shear, secular shear, Eddington-Sweet circulation and Goldreich-Schubert-Fricke instability. Details on the physics of these instabilities and their implementation in the code can be found in Heger et al. (2000).

Chemical mixing and transport of angular momentum due to magnetic fields (Spruit 2002) is included as in Heger et al. (2005). The contribution of magnetic fields to the mixing is also calculated as a diffusion coefficient ($D_{\rm mag}$) that is added to the total diffusion coefficient D that enters Equation 6.1.

We compute evolutionary models of 1.0 $M_\odot$, 1.5 $M_\odot$, 2.0 $M_\odot$ and 3.0 $M_\odot$ at solar metallicity (Z=0.02). The initial equatorial velocities of these models were chosen to be 10, 45, 140 and 250 km s^{-1} (Tassoul 2000); we assume the stars rigidly rotating at the zero-age main sequence. Throughout the evolution of all models, the mass loss rate of Reimers (1975) was used. These models are the same discussed by Suijs et al. (2008), even if for this work some late evolutionary phases have been re-run with a different value of $\alpha_{\rm th}$.

6.4 Mixing on the Giant Branch

The evolutionary calculations presented are the same as in Suijs et al. (2008), to which we refer for the details of their main sequence evolution.

The surface composition of low mass stars is substantially changed during the first dredge-up: lithium and carbon abundances as well as the carbon isotopic ratio decline,^{3}He and nitrogen abundances increase. After the first dredge-up the hydrogen burning shell is advancing while the convective envelope retreats; the shell source then enters the chemically homogeneous part of the envelope. EDL06 and CZ07 have shown that in this situation an inversion in the molecular weight is created by the reaction ^{3}He(^{3}He,2p)^{4}He in the outer wing of the hydrogen burning shell in models of 1.0 and 0.9 $M_\odot$. Such inversion was already predicted by Ulrich (1972).

We compute stellar models of 1.0, 1.5, 2.0 and 3.0 $M_\odot$ with solar metallicity. We confirm the presence of an inversion in the mean molecular weight in the outer wing of the H-burning shell. This inversion occurs after the luminosity bump on the red giant branch in the 1.0, 1.5

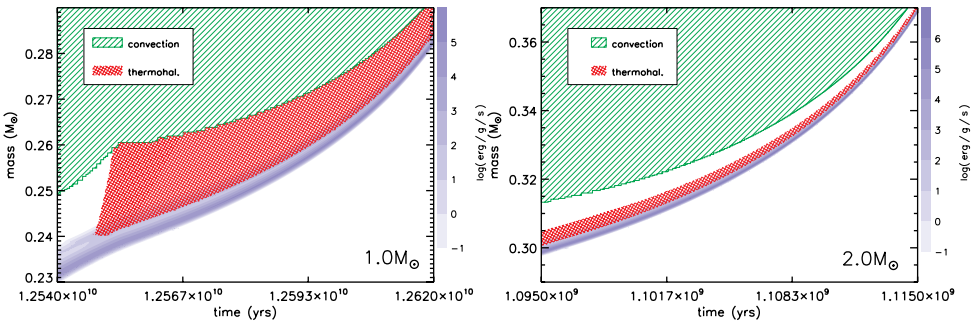

Figure 6.2: *Left:* Evolution of the region between the H burning shell source and the convective envelope in the RGB phase after the onset of thermohaline mixing for a 1.0 $M_\odot$ star. Green hatched regions indicate convection and red cross hatched regions indicate thermohaline mixing, as displayed in the legend. Blue shading shows regions of nuclear energy generation, tracing the H-burning shell. *Right:* Evolution of the region between the H burning shell source and the convective envelope in the RGB phase after the onset of thermohaline mixing for a 2.0 $M_\odot$ star

and 2.0 $M_\odot$ models. The size of the μ-inversion is depending on the local amount of ^{3}He and in the studied mass range decreases with increasing initial mass[1]. According to Inequality 6.2 this inversion causes thermohaline mixing in the radiative buffer layer, the radiative region between the H-burning shell and the convective envelope. We emphasize that the extension of the region in which the mixing process is active is not chosen arbitrarily, but is calculated self-consistently by the code. This is done at each time step of the evolutionary calculation by checking which grid points fulfill condition 6.2. This is a major difference between models including thermohaline mixing and models where the extra mixing is provided by magnetic buoyancy (Busso et al. 2007; Nordhaus et al. 2008; Denissenkov et al. 2009). In fact for the latter, a self-consistent implementation is still not available in 1D stellar evolution codes, and the extension of the extra mixing has to be set arbitrarily.

In our 1 $M_\odot$ model, thermohaline mixing developes at the luminosity bump and transports chemical species between the H-burning shell and the convective envelope (see Fig. 6.2). This results in a change of the stellar surface abundances. Figure 6.3 shows the evolution of ^{3}He surface abundance and of the ratio ^{12}C/^{13}C, qualitatively confirming the result of EDL06 and CZ07, namely that thermohaline mixing is depleting ^{3}He and lowering the ratio ^{12}C/^{13}C on the giant branch. As already observed by CZ07 surface abundance of ^{16}O is not affected because thermohaline mixing is not transporting chemical species deep enough in the H-burning shell.

Unlike the 1.0 $M_\odot$ and the 1.5 $M_\odot$ model, in the 2.0 $M_\odot$ model thermohaline mixing starts but never connects the H-burning shell to the convective envelope. This is a direct consequence of the lower ^{3}He abundance, which results in a smaller μ-inversion and therefore in a

[1]During the main sequence of these stars, the pp chain operates partially burning hydrogen to ^{3}He but not beyond in a wide zone outside the main energy-producing region. At the end of core H burning the first dredge up mixes this ^{3}He in the stellar envelope. Since the main sequence lifetime is longer for lower mass stars, these are able to produce bigger amounts of ^{3}He.

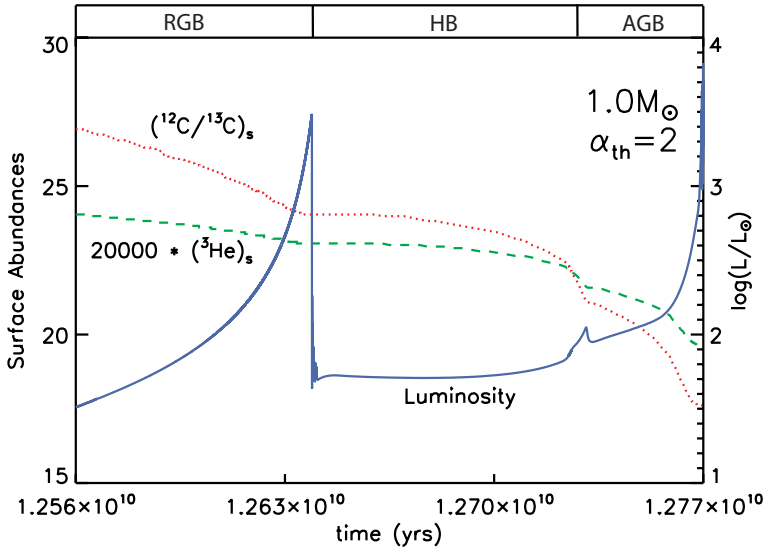

Figure 6.3: Evolution of the surface abundance profiles of the $^{12}C/^{13}C$ ratio (dotted red line) and ^{3}He (dashed green line), and of the luminosity (solid blue line) from the onset of thermohaline mixing up to the AGB for a 1.0 $M_{\odot}$ star.

slower thermohaline mixing, according to Eq. 6.3. It is surprising that thermohaline mixing, once started in the outer wing of the hydrogen burning shell, is not spreading through the whole radiative buffer layer. In fact the H-shell burns in a chemically homogeneous region, meaning that no compositional barrier is expected to stop the instability. The reason is that the region unstable to thermohaline mixing is moving too slow in mass coordinate, and it never catches-up with the quicker receding envelope. This situation is shown in the right panel of Fig. 6.2. As a result no change in the stellar surface composition due to thermohaline mixing is observed during the RGB phase of the 2.0 $M_{\odot}$ model.

In our 3.0 $M_{\odot}$ model the H-burning shell never penetrates the homogeneous region left by the 1DUP. Accordingly thermohaline mixing is not occurring during this phase.

In conclusion our models predict that, before He-core burning, thermohaline mixing is able to change surface abundances only in stars with $M \lesssim 1.5\,M_{\odot}$.

During the RGB evolution the choice of $\alpha_{\rm th} = 2.0$, roughly corresponding to the prescription of Kippenhahn et al. (1980) for the thermohaline mixing, allows our stellar models to reach helium ignition without having depleted too much ^{3}He in the envelope. The presence of leftover ^{3}He allows thermohaline mixing to play a role also during later evolutionary phase, as we show in the next section. On the other hand, CZ07 chose the prescription of Ulrich (1972), and their efficiency parameter corresponds to $\alpha_{\rm th} = 667$, i.e. a mixing efficiency more than 300 times higher than in our case. Consequently in their 0.9 $M_{\odot}$ model ^{3}He is almost completely depleted in the envelope already at the end of the RGB phase. While using the Ulrich (1972) prescription one can reproduce quantitatively the extent of surface abundances

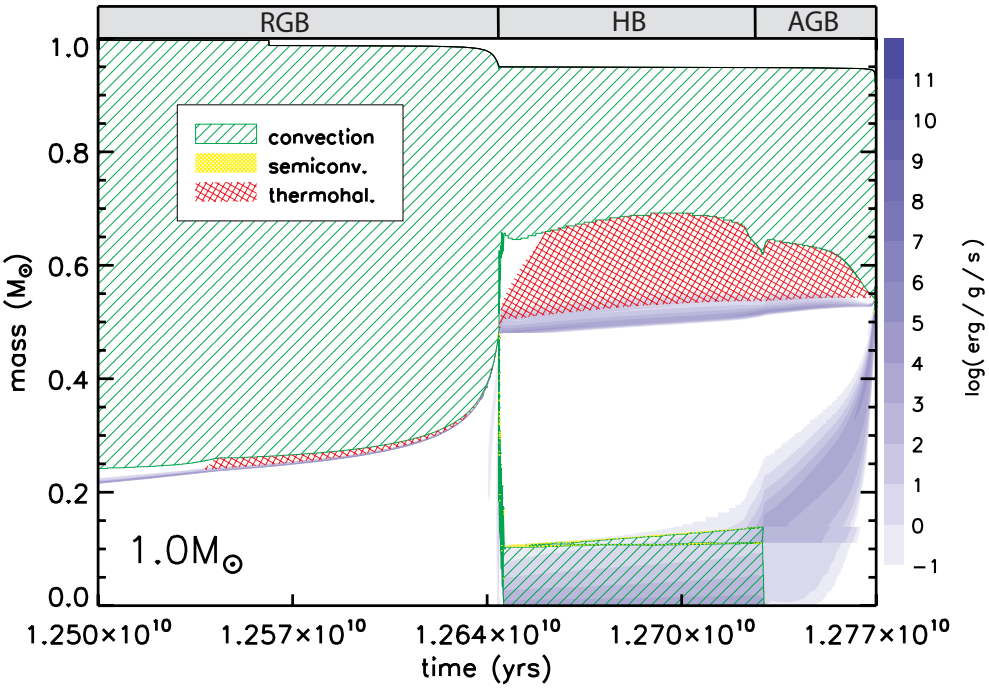

Figure 6.4: Evolution of the internal structure of a 1.0 $M_\odot$ star from the onset of thermohaline mixing to the asymptotic giant branch. Green hatched regions indicate convection, yellow filled regions represent semiconvection and red cross hatched regions indicate thermohaline mixing, as displayed in the legend. Blue shading shows regions of nuclear energy generation.

variation at the luminosity bump (Charbonnel & Zahn 2007), this is not a sufficient reason to prefer one prescription over another. We discussed in Sect. 6.2.2 why we believe that the Kippenhahn et al. (1980) is a better physical description of thermohaline mixing in stellar interiors. Such statement will need to be confirmed by realistic simulations of thermohaline mixing. If true, then a different mechanism, or the interaction of thermohaline mixing with other physical phenomena, is required to explain the rapid change of surface abundances at the luminosity bump.

6.5 Beyond the RGB: mixing on the horizontal branch and during the AGB stage

While CZ07 and EDL07 investigate thermohaline mixing only during the RGB, we followed the evolution of our models until the thermally-pulsing AGB stage (TP-AGB). Infact a μ-

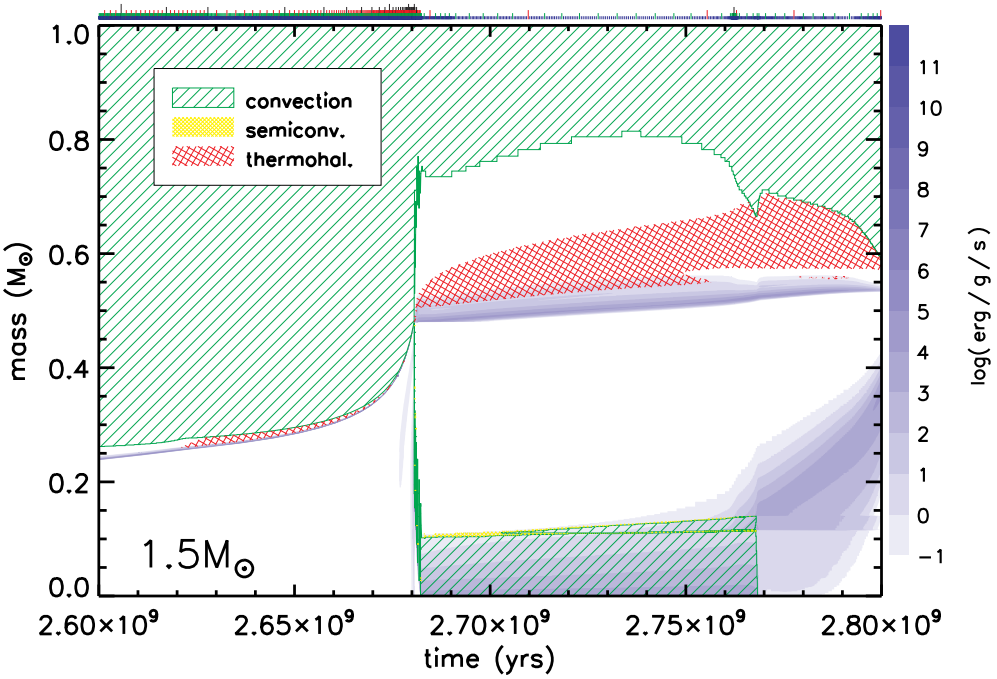

Figure 6.5: Evolution of the internal structure of a 1.5 $M_\odot$ star from the onset of thermohaline mixing to the AGB phase. Green hatched regions indicate convection, yellow regions represent semiconvection and regions of thermohaline mixing are red cross hatched, as is displayed in the legend. Blue shading shows regions of nuclear energy generation.

inversion is always created if a H-burning shell is active in a chemically homogeneous layer, the size of the inversion depending on the local abundance of ^{3}He. This happens not only during the RGB, but also during the horizontal branch (HB) and the AGB. As a result thermohaline mixing can operate also during these evolutionary phases.

Depending on the efficiency of thermohaline mixing during the RGB, the ^{3}He can be exhausted at the end of this phase (e.g in the models of CZ07). However, stars that avoid extra mixing during the RGB are observed (Charbonnel & Do Nascimento 1998). For these stars the ^{3}He reservoir is intact at He ignition, and thermohaline mixing has the potential to play an important role during the HB and AGB phases. This is confirmed by the evolutionary calculations presented in Section 6.5.1 and 6.5.2.

6.5.1 Horizontal Branch

After core He-flash, helium is burned in the core, while a H-burning shell is still active below the convective envelope. In our 1 $M_\odot$ model we found that during this phase thermohaline mixing is present and can spread through the whole radiative buffer layer. This is clear in

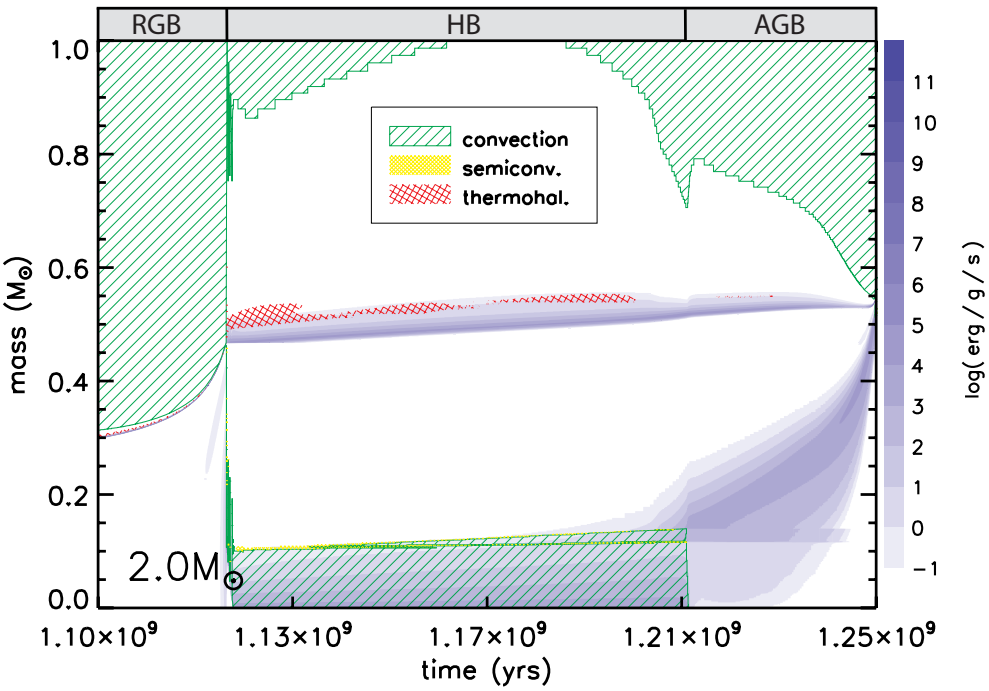

Figure 6.6: Evolution of the internal structure of a 2.0 $M_\odot$ star from the onset of thermohaline mixing to the AGB phase. Green hatched regions indicate convection, yellow regions represent semiconvection and regions of thermohaline mixing are red cross hatched, as is displayed in the legend. Blue shading shows regions of nuclear energy generation.

Fig. 6.4 where thermohaline mixing (red, cross hatched region) extends from the H-shell to the convective envelope also after ignition of core He-burning (HB label in the plot). Accordingly surface abundances change during this phase, as shown in Fig. 6.3. Here a change of surface abundances is visible also after the luminosity peak corresponding to the core He-flash.

Contrary to the 1 $M_\odot$ model, in our 1.5 and 2.0 $M_\odot$ models thermohaline mixing is not changing surface abundances during the HB phase. In the 1.5 $M_\odot$ the instability succeeds to connect the H-shell and the convective envelope only at the end of core He-burning, while in the 2.0 $M_\odot$ this is never achieved (see Fig. 6.6). In the latter case thermohaline diffusion is confined to a tiny layer on top of the H-burning shell, never spreading through the radiative layer (the red, cross hatched region in Fig. 6.6). This is due to the presence of a μ barrier which stops the development of the instability. In Fig. 6.7 we show the profile of $1/\mu$ for the 2.0 $M_\odot$ model at three successive times during core Helium burning: the initial peak created by the reaction ^{3}He(^{3}He,2p)^{4}He gets smaller while a dip begins to be visible at slightly higher mass coordinate, i.e. at a lower temperature. This μ-barrier is responsible for stopping the

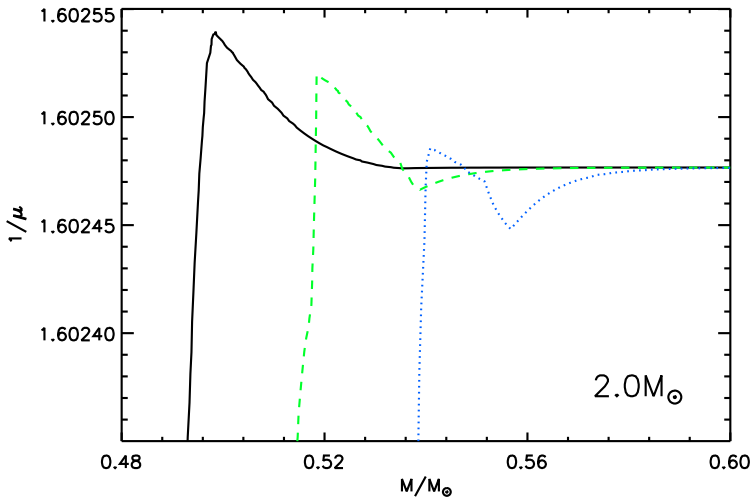

Figure 6.7: Profiles of reciprocal mean molecular weight ($1/\mu$) in the region above the H-burning shell. The plot shows three successive times in a $2\,M_\odot$ model during the horizontal branch. The black, continuous line represents the model at t = 1.13×10^9; the green, dashed line shows the same model at t = 1.16×10^9, while the blue, dotted line is the $1/\mu$ profile at t = 1.21×10^9.

instability; this process is discussed in greater details in Appendix A.

In the $3.0\,M_\odot$ model the H-burning shell enters for the first time the chemically homogeneous region after igniting He in the core. However, also in this case, thermohaline mixing is not changing surface abundances since is not able to connect the H-burning shell with the convective envelope.

We conclude that in our models thermohaline mixing during the HB is changing the surface abundances only in stars with $M < 1.5\,M_\odot$.

6.5.2 Asymptotic Giant Branch

The subsequent evolutionary phase is characterized by the presence of two burning shells and a degenerate core. The star burns H in a shell and the ashes of this process feed a underlying He-burning shell. This is referred to as the Asymptotic Giant Branch (AGB phase).

During the low luminosity part of the AGB thermohaline mixing is working under the same conditions present in the last part of the HB phase (see Fig. 6.4, label AGB). In 1.0 and $1.5\,M_\odot$ models, thermohaline mixing connects the shell source to the envelope. As a consequence surface abundances change, as shown for our $1.0\,M_\odot$ model in Fig. 6.3 (label AGB). Similarly to the RGB and HB phases, no thermohaline mixing is present in models with initial mass higher than $1.5\,M_\odot$.

During the most luminous part of the AGB the He shell periodically experiences thermal pulses (TPs); in stars more massive than $\sim 2\,M_\odot$ these thermal pulses are associated with a

deep penetration of the convective envelope, the so-called third dredge-up (3DUP). In our $1\,M_\odot$ model we find thermohaline mixing to be present also on the TP-AGB. The instability propagates through the thin radiative buffer region (thin in mass coordinate), and reaches the convective envelope. This situation is illustrated in Fig. 6.10. However in this case thermohaline mixing leads only to negligible changes in the surface abundances. This is due to the very short timescale of this evolutionary stage and to the fact that most of the ^{3}He has already been burned in previous evolutionary phases. Overall in our models we found no impact of thermohaline mixing on the surface abundances during the TP-AGB phase.

We want to stress here that the presence and impact on surface abundances of thermohaline mixing during the TP-AGB, depends critically on the local ^{3}He abundance and on the value of the efficiency factor $\alpha_{\rm th}$. This is because the local ^{3}He abundance is related to the previous history of mixing, that in turns also depends on the efficiency $\alpha_{\rm th}$ of the diffusion process.
We do not know the correct value of $\alpha_{\rm th}$ in stellar interiors. In fact $\alpha_{\rm th}$ could also depends on stellar parameters such as rotation, metallicity or magnetic fields (see Sect. 6.6), and it could well be that it changes in the same star through different evolutionary phases. Therefore our predictions for the changes of surface abundances due to thermohaline mixing, especially during the TP-AGB phase, are strongly affected by these uncertainties. Further study is needed to clarify the picture.

6.6 Thermohaline mixing, rotational mixing and magnetic diffusion

In our $1.0\,M_\odot$ and $1.5\,M_\odot$ models we found that in the relevant layers thermohaline mixing has generally higher diffusion coefficients than rotational instabilities and magnetic diffusion. Figure 6.8 clearly shows that rotational and magnetic mixing are negligible compared to the thermohaline mixing in our $1.0\,M_\odot$ model. The only rotational instability acting on a shorter timescale is the dynamical shear instability, visible in Fig. 6.8 as a spike present at the lower boundary of the convective envelope. This instability works on the dynamical timescale in regions of a star where a high degree of differential rotation is present; it sets in if the energy that can be gained from the shear flow becomes comparable to the work which has to be done against the potential for an adiabatic turn-over of a mass element ("eddy") (Heger 1998). However, if present, this instability acts only in a very small region (in mass coordinate) at the bottom of the convective envelope. As a result thermohaline mixing is still setting the timescale for the diffusion of chemical species from the convective envelope to the hydrogen burning shell.

In models of $2.0\,M_\odot$ and $3.0\,M_\odot$ thermohaline mixing is less efficient due to the lower abundance of ^{3}He. At the same time rotational instabilities and magnetic diffusion have bigger diffusion coefficients, mainly because these models have initial equatorial velocities of 140 and 250 $\mathrm{km\,s^{-1}}$ respectively. Fig. 6.9 shows how in the $2\,M_\odot$ model during core He burning rotational mixing and magnetic diffusion become more important than thermohaline mixing. The radiative buffer layer is dominated by the Eddington-Sweet circulation, dynamical shear and magnetic diffusion. However the rotational mixing diffusion coefficient is still

too small to allow surface abundances to change appreciably in this phase, in agreement with results from Palacios et al. (2006). The same conclusion is valid for magnetic diffusion, which has the same order of magnitude as rotational diffusion in the radiative buffer layer. Our models are calculated with the Kippenhahn et al. (1980) prescription for thermohaline mixing, that implies a smaller diffusion coefficient respect to the one proposed by Ulrich (1972). As a consequence the result that thermohaline mixing has in general a higher impact than rotational mixing and magnetic diffusion in the relevant layers is valid regardless of the choice between the two prescriptions.

The discussion of the interactions of thermohaline motions with the rotational instabilities and magnetic fields is more complex. In this respect Canuto (1999) argues that shear due to differential rotation decreases the efficiency of thermohaline mixing. Not only, Denissenkov & Pinsonneault (2008) claim that rotation-induced horizontal turbulent diffusion may suppress thermohaline mixing. This is because horizontal diffusion (molecular plus turbulent) may change the mean molecular weight of the fluid element during its motion. They argue that this horizontal diffusion is able to halt thermohaline mixing. We think this argument is correct in an ideal situation in which a single blob of material is crossing an infinite, parallel slab. However, in a star horizontal turbulence is acting on a shell, which can be locally approximated to a parallel slab with periodic boundary conditions in the horizontal direction. Such horizontal layer (shell) is rapidly homogenized by the horizontal turbulence. Fingers trying to cross this horizontal layer are quickly disrupted and mixed. This results in a rapid increase of the mean molecular weight μ in the shell, such that the region will become unstable to thermohaline mixing. A new generation of fingers is therefore expected. However the presence of horizontal turbulence is probably making fingers an unlikely geometrical configuration: blobs that travel a small distance before turbulence is mixing them on a horizontal layer are more likely. This way thermohaline mixing is not stopped, but only slowed down. This scenario would favour the Kippenhahn et al. (1980) prescription, which actually predicts blobs traveling a distance comparable to their size.

Another interesting idea has been proposed by Charbonnel & Zahn (2007). They claim that internal magnetic fields can play a stabilizing role, trying to counteract the destabilizing effect of the inverse μ gradient. Their conclusion is that thermohaline mixing can be inhibited by the presence of a magnetic field stronger than 10^4 – 10^5 Gauss. However they warn that their analysis ignores both stellar rotation and spatial variation of B, which results in neglecting any possible instability of the magnetic field itself (Spruit 1999).

The instability of magnetic fields below the convective envelope of RGB and AGB stars has been discussed by Busso et al. (2007); Nordhaus et al. (2008). They argue that dynamo-produced buoyant magnetic fields could provide the source of extra mixing in these stars.

6.7 Lithium rich giants

Lithium is a fragile element which is destroyed at temperatures higher than about 3×10^6K. For this reason it is expected that lithium should decrease from its initial value during the evolution of stars. On the other hand, observations have shown that about 2% of giants show

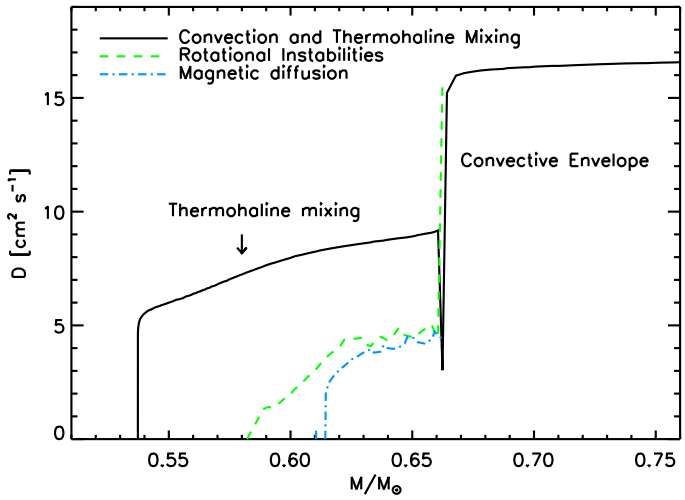

Figure 6.8: Diffusion coefficients in the region between the H burning shell and the convective envelope for the 1.0 $M_\odot$ model during the HB (t= 1.267×10^{10}). The initial equatorial velocity of the model is 10 km s^{-1}. The black, continuous line shows convective and thermohaline mixing diffusion coefficients, the green, dashed line is the sum of the diffusion coefficients due to rotational instabilities while the blue, dot-dashed line shows the magnitude of magnetic diffusion coefficient.

strong Li lines (e.g., Wallerstein & Sneden 1982; Brown et al. 1989). Some of these stars even show surface Li abundances higher than the interstellar values.

In intermediate mass stars a possible solution was proposed by Cameron & Fowler (1971), who showed how a net production of ^{7}Li can be achieved during hot bottom burning (HBB). During HBB the convective envelope penetrates into the H-shell burning, where ^{7}Be is produced by the pp-chain. In this situation the unstable isotope ^{7}Be can be transported to cooler temperatures by the convective motions, decaying into ^{7}Li in regions of the envelope where the temperature is low enough for lithium to survive. This results in Li enrichment at the surface.

At solar metallicity stars below $\sim 5\,M_\odot$ do not experience hot bottom burning (Forestini & Charbonnel 1997), whereas at $Z = 0$ hot-bottom burning is found down to $3\,M_\odot$ (Siess et al. 2002). For stars avoiding hot-bottom burning, some other mechanism is needed in order to increase the Li surface abundance. A possibility is that some kind of extra mixing is connecting the H-burning shell and the convective envelope, which in the literature is often referred to as Cool Bottom Process (CBP). The work of Charbonnel & Balachandran (2000) supports this hypothesis. In fact they found Li-rich stars to be either red giants at the luminosity bump or early-AGB stars before the second dredge-up, in agreement with the idea that some internal mixing is occurring when the H-burning shell enters a chemically homogeneous region.

Recently Uttenthaler et al. (2007) reported the detection of low-mass, Li-rich AGB stars in the galactic bulge. Interestingly two of the four stars which show surface Li enhancement

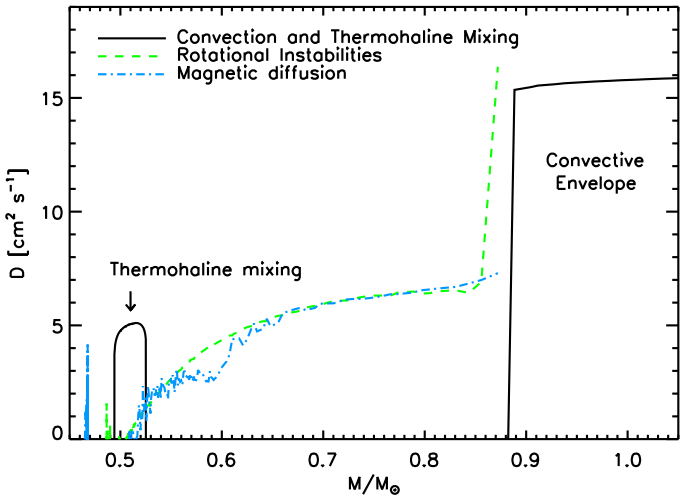

Figure 6.9: Diffusion coefficients in the region between the H burning shell and the convective envelope for the 2.0 $M_\odot$ model during core Helium burning (t= 1.124×10^9). The initial equatorial velocity of the model is 140 km s^{-1}. The black, continuous line shows convective and thermohaline mixing diffusion coefficients, the green, dashed line is the sum of the diffusion coefficients due to rotational instabilities while the blue, dot-dashed line shows the magnitude of magnetic diffusion coefficient.

present no evidence for third dredge-up, and thermohaline mixing is advocated as a possible source for the extra mixing.

In our calculations we found that the Li surface abundance is affected by the presence of thermohaline mixing during the evolution of low mass stars. While Li is burned during the RGB and HB, thermohaline mixing has the potential to enhance the Li surface abundance during the TP-AGB phase. To show this, we computed stellar evolution calculations of the TP-AGB phase in 1 and 3 $M_\odot$ with different values of $\alpha_{\rm th}$. An example of the evolution of the lithium surface abundance in the 3 $M_\odot$ model during one thermal pulse is shown in Fig. 6.11. Our models confirm qualitatively that this instability can enhance the surface Li abundances in low mass AGB stars, even if we can not reproduce quantitatively the high level of enrichment observed by Uttenthaler et al. (2007). To reach the values of Uttenthaler et al. (2007) a value of $\alpha_{\rm th}$ much bigger than the ones proposed by Kippenhahn et al. (1980) and Ulrich (1972) is needed. As discussed in Sect. 6.5.2, a quantitative study requires a better knowledge of the efficiency parameter for thermohaline mixing $\alpha_{\rm th}$.

The observations of Uttenthaler et al. (2007) show that only 4 of 27 galactic bulge stars are Li enriched. If thermohaline mixing is the physical process providing the high Li enrichment observed, we still have to understand why only 15% of the sample shows such a strong enhancement. One possibility is that such stars did not experience thermohaline mixing in previous evolutionary phases. This would leave the ^{3}He reservoir intact, leading to a much more efficient mixing during the TP-AGB phase.

This scenario requires a way to inhibit the extra mixing during the RGB and HB phases. Charbonnel & Zahn (2007) have proposed that strong magnetic fields stop thermohaline mixing in those red giants stars that are the descendants of Ap stars. They call these stars “thermohaline deviant stars".
Since the fraction of Ap stars relative to A stars (5-10 %), the amount of red giants that seem to avoid the extra mixing ($\sim$ 4%) and the observed fraction of Li-enriched AGB stars (15%) are similar, it may be possible that we are looking at the same group of stars at different evolutionary stages. If this is the case, it remains to be understood why the process that inhibits the mixing during the RGB and HB phases is not at work during the AGB.

A further complication comes from the observations of Drake et al. (2002), showing that the incidence of Li-rich giants is much higher among fast rotating objects. They consider single K giants and find that among rapid rotators ($v \sin i \geq 8\,\mathrm{km\,s^{-1}}$) a very large proportion ($\sim$ 50%) is Li-rich, in contrast with a very low proportion ($\sim$ 2%) of Li-rich stars among the much more common slowly rotating giants. Thermohaline mixing is not driven by rotational energy and if any effect would be expected, it would be a lower efficiency of the mixing with increasing shear and horizontal turbulence (Canuto 1999; Denissenkov & Pinsonneault 2008). On the other hand, an increase in the mixing efficiency with the rotation rate is expected if the physical mechanism behind the extra mixing is magnetic buoyancy (Busso et al. 2007; Nordhaus et al. 2008; Denissenkov et al. 2009). In this case rotation is necessary to amplify the magnetic field below the convective envelope.
Another possibility is that lithium has an external origin, resulting from accretion and ingestion of planets or a brown dwarf by an expanding red giant (e.g., Siess & Livio 1999a,b). Mass transfer or wind accretion in a binary system is also a possible scenario.

The far-IR excess which is observed in all the fast rotating, Li enriched giants is another interesting piece of the puzzle (Drake et al. 2002; Reddy & Lambert 2005). While models in which some kind of accretion process is occurring could explain the IR excess, internal production of lithium has problems with reproducing such observations (but see Palacios et al. 2001). We refer to Drake et al. (2002) for a nice review of the proposed mechanism for the formation of Li-rich giants.

6.8 Conclusion

We qualitatively confirm the results of CL07: thermohaline mixing in low mass giants is capable of destroying large quantities of ^{3}He, as well as decreasing the ratio ^{12}C/^{13}C. Thermohaline mixing indeed starts when the hydrogen burning shell source moves into the chemically homogeneous layers established by the first dredge-up. At solar metallicity we find that this process is working only in stars with mass below $1.5\,\mathrm{M}_\odot$. This result is sensitive to the choice of the α_{th} parameter which regulates the speed of thermohaline mixing.

Our models show further that thermohaline mixing remains important during core helium burning, and can also operate on the AGB — including the termally-pulsing AGB stage. Depending on the efficiency of the mixing process, this can result in considerable Lithium enrichment.

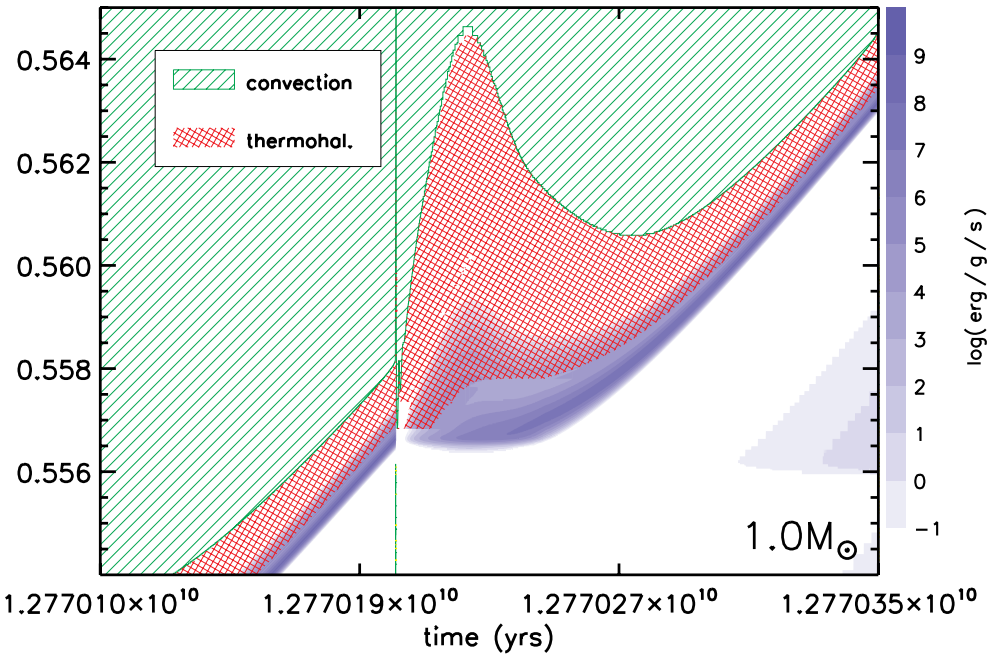

Figure 6.10: Evolution of the region between the H burning shell source and the convective envelope during a thermal pulse in a 1.0 $M_\odot$ star. Green hatched regions indicate convection and regions of thermohaline mixing are red cross hatched, as is displayed in the legend. Blue shading shows regions of nuclear energy generation. This model is evolved from the zero age main sequence to the TP-AGB with $\alpha_{\rm th}$ =2.

Our calculations show that in the relevant layers thermohaline mixing has generally a higher diffusion coefficient than rotational instabilities and magnetic diffusion. However, we can not address the interaction of thermohaline motions with differential rotation and magnetic fields, for which hydrodynamic calculations are required.

In stellar evolution codes thermohaline mixing is implemented as a diffusive process. This process acts on a thermal timescale, but the exact velocity of the motion depends on a parameter $\alpha_{\rm th}$. This parameter is related to the geometry of the fingers (or blobs) displacing the stellar material and is still a matter of debate. The two widely used prescriptions have a parameter $\alpha_{\rm th}$ that differs by two orders of magnitude. In this paper we used Kippenhahn et al. (1980) prescription, even if we also investigated the effect of using different values of $\alpha_{\rm th}$ in a few calculations. CZ07 used a much more efficient thermohaline mixing (Ulrich 1972), justifying their choice on the basis of laboratory experiments of thermohaline mixing performed in water, and on the observations of surface abundances of red giants.
However the physical conditions inside a star are very different than in these laboratory experiments, which clearly can not be used for a quantitative study of this hydrodynamic instability. Moreover it is not clear if thermohaline mixing is the only physical process responsible for

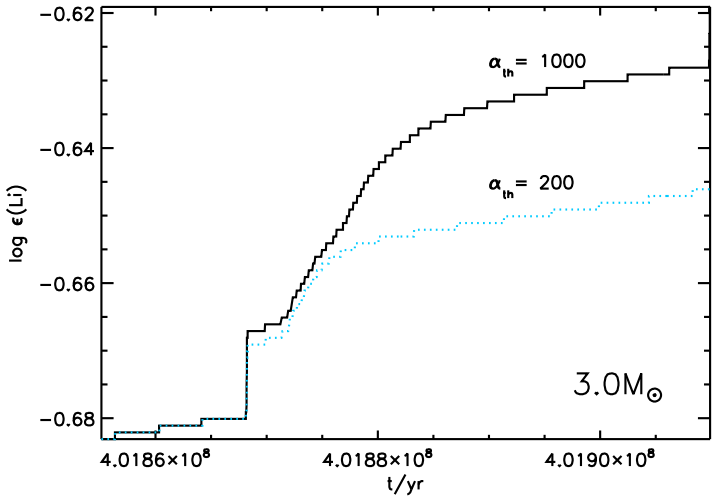

Figure 6.11: Evolution of Lithium surface abundance during one thermal pulse in a $3\,M_{\odot}$ model. The black, continuous line shows a model evolved with $\alpha_{\rm th} = 1000$; the blue, dotted line refers to the same model evolved with a thermohaline mixing efficiency $\alpha_{\rm th} = 200$. In both cases the model is experiencing third dredge-up. The evolution of the star prior to the TP-AGB has been calculated with $\alpha_{\rm th} = 2$.

the extra mixing, and therefore it is not possible to calibrate its efficiency against the observations.

We argue that is not possible at this stage to firmly identify thermohaline mixing as the cause of the observed surface abundances in low-mass giants (Gratton et al. 2000). In particular the long standing ^{3}He problem can not be considered solved. In agreement with CZ07 we claim that to clarify the picture it would be desiderable to have realistic hydrodynamic simulations of thermohaline mixing.

Acknowledgments MC wishes to thank Steve N. Shore, Maria Lugaro, Onno Pols, Evert Glebbeek, Selma de Mink and John Lattanzio for helpful discussions. MC acknowledges support from the International Astronomical Union and from the Leids Kerkhoven-Bosscha Fonds.

APPENDIX A

Halting thermohaline mixing

For models of $M > 1.5\,M_{\odot}$ we found two situations in which thermohaline mixing fails connecting the H-burning shell with the convective envelope:

1. The envelope is receding in mass coordinate and the thermohaline mixing is not fast enough to catch-up. This situation is shown in the right panel of Fig. 6.2.

2. A chain of reactions rising the mean molecular weight can create a barrier that stops the mixing process.

The second scenario occurs depending on the efficiency of the reactions rising the molecular weight in the outer wing of the H-burning shell. The reactions responsible for creating this compositional barrier are ^{3}He (^{4}He,γ) ^{7}Be (e^{-},ν) ^{7}Li (^{1}H,^{4}He) ^{4}He.
In the first one ^{3}He and ^{4}He produce ^{7}Be that rapidly decays into ^{7}Li. The lithium easily reacts with a proton producing two α-particles; this way the initial molecular weight of $7/6$ rises to the value $4/3$. This occurs in the outer wing of the H-burning shell, at a lower temperature respect to the region where the mean molecular weight inversion discussed by EDL06 and CZ07 is present. As a consequence thermohaline mixed is halted (see Fig. 6.6 and Fig. 6.7).

Therefore two sets of reactions play a role in the evolution of thermohaline mixing in the region between the H-burning shell and the convective envelope:

$$^{3}\mathrm{He} + ^{3}\mathrm{He} \longrightarrow 2\,^{1}\mathrm{H} + ^{4}\mathrm{He} \qquad \mu : 1 \rightarrow 6/7 \tag{A.1}$$

$$\left.\begin{array}{l} ^{3}\mathrm{He} + ^{4}\mathrm{He} \longrightarrow ^{7}\mathrm{Be} + \gamma \\ ^{7}\mathrm{Be} + \mathrm{e}^{-} \longrightarrow ^{7}\mathrm{Li} + \nu \\ ^{7}\mathrm{Li} + ^{1}\mathrm{H} \longrightarrow 2\,^{4}\mathrm{He} \end{array}\right\} \quad \mu : 7/6 \rightarrow 4/3 \tag{A.2}$$

As a consequence, the efficiency in starting and stopping thermohaline mixing is regulated by the local abundance of ^{3}He and ^{4}He. The first reaction in the chain A.2 has a lower rate than reaction A.1 at the temperatures in the region of interest. However ^{3}He (^{4}He,γ) ^{7}Be depends linearly on the local abundance of ^{3}He and ^{4}He, while reaction A.1 depends quadratically on the abundance of ^{3}He. Increasing the initial mass of the stellar model, the ratio ^{3}He/^{4}He decreases in the radiative buffer layer (e.g., Boothroyd & Sackmann 1999). Consequently increasing the initial mass, at some point the set of reactions A.2 becomes more important than A.1, meaning that a compositional barrier is created. This explains why we observe a threshold in mass at about 1.5 $M_\odot$, above which thermohaline mixing is not efficient anymore.

It is important to stress here that both scenarios 1. and 2. depend on $\alpha_{\rm th}$, i.e. on the speed of the mixing process. Increasing the value of $\alpha_{\rm th}$ makes thermohaline mixing more difficult to be stopped; therefore the value of the mass threshold depends on the choice of $\alpha_{\rm th}$.

Samenvatting in het Nederlands

Dankzij de sterren, die alle elementen behalve waterstof gemaakt hebben en blijven maken, is het leven op aarde mogelijk.

Om de details van dit proces te begrijpen, wat ook wel nucleosynthese wordt genoemd, moeten we de levencyclus en de evolutie van sterren bestuderen. Sterren leven niet oneindig lang. Ze worden geboren, leven en sterven. In het algemeen is het niet mogelijk om de evolutie van sterren te zien gebeuren omdat, met een paar uitzonderingen, sterren alleen veranderingen laten zien op een tijdschaal die veel groter is dan het leven van een mens. Zodra een ster gevormd is kan deze enkele miljoenen tot tientallen miljarden jaren leven.

Daarom, voor de bestudering van sterren, moeten we vertrouwen op modellen en simulaties. Met behulp van moderne computers die berekeningen uitvoeren van de belangrijkste fysische effecten in een ster, is het mogelijk om de evolutie van sterren te verkennen.

Fysische modellen zijn niet altijd goede benaderingen van de realiteit. Ze kunnen te eenvoudig opgesteld zijn, belangrijke fysische processen niet meenemen, of gewoon verkeerd zijn. Om de huidige modellen te verfijnen is het nodig om waarnemingen te doen van de sterren. Alleen door de constante vergelijking tussen de modellen en de waarnemingen kunnen we er op vertrouwen dat onze kennis verbeterd en dat we de goede kant op gaan.

In dit proefschrift worden de resultaten van hypermoderne simulaties getoond. Deze berekeningen bevatten processen waarvan het duidelijk is dat deze belangrijk zijn voor de evolutie van sterren. Rotatie, wat in principe een eenvoudig proces is, is één van de voorbeelden: het veranderd niet alleen de vorm van de ster, van bolvormig naar afgeplat, maar veroorzaakt ook interne circulatie die het gas mengt en de structuur en de compositie veranderd (hoofdstuk 3 en 4). Dit betekend dat het interieur van een ster niet constant is maar dat het beïnvloed wordt door processen die de binnenste lagen mengen. Het is opvallend dat de modellen laten zien dat het toevoegen van dit enkele proces grote waarneembare gevolgen heeft, die dus kunnen worden getoetst met de waarnemingen.

De toevoeging van rotatie en andere processen zoals interne magnetische velden resulteert in dramatische veranderingen voor de evolutie van sterren. De helderste explosies in het heelal, lange gamma-flitsen, kunnen worden veroorzaakt door sterren die heel snel roteren aan het eind van hun leven (hoofdstuk 4).

De meeste fysische processen die besproken worden in dit proefschrift hebben een destabilizerend effect op het interieur van de sterren (hoofdstuk 2 en 6), wat verborgen is voor directe studie, en daarom hebben geprobeerd te focussen op het observationele effect van hun toevoeging, wat dus de "Observationele consequenties van het onstabiele interieur van sterren" zijn.

Dit proefschrift

De vragen die ten grondslag liggen aan de onderwerpen die in dit proefschrift behandeld worden

- **Wat is convectie?**
  Iedereen die een pan water op het vuur zet, kan zien wat convectie is. In het begin is het water rustig, maar terwijl het water van onderaf verwarmd wordt, komt het in beweging. Waterbubbels beginnen van onder naar boven te bewegen en het wateroppervlak begint te trillen. Dat laatste kun je ook horen. De bewegingen zijn het gevolg van het principe van Archimedes. Het water onderin wordt heet, zet uit en drijft naar boven, net zoals bij een heteluchtballon. In sterren zijn er, net als in een pan met kokend water, lagen die convectief zijn. In **Hoofdstuk 2** bestuderen we welke effecten hiervan aan het oppervlak zichtbaar zijn.

- **Wat is een dubbelster?**
  Wanneer twee sterren om elkaar heen draaien, spreekt men van een dubbelster. Het is gebleken dat de meeste sterren dubbelsterren zijn of soms zelfs deel uitmaken van een systeem met drie of meer sterren. Dubbelsterren zijn van groot belang voor de sterrenkunde omdat ze ons in staat stellen essentiéle eigenschappen van sterren te bepalen, zoals de massa en de afmeting. Door de snelheid te meten waarmee de sterren om elkaar heen draaien, kunnen de massa's van de sterren worden berekend. Sommige systemen vertonen verduisteringen: hierbij bewegen de sterren voor en achter elkaar langs. Voor deze dubbelsterren kan bepaald worden wat de afmetingen van de sterren zijn. Zeker niet onbelangrijk is dat de sterren in een dubbelster elkaar kunnen beïnvloeden, bijvoorbeeld via de getijdenwerking. Net zoals de maan zwaartekracht uitoefent op de oceanen op aarde en daarmee eb en vloed veroorzaakt, zo kan getijdewerking in een dubbelster zo sterk zijn dat het zelfs de rotatiesnelheid van de sterren beïnvloedt. In **Hoofdstuk 3** wordt gebruik gemaakt van dit fenomeen. Een ander proces dat van groot belang is in dubbelsterren, is massa-overdracht. Stel je twee sterren voor die om elkaar heen draaien. Als een astronaut zich precies tussen beide sterren in zou bevinden, dan zou hij gewichtsloos zijn omdat hij even sterk door de zwaartekracht van beide sterren wordt aangetrokken. Als hij echter een duwtje zou krijgen in de richting van één van

beide sterren, dan zou de arme kerel op de ster te pletter vallen. Precies hetzelfde gebeurt met stermateriaal, als één van de sterren zó groot wordt, dat het oppervlak in de buurt van dit punt komt. Dan begint stermateriaal naar de andere ster te vallen, waarbij het “duwtje” gegeven wordt door de gasdruk. Hierdoor wordt de massaverliezende ster steeds lichter. De massaontvangende ster wordt steeds zwaarder en begint bovendien steeds sneller te draaien. Dit wordt besproken in **Hoofdstuk 4** waarin we laten zien dit proces ten grondslag kan liggen aan de vorming van zogenaamde gamma-flitsen (zie ook "Wat zijn gamma-flitsen?").

- **Wat is menging door rotatie?**
  Rotatie kan ervoor zorgen dat een ster afgeplat wordt. Hierdoor wordt de ster heter bij de polen en koeler bij de evenaar van de ster. Verder kan rotatie ook het binnenste van sterren dusdanig verstoren dat verschillende lagen van de ster met elkaar gemengd worden. Er zijn verschillende mengprocessen die een rol kunnen spelen, maar de belangrijkste is een direct gevolg van de verstoring van het warmte-evenwicht. Dit leidt tot stromingen in het binnenste van de ster van de polen naar de evenaar en weer terug. Hoe sneller de ster draait, des te efficiënter de ster gemengd wordt. Deze processen komen aan de orde in **Hoofdstuk 3, 4** en **5**.

- **Wat zijn gamma-flitsen?**
  De zogenaamde lange gamma-flitsen zijn afkomstig van de zwaarste en helderste ontploffingen in het universum. Om de paar dagen wordt de aarde geraakt door lichtstralen afkomstig van gamma-flitsen uit verafgelegen sterrenstelsels. Dit licht heeft er miljarden jaren over gedaan om onze telescopen te bereiken. Bij deze explosies komt een enorme hoeveelheid energie vrij. In slechts een seconde tijd komt alle energie van de ster vrij. Ter vergelijking: tijdens een gamma-flits van één seconde komt er net zo veel energie vrij als de zon uitstraalt in zijn hele leven, zo’n 10 miljard jaar. Deze buitengewoon grote hoeveelheid energie wordt uitgezonden in een smalle bundel. Wanneer deze bundel toevallig in de richting van de aarde wordt uitgezonden, dan kunnen we deze waarnemen, zelfs als deze van extreem grote afstand afkomstig is, zoals de afstanden tot de verste sterrenstelsels. We denken dat gamma-flitsen worden geproduceerd aan het einde van het leven van sommige zeer zware sterren. In **Hoofstuk 4** behandelen we de levensloop van zware sterren in dubbelstersystemen en we tonen aan dat deze systemen onder bepaalde omstandigheden gamma-flitsen kunnen uitzenden.

- **Wat is een supernova?**
  Zware sterren eindigen hun leven in spectaculaire explosies die supernovae genoemd worden. Dit gebeurt wanneer hun nucleaire brandstof uitgeput raakt en de ster door zijn eigen zwaarte kracht ineenstort. Net als gamma-flitsen zijn supernova-explosies zeer helder. Zeer zware sterren exploderen als een speciaal type supernova, die nog helderder zijn dan normale supernovae. Bij deze sterren zijn het vooral de fotonen die verantwoordelijk zijn voor de hoge druk in het centrum van de ster. Vlak voor de ontploffing gaan deze fotonen over in zogenaamde electron-positron paren waardoor de druk plotseling wegvalt en de kern van de ster ineenstort. In **Hoofdstuk 5** bespreken we welk type sterren op deze manier exploderen.

- **Wat is thermohaliene menging?**
  Thermohaliene circulatie is een bekend verschijnsel bij natuurkundigen die de oceaan bestuderen. Wanneer de bovenste laag van het water in de oceaan verdampt, blijft het zout achter. Hierdoor ontstaat een laag warm en zout water boven een laag koud en minder zout water. Wanneer het zoute water afkoelt, zinkt het naar beneden in verticale structuren die er uit zien als lange dunne vingers. In het Engels wordt dit effect ook wel “salt-fingers” genoemd. Uiteindelijk verdwijnen de structuren en zijn de twee lagen met elkaar gemengd. Het wonderlijke is dat hetzelfde proces optreedt in sterren wanneer de gemiddelde moleculaire dichtheid in een bepaalde laag hoger is dan in de laag eronder. In **Hoofdstuk 6** laten we zien dat dit proces tot menging kan leiden in sterren, wat grote gevolgen kan hebben voor de nucleaire processen.

English Summary

Life is possible because, besides hydrogen, stars have produced – and continue to synthesize – all of the elements of which we and all living things are composed. To understand the details of this process, which is called stellar nucleosynthesis, requires to study the life cycle of the stars, their evolution. But they are not eternal. Stars are born, live and die. In general, we cannot observe stars evolve in real time because, with a few exceptions, they only show major changes of their properties on a time much longer than human lifetime. Once formed, a star can live from a few millions years up to tens of billions of years.

Therefore, to study stars, one must rely on models and simulations. It is possible to explore the evolution of stars using modern computers, which run codes including what we think are the most important physical effects.

Physical models are not always good approximations of the reality. They may be too simplified, lack the inclusion of some important physical processes, or simply be wrong. What is required are observations of nature, in this case of real stars, that constrain and show how to refine existing models. Only with this constant confrontation of theory and observations can we be confident that our understanding is improving, that we are on the right track.

In this thesis, state-of-the-art computer simulations of stars have been performed. These calculations include processes that have been recognized to be important for the evolution of stars. Rotation, a simple thing in principle, is an example: It not only changes the shape of a star, from spherical to flattened, but induces internal circulations that can mix the gas and alter its structure and composition (Chapter 3 and 4). This means that the interior of a rotating star is not quiet, but is affected by a transport process that mixes its inner layers. Interestingly the models show that including this single physical effect produces major observational consequences for the star, and these predictions can be tested against the observations.

The inclusion of rotation and other processes, like internal magnetic fields, results in dramatic changes for the evolution of stars. The brightest explosions in the universe, long gamma-ray bursts, might be caused by massive stars that rotate very fast at the end of their life (Chapter 4).

Most of the physical processes discussed in the thesis tend to destabilize the stellar interior (Chapter 2 to 6), the part hidden from direct study by its opacity, and we tried to focus on the observable effects of their inclusion, that is the "Observational consequences of unstable stellar interiors".

This thesis

Several questions underly and link the research topics of the thesis.

- **What is convection?**
  If you have ever left a pot of water sitting on a stove, you are familiar with the concept of convection. The burner warms the water from below, which at some point ceases to be static and you see vertical, disordered motion of blobs of water and ripples are easily seen on the surface. You also hear noise radiated by the rippling surface. The motion is driven by buoyancy. Within a star there are regions which, like the pot of water sitting on the flame, are convective. If such convective layers are close to the stellar surface, one can ask if the turbulent motions and sound can affect the outer layers of the star and result in "observational consequences". This is the topic of **Chapter 2**.

- **What is a binary star?**
  A binary system consists of two stars orbiting around a common center of mass. It now appears that most stars are part of either binary or multiple systems. Binaries are very important in astrophysics because observing their orbital velocity projected along the line of sight permits a direct determination of the masses of the individual components from which other stellar parameters, such as the stars' radii, can be indirectly estimated or – if they mutually eclipse – actually directly measured. Even more important is that these stars are not wholly independent. In a binary the two components can interact and influence each other's evolution. One way is through the action of tides. This is a familiar concept: due to the gravitational effect of the Moon, the level of the sea on Earth can change rather spectacularly (think of Mont S. Michel in Normandy). In a binary system, these tides can be so strong that they affect the whole star, changing its rotational velocity. This phenomenon, peculiar of binary stars, have been exploited in the study presented in **Chapter 3**. Another very important process occurring in a binary system is mass transfer. Imagine two stars of the same mass orbiting each other. An astronaut placed exactly halfway between them feels the same attraction in both directions and remains motionless. But if pushed ever so slightly toward one of the two stars, the poor character will ultimately fall toward the surface of the star in the direction as the shove. The same thing happens to stellar material should its radius increase to this critical point: gas start falling on the other star pushed past the stable point by internal pressure. This results in a transfer of mass from one to the other

component, increasing the mass of the gainer (at the expense of its companion) and changing its rotational velocity. This is the key-process discussed in **Chapter 4**, where we show that this kind of binary interaction can lead to the production of a gamma-ray burst (see below "What is a gamma-ray burst?").

- **What is rotational mixing?**
  Rotation not only makes a distort – flatten – star, but induces processes that tend to mix its interior. The most important is due to the fact that this rotational distortion leaves the pole of the star hotter than the equator. This thermal imbalance needs to be restored by an energy-transporting circulation of mass, and such circulation has the effect of mixing the stellar interior. The faster the star rotates, the more efficient the mixing. Rotational mixing is discussed in **Chapter 3, 4** and **5**.

- **What is a gamma-ray burst?**
  Long gamma ray-bursts (GRBs) are the brightest explosions in the Universe. Once every few days, a beam of light coming from some remote galaxy hits the Earth. Such light has traveled up to billions of years before reaching our telescopes. A GRB is extremely powerful. In just one second it releases virtually the rest energy of a star – the energy that is liberated by a GRB is hundred times the total energy released by the Sun during its roughly 10 billions year lifetime. This tremendous amount of energy emerges in a narrow beam and travels at the speed of light. If this beamed light happens by chance to point toward us, we can see it over astonishingly long distances, those of the farthest galaxies. GRBs are believe to be produced by the death of massive stars. In **Chapter 4** we study the evolution of massive stars in a binary system, and show that, under certain circumstances, this can lead to the formation of a GRB.

- **What is a pair creation supernova?**
  Massive stars end their lives in spectacular explosions called Supernovae. These are the consequence of the exhaustion of nuclear fuel in the stellar interior and subsequent gravitational collapse of the core. Like GRBs, supernovae are extremely luminous. During a very short interval, days to weeks, a supernova radiates as much energy as the Sun could emit over its life span. Very massive stars can explode as pair creation supernovae (PCSN) that are even more luminous than the normal variety. Their designation specifies the mechanism responsible for their initiation: the sudden reduction of the pressure, leading to the initial phase of collapse, by the creation of electron-positron pairs. The photons, which in a very massive star account for most of the pressure in the stellar interior, suddenly disappear when their energy is sufficient to create the pairs. This leads to a sudden drop of the internal pressure and to the initial collapse of the core. Which stars can actually explode as PCSN is the research topic of **Chapter 5**.

- **What is thermohaline mixing?**
  Thermohaline instability, also known as salt fingers, is an hydrodynamic phenomenon that, until very recently, was better known in geophysics than astrophysics. In the oceans this instability can be found, for example, in regions where the evaporation leaves a warm layer of saltier water on top of less salty, cooler water. The saltier water can sink only after exchanging its heat excess, producing long "fingers" of salty

water penetrating the fresh water (see Fig. 1.5). The instability ultimately mixes the two layers. It is intriguing that such process can also occur in stars. Of course there is no water or salt there, but there can be an analogous inversion of the mean molecular weight. In the stellar plasma, this can do the trick, as shown in **Chapter 6**. As discussed in the chapter, thermohaline mixing may have profound implications for stellar nucleosynthesis.

Sommario in italiano

La vita sulla Terra è possibile perché, a parte l'idrogeno, tutti gli elementi di cui il nostro corpo è composto sono stati prodotti all'interno delle stelle. Questo processo è chiamato nucleosintesi ed è tuttora in corso, per esempio, all'interno del sole. Per capire i dettagli della nucleosintesi bisogna studiare la vita delle stelle, il loro ciclo evolutivo. Le stelle infatti non sono eterne. Un po' come noi nascono, vivono e muoiono. La durata di questo ciclo è molto lunga: una volta formata, una stella può vivere da alcuni milioni fino a decine di miliardi di anni. Di conseguenza è impossibile, a parte in alcuni casi, osservarne i cambiamenti indotti dalla loro evoluzione.

Per questo motivo lo studio dell'evoluzione delle stelle si avvale di modelli e simulazioni. È possibile studiare l'evoluzione di una stella con i moderni computers. Questi utilizzano dei programmi di simulazione che includono i processi fisici ritenuti importanti.

Tuttavia i modelli non rappresentano sempre una buona approssimazione della realtà. A volte si rivelano troppo semplici, altre volte non includono alcuni importanti effetti fisici, altre volte sono semplicemente sbagliati. Quel che serve sono osservazioni, in questo caso delle stelle, che permettano di verificare i modelli. Soltanto confrontando costantemente i risultati delle simulazioni con le osservazioni possiamo essere sicuri di essere sulla giusta strada.

Per questa tesi sono state utlizzate delle simulazioni al computer che sfruttano un programma tra i più avanzati in circolazione. Queste simulazioni includono alcuni processi che sono ritenuti di estrema importanza per l'evoluzione delle stelle. La rotazione, in principio un fenomeno molto semplice, ne è un esempio: non solo cambia la forma della stella da sferica a ellissoidale, ma induce all'interno delle circolazioni che possono mescolarne il gas. Questo ha delle importanti conseguenze sia per per la struttura che per la composizione della stella (Capitolo 3 e 4). La parte interna di una stella in rotazione è condizionata da dei moti che la rimescolano, e le simulazioni che includono questo effetto mostrano importanti ripercus-

sioni sull'evoluzione della stella. Queste conseguenze sono osservabili e rappresentano un importante test per i modelli.

Talvolta l'inclusione della rotazione e di altri processi fisici, come la presenza di campi magnetici, porta a risultati sorprendenti. Ad esempio le esplosioni più energetiche dell'universo, i lampi di raggi gamma, potrebbero essere causate da stelle massicce che ruotano molto velocemente alla fine della loro vita (Capitolo 4).

La maggior parte dei processi fisici discussi in questa tesi tendono a destabilizzare l'interno delle stelle (Capitoli da 2 a 6). Queste regioni non sono osservabili direttamente, ma l'incusione di questi fenomeni ha delle conseguenze osservative, "Observational consequences of unstable stellar interiors".

In questa tesi

Il modo più semplice per capire meglio gli argomenti di ricerca trattati in questa tesi, è rispondere ad alcune domande.

- **Cos'è la convezione?**
  Ogni volta che fate bollire dell'acqua in una pentola, avete la possibilità di assistere a un esperimento sulla convezione. La fiamma riscalda l'acqua vicino al fondo del contenitore e dopo un po' di tempo l'acqua comincia a muoversi. La causa sta nel fatto che l'acqua più calda e più leggera che si trova a contatto con il fondo galleggia verso la superficie, mentre l'acqua più fredda e pesante che si trova in superficie tende ad affondare. Questo genera moti verticali e disordinati all'interno della pentola e la superficie dell'acqua si increspa. L'acqua, ribollendo, provoca anche un tipico rumore. Dentro una stella vi sono zone che, come una pentola piena d'acqua sul fuoco, diventano convettive. Se queste zone sono vicine alla superficie della stella, ci possiamo chiedere se vi sono conseguenze osservabili dovute alla presenza di questi moti convettivi e del suono da loro generato. Questo è l'argomento trattato nel **Capitolo 2**.

- **Cos'è una stella binaria?**
  Un sistema binario consiste di due stelle che orbitano attorno a un centro di massa comune. Apparentemente la maggior parte delle stelle non è isolata, ma fa parte di un sistema binario o multiplo. Le stelle binarie sono molto importanti in astrofisica, in quanto osservando il loro moto orbitale si può ottenere una misura precisa della massa delle stelle. Nel caso in cui le stelle si eclissano a vicenda, è anche possibile misurarne con precisione il raggio. In un sistema binario le due stelle possono interagire, influenzando la loro evoluzione. Un primo importante effetto è l'azione delle maree. Questo è un concetto abbastanza familiare: la Luna, orbitando attorno alla Terra, influenza il livello del mare attraverso il suo campo gravitazionale, dando vita a spettacolari maree (per esempio a Mont S. Michel, in Normandia). In un sistema binario le maree possono essere così intense da influenzare la velocità di rotazione dell'intera stella. Questo effetto è stato utilizzato per lo studio presentato nel **Capitolo 3**. Un altro importante processo che avviene nelle stelle binarie è il trasferimento di massa. Si prendano due

stelle della stessa massa che orbitano l'una attorno all'altra. Un astronauta che si trova esattamente a metà strada tra le due stelle, sente la stessa attrazione gravitazionale nelle due direzioni e quindi rimane immobile nel centro di massa del sistema. Ma nel momento in cui viene anche solo leggermente spinto in una delle due direzioni, il suo destino è segnato. L'astronauta cade sulla superficie della stella verso cui è stato spinto. La stessa cosa accade al materiale che compone una stella quando il raggio stellare cresce oltre un punto critico: il gas comincia a cadere verso l'altra stella, inizialmente sospinto dalla pressione interna e successivamente dall'attrazione gravitazionale. Questo contribuisce a incrementare la massa della stella su cui cade il materiale, a spese dell'altra componente del sistema binario. Anche la velocità di rotazione delle due stelle viene condizionata da questo processo, in quanto il materiale cadendo ha lo stesso effetto di un impulso data a una trottola. Questo è il processo fisico alla base del lavoro presentato nel **Capitolo 4**, dove viene mostrato che questo tipo di interazione in un sistema binario può portare alla formazione di un lampo di raggi gamma (vedi di seguito "Cos'è un lampo di raggi gamma?").

- **Cos'è un lampo di raggi gamma?**
  I lampi di raggi gamma (GRBs) sono prodotti dalle esplosioni più luminose dell'universo. All'incirca una volta al giorno, un fascio di luce proveniente da una qualche remota galassia colpisce la Terra. La luce che lo compone può aver viaggiato anche miliardi di anni prima di raggiungere i nostri telescopi. Un GRB è estremamente potente: in un solo secondo rilascia l'intera energia a riposo di una stella. Per capire quanto sia eccezionale questo evento, basti pensare che l'energia liberata da un GRB è cento volte l'energia totale emessa dal Sole durante i suoi 10 miliardi di anni di vita. Questa incredibile quantità di energia viene emessa in un fascio collimato e viaggia alla velocità della luce. Se il fascio punta nella direzione della Terra, possiamo osservare il GRB da distanze enormi: l'oggetto celeste più lontano mai osservato dall'uomo è infatti un lampo di raggi gamma formatosi circa 13 miliardi di anni fa, quando l'universo aveva solo 600 milioni di anni. Si pensa che i GRBs vengano prodotti durante le fasi finali dell'evoluzione di stelle massicce. Nel **Capitolo 4** si discute l'evoluzione di stelle massicce in un sistema binario, mostrando come, in certe particolari condizioni, questo possa formare proprio un lampo di raggi gamma.

- **Cos'è il mescolamento rotazionale?**
  Una stella in rotazione non viene solo distorta dalla forza centrifuga: infatti al suo interno avvengono anche dei processi, indotti dalla rotazione, che tendono a mescolarne il gas. Il più importante di questi processi è dovuto al fatto che la distorsione indotta dalla rotazione fa sì che i poli della stella siano più caldi dell'equatore. Per ripristinare l'equilibrio termico, si sviluppa una circolazione che ha l'effetto di mescolare l'interno della stella. Più la stella ruota velocemente, maggiore il mescolamento del gas. Il mescolamento rotazionale è uno dei concetti chiave negli studi presentati nei **Capitoli 3, 4** e **5**.

- **Cos'è una supernova ad instabilità di coppia?**
  Quando muoiono, le stelle massicce producono delle spettacolari esplosioni, chiamate

supernovae. L'esplosione è provocata dal collasso gravitazionale che segue l'esaurimento del combustibile nucleare. Come i lampi di raggi gamma, le esplosioni di supernovae sono molto luminose, anche se sono visibili da distanze minori non essendo in questo caso la luce collimata in un fascio. In un intervallo di giorni o al più settimane, una supernova irraggia l'energia emessa dal Sole durante tutta la sua esistenza. Stelle molto massicce possono esplodere come supernove ad instabilità di coppia (PC-SN), che sono ancora più luminose delle normali supernovae. Il loro nome deriva dal meccanismo che innesca il collasso gravitazionale della stella: la repentina riduzione della pressione interna dovuta alla creazione di coppie elettrone-positrone. I fotoni, che in una stella massiccia contribuiscono in maniera essenziale alla pressione interna, vengono rimossi all'improvviso quando la loro energia è sufficiente a creare le coppie elettrone-positrone. Questo determina la repentina perdita di pressione e il conseguente collasso del nucleo. Quali stelle esplodono come supernovae a instabilità di coppia è il tema trattato nel **Capitolo 5**.

- **Cos'è il mescolamento termoalino?**
  L'instabilità termoalina è un fenomeno idrodinamico ben conosciuto in ambito geofisico, che solo recentemente ha ottenuto visibilità anche in campo astrofisico. Negli oceani questo fenomeno può essere osservato in regioni dove l'evaporazione crea uno strato di acqua calda e salata sovrastante uno strato di acqua fresca e dolce. L'acqua più salata tenderebbe ad affondare, se non fosse per il fatto che allo stesso tempo è anche più calda. Prima di poter affondare e mescolarsi con l'acqua più fresca, lo strato d'acqua più caldo deve prima perdere del calore. Si formano così delle strutture simili a "dita" di acqua salata che penetrano l'acqua fresca (vedi Fig. 1.5), poiché questa configurazione ottimizza lo scambio di calore. La cosa affascinante è che questo processo può avvenire anche all'interno delle stelle. Nelle stelle non vi sono né acqua né sale, ma in particolari condizioni si può verificare un'inversione analoga del peso medio molecolare. Questo può avere importanti conseguenze per la nucleosintesi stellare, come discusso nel **Capitolo 6**.

Curriculum Vitae

Date and place of birth:	28 October 1979, Cecina, Italy
Bachelor of Science:	Physics, Pisa University, Italy (1998 – 2003) Thesis: Extrasolar planet detections Advisor: R.Poggiani
Master of Science:	Astrophysics, Pisa University, Italy (2003 – 2005) Thesis: Large and small scale structure of the ISM toward the Orion OB1 association Advisor: S.N.Shore
Doctorate:	Astrophysics, Astronomical Institute, Utrecht University, The Netherlands (2005 – 2009) Thesis: Observational consequences of unstable stellar interiors Advisor: N.Langer

List of publications

Published in refereed journals

1. Cantiello, Langer, Brott, de Koter, Shore, Vink, Voegler, Lennon & Yoon 2009, A&A, 499, 279 *Sub-surface convection zones in hot massive stars and their observable consequences*

2. de Mink, Cantiello, Langer, Pols, Brott & Yoon 2009, A&A, 497, 243 *Rotational mixing in massive binaries. Detached short-period systems*

3. Langer, Norman, de Koter, Vink, Cantiello & Yoon 2007, A&A, 475, L19 *Pair creation supernovae at low and high redshift*

4. Cantiello, Yoon, Langer & Livio 2007, A&A, 465, L29 *Binary star progenitors of long gamma-ray bursts*

5. Cantiello, Langer, Brott, de Koter, Shore, Vink, Voegler & Yoon 2009, Communications in Asteroseismology, Vol. 158, 61 *On the origin of microturbulence in hot stars*

6. de Mink, Cantiello, Langer & Pols 2009, Communications in Asteroseismology, Vol. 158, 94 *Rotational mixing in tidally locked massive main sequence binaries*

Submitted to refereed journals

1. Cantiello & Langer 2009, A&A, *Thermohaline mixing in evolved low mass stars*

Published in conference proceedings

1. Evans, Bastian, Beletsky, Brott, Cantiello et al. 2009, IAU Symposium 266 *The VLT-FLAMES Tarantula Survey*

2. de Mink, Cantiello, Langer, Yoon, Brott, Glebbeek, Verkoulen & Pols 2008, IAU Symposium 252, 365 *Rotational mixing in close binaries*

3. Cantiello & Langer 2008, IAU Symposium 252, 103 *Thermohaline mixing in low-mass giants*

4. Yoon, Langer, Cantiello, Woosley & Glatzmaier 2008, IAU Symposium 250, 231 *Evolution of Progenitor Stars of Type Ibc Supernovae and Long Gamma-Ray Bursts*

5. Langer, Cantiello, Yoon, Hunter, Brott, Lennon, de Mink & Verheijdt 2008, IAU Symposium 250, 167 *Rotation and Massive Close Binary Evolution*

6. Yoon, Cantiello & Langer 2008, First Stars III, AIP Conference Proceedings, 990, 225 *Evolution of Massive Stars at Very Low Metallicity, Including Rotation and Binary Interactions*

7. Cantiello, Yoon, Langer & Livio 2007, Unsolved Problems in Stellar Physics, AIP Conference Proceedings, 948, 413 *Long GRBs from Binary Stars: Runaway, Wolf-Rayet Progenitors*

8. Cantiello, Hoekstra, Langer & Poelarends 2007, Unsolved Problems in Stellar Physics, AIP Conference Proceedings, 948, 73 *Thermohaline Mixing in Low-mass Giants: RGB and Beyond*

Acknowledgements

There is always this unique feeling when an important period of my life comes to an end. My mind tries to organize and store the memories in a safer place, and doing that it always realizes an undeniable truth: how lucky I am.
It's about the experiences and the great moments, the ups and downs of life, the things I learned and the emotions I felt. And most of these things I owe to the people around me. Those people who made unforgettable every moment spent during the last four years of my life. Saying "Thank you" to some of them it's a pleasure and a chance I don't want to miss.

A mia madre e mio fratello, per essermi stati vicini tutto il tempo e per aver creduto in me. Vi voglio bene. Caro Francesco, nelle pagine di questa tesi ci sono tutte le cose che mi hanno occupato in questi anni, e che soprattutto hanno rallentato la costruzione dell'amata macchina del tempo.

It is a great pleasure to thank my advisor Norbert Langer. Norbert, I learned a great deal from you. You gave me the freedom to work on many exciting physical problems, and I am grateful for this. I admire the way you can always find the important bit of information and the right direction to go in order to solve a physical problem; I am very fortunate to work with you. Sung-Chul Yoon, you also helped me a lot during these years. You are a very good scientist and I am very glad to be your collaborator. Also thanks to Alex de Koter, for the many useful discussions we had, about science and not only. A special thank to Steve N. Shore, which, from the very moment we met in Pisa, has been a constant source of inspiration and a good friend.

I always felt at home at the Sterrekunding Instituut. It is a very friendly place and I had such a good time there. For this reason I would like to say thank to some of the people who I met at the institute. Selma, I am very happy to have come to you that day and talk about rotational mixing in binaries. I think we did very good together. I would also like to thank you, Erik and Bob for the translation of the dutch summary. In no special order I want to thank Bob, Sabina, Frans, Hector, Esteban, Ana, Martijn, Sandra, Axel, Marc, Evert, Klara, Heveline, Onno, Christoph, Mark, Maria, Vanna, Nanda, Rob Izzard, Remco, Ines, Peter, Marion, Allard-Jan, Arend-Jan and Pit. Many of you helped me during these years, many have become my friends. With some of you I had very good time traveling. Each of you knows what I am talking about. Thank to Mark Gieles, Remco Scheepmaker and Sung-Chul Yoon for providing me their thesis LaTeX–template. I want to express my gratitude to Huib Henrichs, Christoph Keller, Alex de Koter and Brahm Achterberg for carefully reading the manuscript.

In Utrecht, as in any other university place, people come and go every year. I met extremely interesting persons during my PhD, and even if some of them now live far away, I have great memories of the time spent together and hope the friendship will last for many years to come. I can ideally divide my time here in the Netherlands in three phases:

- The "Cambridgelaan era". I arrived in Utrecht in November, it was rainy and dark and I was completely alone. Then I was invited for a dinner in one of Cambridgelaan's apartments and my world turned upside down. Thank to Alejandro, Nicolle, Ryan, Sonia, Zorica, Joe, Birka, Yolanda, Santiago, Martin, Juliana, Emilia, Tanja, Tina, Olga, Yukina, Wilem, Angeles, Watse, Wiebke, Takeshi, Lih King, Anand, Vicky, Caro, Lo, Julian... for the unforgettable time together.

- The "Erasmus era". During this period I was living in Croeselaan, with Hinze and Asia. Great, great times. I was going out a lot, living the crazy Erasmus lifestyle. During this period I met Kimberley and Chiara, who I thank for the amazing time we shared. Thank to Frank and Viviana, which for sure have wonderful memories of this period as well. These were the years of the Tigers (!!!), the football team I had so much fun with. Thank to Tom, Jon, Joe, Andrea, Max and Paulo!

- The "Hopakker era". Living in the center of Utrecht was great. Especially because of the people I was living/going out with. Davide, Andrea, Max, Emanuele e Bruno. Grazie per avermi fatto sempre sentire a casa e per le bellissime serate passate insieme. Per tutte le cazzate sparate, i discorsi sull'Islam, le donne e i bubu. A bombà! Davide, un grazie speciale per essere stato amico e compagno di casa ideale in questi due anni. A special thank to Lucy for the wonderful moments we had. With the Tigers still alive and kicking, we started another football team: Hercules 16. Thanks Marcoleon for being "Il capitano". Un grazie a Fabio, Alberto e Antonio, per aver lasciato Manduria e aver incrociato la mia strada. Traveling around I met wonderful people. I can not mention all of them, but here I would like to name two. Thank Ofer for being a good friend since we met for the first time during a great conference in China. And thank Chris, for the good time and nice conversations we had in various parts of the world.

Un grazie di cuore a tutto il dipartimento di oncoematologia pediatrica del Santa Chiara di Pisa. Inoltre vorrei ringraziare la Menni, per avermi molto aiutato in questi anni in alcuni momenti difficili.

Un ringraziamento speciale ai miei grandi amici Fulvio, Elena, Fabio, Fabiano e Boris. Voi ci siete da così tanto tempo che a volte pare scontato, ma la vostra amicizia ha reso ogni momento passato insieme indimenticabile. Voi mi accompagnate lungo la strada rendendola a ogni passo migliore, poiché siete per me una costante fonte di ispirazione. Grazie davvero! Un grazie per tutti i bei momenti passati assieme anche a Giacomo, Carlo, Eva, Walter, Silvia, Ferdi, Chiara, Jacopo, Sama, Cinzia, France, Nadia, Ciro, Simona, Roberta e Antonio.

Antoine de Saint-Exupéry wrote one of the most beautiful books I ever read: "The Little Prince". It was my first book. Here I want to pay my tribute to the poetry and to the delicate charm of Saint-Exupéry's writing, the writing and the whimsical drawings that shaped my childhood and my hearth.

It was then that the fox appeared.

[. . .] “I cannot play with you,” the fox said.“I am not tamed.”

[. . .] “But if you tame me, it will be as if the sun came to shine on my life. I shall know the sound of a step that will be different from all the others. Other steps send me hurrying back underneath the ground. Yours will call me, like music, out of my burrow. And then look: you see the grain-fields down yonder? I do not eat bread. Wheat is of no use to me. The wheat fields have nothing to say to me. And that is sad. But you have hair that is the colour of gold. Think how wonderful that will be when you have tamed me! The grain, which is also golden, will bring me back the thought of you. And I shall love to listen to the wind in the wheat. . . ”

[. . .] “All men have the stars,” he answered, “but they are not the same things for different people. For some, who are travelers, the stars are guides. For others they are no more than little lights in the sky. For others, who are scholars, they are problems. For my businessman they were wealth. But all these stars are silent. You –you alone– will have the stars as no one else has them”

[. . .] “The stars are beautiful, because of a flower that cannot be seen.”

Antoine de Saint-Exupéry, “Le Petit Prince sur l’astéroïde B612”. © Éditions Gallimard

References

Abbett, W. P., Beaver, M., Davids, B., et al. 1997, ApJ, 480, 395
Aerts, C., Puls, J., Godart, M., & Dupret. 2008, ArXiv e-prints
Alongi, M., Bertelli, G., Bressan, A., et al. 1993, A&AS, 97, 851
Anders, E. & Grevesse, N. 1989, Geochimica et Cosmochimica Acta, 53, 197
Arzoumanian, Z., Chernoff, D. F., & Cordes, J. M. 2002, ApJ, 568, 289
Asplund, M., Grevesse, N., & Sauval, A. J. 2005, in Astronomical Society of the Pacific Conference Series, Vol. 336, Cosmic Abundances as Records of Stellar Evolution and Nucleosynthesis, ed. T. G. Barnes, III & F. N. Bash, 25
Asplund, M., Nordlund, Å., Trampedach, R., & Stein, R. F. 1999, A&A, 346, L17
Azzopardi, M., Lequeux, J., & Maeder, A. 1988, A&A, 189, 34
Babel, J. & Montmerle, T. 1997, ApJL, 485, L29
Badnell, N. R., Bautista, M. A., Butler, K., et al. 2005, MNRAS, 360, 458
Ballero, S. K., Matteucci, F., & Chiappini, C. 2006, New Astronomy, 11, 306
Baraffe, I., Heger, A., & Woosley, S. E. 2001, ApJ, 550, 890
Bascoul, G. 2007a, Ph.D. Thesis
Bascoul, G. P. 2007b, in IAU Symposium, ed. T. Kuroda, H. Sugama, R. Kanno, & M. Okamoto, Vol. 239, 317–319
Belczynski, K., Kalogera, V., & Bulik, T. 2002, ApJ, 572, 407
Böhm-Vitense, E. 1958, Zeitschrift fur Astrophysik, 46, 108
Bonanos, A. Z., Stanek, K. Z., Udalski, A., et al. 2004, ApJL, 611, L33
Bond, J. R., Arnett, W. D., & Carr, B. J. 1984, ApJ, 280, 825
Boothroyd, A. I. & Sackmann, I.-J. 1999, ApJ, 510, 232
Bouret, J.-C., Lanz, T., & Hillier, D. J. 2005, A&A, 438, 301
Bouret, J.-C., Lanz, T., Hillier, D. J., et al. 2003, ApJ, 595, 1182
Bouwens, R. J., Illingworth, G. D., Thompson, R. I., et al. 2004, ApJL, 606, L25
Braithwaite, J. & Spruit, H. C. 2004, Nature, 431, 819
Brandt, N. & Podsiadlowski, P. 1995, MNRAS, 274, 461
Braun, H. 1997, PhD thesis, Ludwig-Maximilians-Univ. München, (1997)
Brookshaw, L. & Tavani, M. 1993, ApJ, 410, 719
Brott, I., Langer, N., Lennon, D., et al. 2009, in prep.

Brown, J. A., Sneden, C., Lambert, D. L., & Dutchover, E. J. 1989, ApJS, 71, 293
Busso, M., Wasserburg, G. J., Nollett, K. M., & Calandra, A. 2007, ApJ, 671, 802
Cameron, A. G. W. & Fowler, W. A. 1971, ApJ, 164, 111
Cantiello, M., Langer, N., Brott, I., et al. 2009, A&A, 499, 279
Cantiello, M., Yoon, S.-C., Langer, N., & Livio, M. 2007, A&A, 465, L29
Canuto, V. M. 1999, ApJ, 524, 311
Charbonneau, P. & MacGregor, K. B. 2001, ApJ, 559, 1094
Charbonnel, C. & Balachandran, S. C. 2000, A&A, 359, 563
Charbonnel, C. & Do Nascimento, Jr., J. D. 1998, A&A, 336, 915
Charbonnel, C. & Zahn, J.-P. 2007, A&A, 467, L15
Charpinet, S., Fontaine, G., Brassard, P., et al. 1997, ApJL, 483, L123
Chevalier, R. A. & Li, Z.-Y. 2000, ApJ, 536, 195
Chevalier, R. A., Li, Z.-Y., & Fransson, C. 2004, ApJ, 606, 369
Cowley, C. R. 1970, The theory of stellar spectra (Topics in Astrophysics and Space Physics, New York: Gordon and Breach, 1970)
Cranmer, S. R. & Owocki, S. P. 1996, ApJ, 462, 469
Daflon, S., Cunha, K., Butler, K., & Smith, V. V. 2001, ApJ, 563, 325
Davies, B., Oudmaijer, R. D., & Vink, J. S. 2005, A&A, 439, 1107
Davies, B., Vink, J. S., & Oudmaijer, R. D. 2007, A&A, 469, 1045
de Greve, J. P. & Cugier, H. 1989, A&A, 211, 356
De Mink, S. E., Pols, O. R., & Hilditch, R. W. 2007, A&A, 467, 1181
Deng, L. & Xiong, D. R. 2001, MNRAS, 327, 881
Denissenkov, P. A. & Pinsonneault, M. 2008, ApJ, 684, 626
Denissenkov, P. A., Pinsonneault, M., & MacGregor, K. B. 2009, ApJ, 696, 1823
Dessart, L., Langer, N., & Petrovic, J. 2003, A&A, 404, 991
Detmers, R. G., Langer, N., Podsiadlowski, P., & Izzard, R. G. 2008, A&A, 484, 831
Domiciano de Souza, A., Kervella, P., Jankov, S., et al. 2003, A&A, 407, L47
Drake, N. A., de la Reza, R., da Silva, L., & Lambert, D. L. 2002, AJ, 123, 2703
Dupret, M. A. 2001, A&A, 366, 166
Dziembowski, W. A. 2008, ArXiv e-prints
Eddington, A. S. 1925, The Observatory, 48, 73
Eddington, A. S. 1926, The Internal Constitution of the Stars (Cambridge University Press, 1926)
Edmunds, M. G. 1978, A&A, 64, 103
Eggleton, P. P. 1983, ApJ, 268, 368
Eggleton, P. P., Dearborn, D. S. P., & Lattanzio, J. C. 2006, Science, 314, 1580
Eichler, D., Bar Shalom, A., & Oreg, J. 1995, ApJ, 448, 858
Endal, A. S. & Sofia, S. 1978, ApJ, 220, 279
Evans, C. J., Smartt, S. J., Lee, J.-K., et al. 2005, A&A, 437, 467
Eversberg, T., Lepine, S., & Moffat, A. F. J. 1998, ApJ, 494, 799
Ferrario, L. & Wickramasinghe, D. T. 2005, MNRAS, 356, 615
Figer, D. F. 2005, Nature, 434, 192
Figer, D. F., Najarro, F., Morris, M., et al. 1998, ApJ, 506, 384
Fliegner, J., Langer, N., & Venn, K. A. 1996, A&A, 308, L13
Forestini, M. & Charbonnel, C. 1997, A&AS, 123, 241
Fowler, W. A. & Hoyle, F. 1964, ApJS, 9, 201
Friend, D. B. & Abbott, D. C. 1986, ApJ, 311, 701
Fruchter, A. S., Levan, A. J., Strolger, L., et al. 2006, Nature, 441, 463
Fryer, C. L. & Heger, A. 2005, ApJ, 623, 302

Fryer, C. L., Woosley, S. E., & Hartmann, D. H. 1999, ApJ, 526, 152
Fullerton, A. W., Gies, D. R., & Bolton, C. T. 1996, ApJS, 103, 475
Fullerton, A. W., Massa, D. L., & Prinja, R. K. 2006, ApJ, 637, 1025
Fullerton, A. W., Massa, D. L., Prinja, R. K., Owocki, S. P., & Cranmer, S. R. 1997, A&A, 327, 699
Fynbo, J. P. U., Jakobsson, P., Möller, P., et al. 2003, A&A, 406, L63
Gies, D. R. & Lambert, D. L. 1992, ApJ, 387, 673
Glatzel, W. & Mehren, S. 1996, MNRAS, 282, 1470
Goldreich, P. & Kumar, P. 1990, ApJ, 363, 694
Gratton, R. G., Sneden, C., Carretta, E., & Bragaglia, A. 2000, A&A, 354, 169
Grosdidier, Y., Moffat, A. F. J., Joncas, G., & Acker, A. 1998, ApJL, 506, L127
Hammer, F., Flores, H., Schaerer, D., et al. 2006, A&A, 454, 103
Harries, T. J., Hilditch, R. W., & Howarth, I. D. 2003, MNRAS, 339, 157
Harries, T. J., Howarth, I. D., & Evans, C. J. 2002, MNRAS, 337, 341
Heger, A. 1998, Ph.D. Thesis
Heger, A., Fryer, C. L., Woosley, S. E., Langer, N., & Hartmann, D. H. 2003, ApJ, 591, 288
Heger, A. & Langer, N. 1996, A&A, 315, 421
Heger, A. & Langer, N. 2000, ApJ, 544, 1016
Heger, A., Langer, N., & Woosley, S. E. 2000, ApJ, 528, 368
Heger, A. & Woosley, S. E. 2002, ApJ, 567, 532
Heger, A., Woosley, S. E., & Spruit, H. C. 2005, ApJ, 626, 350
Henrichs, H. F., de Jong, J. A., Donati, D.-F., et al. 2000, in Magnetic Fields of Chemically Peculiar and Related Stars, Proceedings of the International Meeting, held in Special Astrophysical Observatory of Russian AS, September 23 - 27, 1999, Eds.: Yu.V. Glagolevskij, I.I. Romanyuk, p.57-60
Herrero, A., Kudritzki, R. P., Gabler, R., Vilchez, J. M., & Gabler, A. 1995, A&A, 297, 556
Herrero, A., Kudritzki, R. P., Vilchez, J. M., et al. 1992, A&A, 261, 209
Herzig, K., El Eid, M. F., Fricke, K. J., & Langer, N. 1990, A&A, 233, 462
Hibbins, R. E., Dufton, P. L., Smartt, S. J., & Rolleston, W. R. J. 1998, A&A, 332, 681
Hilditch, R. W., Howarth, I. D., & Harries, T. J. 2005, MNRAS, 357, 304
Hirschi, R., Meynet, G., & Maeder, A. 2005, A&A, 443, 581
Howarth, I. D. & Prinja, R. K. 1989, ApJS, 69, 527
Huang, W. & Gies, D. R. 2006, ApJ, 648, 591
Hubeny, I., Heap, S. R., & Altner, B. 1991, ApJL, 377, L33
Hubrig, S., Schöller, M., Schnerr, R. S., et al. 2008, A&A, 490, 793
Hunter, I., Brott, I., Lennon, D. J., et al. 2008a, ApJL, 676, L29
Hunter, I., Dufton, P. L., Smartt, S. J., et al. 2007, A&A, 466, 277
Hunter, I., Lennon, D. J., Dufton, P. L., et al. 2008b, A&A, 479, 541
Hurley, J. R., Tout, C. A., & Pols, O. R. 2002, MNRAS, 329, 897
Iglesias, C. A. & Rogers, F. J. 1996, ApJ, 464, 943
Iglesias, C. A., Rogers, F. J., & Wilson, B. G. 1992, ApJ, 397, 717
Jakobsson, P., Björnsson, G., Fynbo, J. P. U., et al. 2005, MNRAS, 362, 245
Kaper, L., Henrichs, H. F., Fullerton, A. W., et al. 1997, A&A, 327, 281
Kato, M. & Iben, I. J. 1992, ApJ, 394, 305
Kippenhahn, R., Ruschenplatt, G., & Thomas, H.-C. 1980, A&A, 91, 175
Kippenhahn, R. & Weigert, A. 1967, Zeitschrift fur Astrophysik, 65, 251
Kippenhahn, R. & Weigert, A. 1990, Stellar Structure and Evolution (Stellar Structure and Evolution, XVI, 468 pp. 192 figs.. Springer-Verlag Berlin Heidelberg New York. Also Astronomy and Astrophysics Library)
Kiriakidis, M., Fricke, K. J., & Glatzel, W. 1993, MNRAS, 264, 50

Korn, A. J., Keller, S. C., Kaufer, A., et al. 2002, A&A, 385, 143
Krishnamurti, R. 2003, Journal of Fluid Mechanics, 483, 287
Kudritzki, R.-P., Lennon, D. J., Haser, S. M., et al. 1996, in Science with the Hubble Space Telescope - II, ed. P. Benvenuti, F. D. Macchetto, & E. J. Schreier, 285
Kudritzki, R. P., Pauldrach, A., Puls, J., & Abbott, D. C. 1989, A&A, 219, 205
Langer, N. 1991, A&A, 252, 669
Langer, N. 1998, A&A, 329, 551
Langer, N., Cantiello, M., Yoon, S.-C., et al. 2008, in IAU Symposium, Vol. 250, IAU Symposium, 167
Langer, N. & El Eid, M. F. 1986, A&A, 167, 265
Langer, N., El Eid, M. F., & Fricke, K. J. 1985, A&A, 145, 179
Langer, N. & Norman, C. A. 2006, ApJL, 638, L63
Langer, N., Yoon, S.-C., Petrovic, J., & Heger, A. 2004, in IAU Symposium, ed. A. Maeder & P. Eenens, P. 535
Lauterborn, D. 1970, A&A, 7, 150
Lefever, K., Puls, J., & Aerts, C. 2007, A&A, 463, 1093
Leibacher, J. W. & Stein, R. F. 1971, ApJL, 7, 191
Lennon, D. J., Dufton, P. L., & Crowley, C. 2003, A&A, 398, 455
Lépine, S. & Moffat, A. F. J. 1999, ApJ, 514, 909
Lepine, S. & Moffat, A. F. J. 2008, ArXiv e-prints, 805
Leushin, V. V. 1988, Soviet Astronomy, 32, 430
Lighthill, M. F. 1967, in IAU Symposium, Vol. 28, Aerodynamic Phenomena in Stellar Atmospheres, ed. R. N. Thomas, 429
Lighthill, M. J. 1952, Royal Society of London Proceedings Series A, 211, 564
Livio, M. 1993, in ASP Conf. Ser. 53: Blue Stragglers, ed. R. A. Saffer, 3
Lobel, A. & Blomme, R. 2008, ApJ, 678, 408
Ludwig, H.-G., Freytag, B., & Steffen, M. 1999, A&A, 346, 111
Lyubimkov, L. S., Rostopchin, S. I., & Lambert, D. L. 2004, MNRAS, 351, 745
MacDonald, J. & Mullan, D. J. 2004, MNRAS, 348, 702
MacFadyen, A. I. & Woosley, S. E. 1999, ApJ, 524, 262
MacGregor, K. B. & Cassinelli, J. P. 2003, ApJ, 586, 480
Maeder, A. 1987, A&A, 178, 159
Maeder, A., Georgy, C., & Meynet, G. 2008, A&A, 479, L37
Maeder, A. & Meynet, G. 2000a, A&A, 361, 159
Maeder, A. & Meynet, G. 2000b, ARA&A, 38, 143
Maeder, A. & Meynet, G. 2001, A&A, 373, 555
Marchenko, S. V., Moffat, A. F. J., St-Louis, N., & Fullerton, A. W. 2006, ApJL, 639, L75
Martins, F., Hillier, D. J., Bouret, J. C., et al. 2008, ArXiv e-prints
Massa, D., Fullerton, A. W., Nichols, J. S., et al. 1995, ApJL, 452, L53
Massey, P., Penny, L. R., & Vukovich, J. 2002, ApJ, 565, 982
Massey, P., Puls, J., Pauldrach, A. W. A., et al. 2005, ApJ, 627, 477
Mendel, J. T., Venn, K. A., Proffitt, C. R., Brooks, A. M., & Lambert, D. L. 2006, ApJ, 640, 1039
Merryfield, W. J. 1995, ApJ, 444, 318
Meynet, G. & Maeder, A. 1997, A&A, 321, 465
Meynet, G. & Maeder, A. 2000, A&A, 361, 101
Meynet, G. & Maeder, A. 2005, A&A, 429, 581
Modjaz, M., Kewley, R., Kirshner, R., et al. 2007, astro-ph/0701246, AJ submitted
Mokiem, M. R., de Koter, A., Evans, C. J., et al. 2007a, A&A, 465, 1003
Mokiem, M. R., de Koter, A., Evans, C. J., et al. 2006, A&A, 456, 1131

Mokiem, M. R., de Koter, A., Vink, J. S., et al. 2007b, A&A, 473, 603
Morel, T., Butler, K., Aerts, C., Neiner, C., & Briquet, M. 2006, A&A, 457, 651
Morel, T., Hubrig, S., & Briquet, M. 2008, A&A, 481, 453
Mullan, D. J. & MacDonald, J. 2005, MNRAS, 356, 1139
Nelson, C. A. & Eggleton, P. P. 2001, ApJ, 552, 664
Nieuwenhuijzen, H. & de Jager, C. 1990, A&A, 231, 134
Nordhaus, J., Busso, M., Wasserburg, G. J., Blackman, E. G., & Palmerini, S. 2008, ApJL, 684, L29
Ober, W. W., El Eid, M. F., & Fricke, K. J. 1983, A&A, 119, 61
Ofek, E. O., Cameron, P. B., Kasliwal, M. M., et al. 2007, ApJL, 659, L13
Orosz, J. A., McClintock, J. E., Narayan, R., et al. 2007, Nature, 449, 872
Orosz, J. A., Steeghs, D., McClintock, J. E., et al. 2008, ArXiv e-prints
Ott, C. D., Burrows, A., Thompson, T. A., Livne, E., & Walder, R. 2006, ApJS, 164, 130
Owocki, S. P. & Puls, J. 1999, ApJ, 510, 355
Palacios, A., Charbonnel, C., & Forestini, M. 2001, A&A, 375, L9
Palacios, A., Charbonnel, C., Talon, S., & Siess, L. 2006, A&A, 453, 261
Pamyatnykh, A. A. 1999, Acta Astronomica, 49, 119
Panaitescu, A. & Kumar, P. 2001, ApJ, 554, 667
Panaitescu, A. & Kumar, P. 2002, ApJ, 571, 779
Parker, E. N. 1975, ApJ, 198, 205
Pavlovski, K. & Hensberge, H. 2005, A&A, 439, 309
Petrovic, J., Langer, N., & van der Hucht, K. A. 2005a, A&A, 435, 1013
Petrovic, J., Langer, N., Yoon, S.-C., & Heger, A. 2005b, A&A, 435, 247
Pinsonneault, M. 1997, ARA&A, 35, 557
Pinsonneault, M. H., Kawaler, S. D., Sofia, S., & Demarque, P. 1989, ApJ, 338, 424
Podsiadlowski, P., Joss, P. C., & Hsu, J. J. L. 1992, ApJ, 391, 246
Podsiadlowski, P., Mazzali, P. A., Nomoto, K., Lazzati, D., & Cappellaro, E. 2004, ApJL, 607, L17
Podsiadlowski, P., Rappaport, S., & Han, Z. 2003, MNRAS, 341, 385
Pols, O. R. 1994, A&A, 290, 119
Prinja, R. K. & Howarth, I. D. 1988, MNRAS, 233, 123
Prinja, R. K., Massa, D., & Fullerton, A. W. 2002, A&A, 388, 587
Puls, J., Markova, N., Scuderi, S., et al. 2006, A&A, 454, 625
Rauw, G., Crowther, P. A., De Becker, M., et al. 2005, A&A, 432, 985
Reddy, B. E. & Lambert, D. L. 2005, AJ, 129, 2831
Reimers, D. 1975, Memoires of the Societe Royale des Sciences de Liege, 8, 369
Rolleston, W. R. J., Brown, P. J. F., Dufton, P. L., & Howarth, I. D. 1996, A&A, 315, 95
Runacres, M. C. & Owocki, S. P. 2002, A&A, 381, 1015
Runacres, M. C. & Owocki, S. P. 2005, A&A, 429, 323
Saio, H. 1993, MNRAS, 260, 465
Saio, H., Kuschnig, R., Gautschy, A., et al. 2006, ApJ, 650, 1111
Sana, H., Gosset, E., Nazé, Y., Rauw, G., & Linder, N. 2008, MNRAS, 386, 447
Sarna, M. J. 1992, MNRAS, 259, 17
Scannapieco, E., Madau, P., Woosley, S., Heger, A., & Ferrara, A. 2005, ApJ, 633, 1031
Schnurr, O., Moffat, A. F. J., St-Louis, N., Morrell, N. I., & Guerrero, M. A. 2008, MNRAS, 389, 806
Schröder, K.-P. & Cuntz, M. 2005, ApJL, 630, L73
Schröder, K.-P. & Cuntz, M. 2007, A&A, 465, 593
Schroder, K.-P., Pols, O. R., & Eggleton, P. P. 1997, MNRAS, 285, 696
Schuessler, M. & Paehler, A. 1978, A&A, 68, 57
Shore, S. N. 1992, An introduction to astrophysical hydrodynamics (San Diego: Academic Press,

|c1992)
Siess, L. 2009, A&A, 497, 463
Siess, L. & Livio, M. 1999a, MNRAS, 304, 925
Siess, L. & Livio, M. 1999b, MNRAS, 308, 1133
Siess, L., Livio, M., & Lattanzio, J. 2002, ApJ, 570, 329
Silverman, J. M. & Filippenko, A. V. 2008, ApJL, 678, L17
Smith, K. C. & Howarth, I. D. 1998, MNRAS, 299, 1146
Smith, N., Li, W., Foley, R. J., et al. 2007, ApJ, 666, 1116
Spiegel, E. A. & Weiss, N. O. 1980, Nature, 287, 616
Spiegel, E. A. & Zahn, J.-P. 1992, A&A, 265, 106
Spitzer, L. 1962, Physics of Fully Ionized Gases (Physics of Fully Ionized Gases, New York: Interscience (2nd edition), 1962)
Spruit, H. C. 1999, A&A, 349, 189
Spruit, H. C. 2002, A&A, 381, 923
Stancliffe, R. J., Glebbeek, E., Izzard, R. G., & Pols, O. R. 2007, A&A, 464, L57
Stankov, A. & Handler, G. 2005, ApJS, 158, 193
Stein, R. F. 1967, Solar Physics, 2, 385
Stern, M. E. 1960, Tellus, 12, 172
Stothers, R. B. & Chin, C.-W. 1992, ApJ, 390, 136
Stothers, R. B. & Chin, C.-W. 1993, ApJL, 408, L85
Suijs, M. P. L., Langer, N., Poelarends, A.-J., et al. 2008, A&A, 481, L87
Tassoul, J.-L. 2000, Stellar Rotation (Cambridge University Press)
Toledano, O., Moreno, E., Koenigsberger, G., Detmers, R., & Langer, N. 2007, A&A, 461, 1057
Townsend, R. H. D., Owocki, S. P., & Groote, D. 2005, ApJL, 630, L81
Trundle, C., Dufton, P. L., Hunter, I., et al. 2007, A&A, 471, 625
Trundle, C. & Lennon, D. J. 2005, A&A, 434, 677
ud-Doula, A. & Owocki, S. P. 2002, ApJ, 576, 413
Ulrich, R. K. 1970, ApJ, 162, 993
Ulrich, R. K. 1972, ApJ, 172, 165
Umeda, H. & Nomoto, K. 2002, ApJ, 565, 385
Umeda, H. & Nomoto, K. 2005, ApJ, 619, 427
Uttenthaler, S., Lebzelter, T., Palmerini, S., et al. 2007, A&A, 471, L41
van der Hucht, K. A. 2001, New Astronomy Review, 45, 135
van Leeuwen, F., van Genderen, A. M., & Zegelaar, I. 1998, A&AS, 128, 117
van Marle, A. J., Langer, N., Achterberg, A., & Garcaía-Segura, G. 2006, A&A, 460, 105
Vanbeveren, D. & de Loore, C. 1994, A&A, 290, 129
Vanbeveren, D., Van Bever, J., & Belkus, H. 2007, ApJL, 662, L107
Vauclair, S. 2004, ApJ, 605, 874
Venn, K. A., Brooks, A. M., Lambert, D. L., et al. 2002, ApJ, 565, 571
Vink, J. S. & de Koter, A. 2005, A&A, 442, 587
Vink, J. S., de Koter, A., & Lamers, H. J. G. L. M. 2001, A&A, 369, 574
Vogt, H. 1925, Astronomische Nachrichten, 223, 229
von Zeipel, H. 1924, MNRAS, 84, 665
Vrancken, M., Lennon, D. J., Dufton, P. L., & Lambert, D. L. 2000, A&A, 358, 639
Wade, G. A., Fullerton, A. W., Donati, J.-F., et al. 2006, A&A, 451, 195
Walborn, N. R. 1976, ApJ, 205, 419
Walborn, N. R., Morrell, N. I., Howarth, I. D., et al. 2004, ApJ, 608, 1028
Wallerstein, G. & Sneden, C. 1982, ApJ, 255, 577

Wedemeyer, S., Freytag, B., Steffen, M., Ludwig, H.-G., & Holweger, H. 2004, A&A, 414, 1121
Wellstein, S. 2001, PhD thesis, University of Potsdam
Wellstein, S. & Langer, N. 1999, A&A, 350, 148
Wellstein, S., Langer, N., & Braun, H. 2001, A&A, 369, 939
Williams, S. J., Gies, D. R., Henry, T. J., et al. 2008, ApJ, 682, 492
Witte, M. G. & Savonije, G. J. 1999, A&A, 350, 129
Woosley, S. E. 1993, ApJ, 405, 273
Woosley, S. E. & Heger, A. 2006, ApJ, 637, 914
Yao, Y., Wang, Q. D., & Nan Zhang, S. 2005, MNRAS, 362, 229
Yoon, S.-C. & Langer, N. 2005, A&A, 443, 643
Yoon, S.-C., Langer, N., & Norman, C. 2006, A&A, 460, 199
Young, T. R. 2004, ApJ, 617, 1233
Zahn, J.-P. 1974, in IAU Symposium, Vol. 59, Stellar Instability and Evolution, ed. P. Ledoux, A. Noels, & A. W. Rodgers, 185
Zahn, J.-P. 1975, A&A, 41, 329
Zahn, J.-P. 1977, A&A, 57, 383
Zahn, J.-P. 1989, A&A, 220, 112